The influence of plankton food-web structure on the efficiency of the biological carbon pump

Dissertation

zur Erlangung des akademischen Grades

eines Doktors der Naturwissenschaften

-Dr. rer. nat.-

an der Mathematisch-Naturwissenschaftlichen Fakultät

der Christian-Albrechts Universität zu Kiel

vorgelegt von

Paul Stange

Kiel, April 2017

GEOMAR
Helmholtz Centre for Ocean Research Kiel

C | A | U

1. Gutachter:	Prof. Dr. Ulf Riebesell
2. Gutachter:	Prof. Dr. Eric Achterberg
Tag der Disputation:	01.06.2017
Zum Druck genehmigt:	01.06.2017

Für Anja

Contents

Zusammenfassung

Die biologische Kohlenstoffpumpe (BKP) ist ein komplexes Zusammenspiel aus Prozessen, welche in ihrer Gesamtheit für den Transport von organischer Materie aus dem Oberflächenozean in die Tiefe verantwortlich ist. Als solches spielt sie gleichzeitig eine wichtige Rolle in der Sequestrierung von atmosphärischem Kohlenstoffdioxid (CO_2) und seiner Speicherung in der Tiefe über Zeiträume von Jahrzehnten bis Jahrtausenden. Dies hat besondere Bewandtnis im Anbetracht der steigenden anthropogenen CO_2 Emissionen, welche beispiellos sind in der jüngsten geologischen Geschichte dieses Planeten. Trotz ihrer zweifelslosen Bedeutung sind wir noch immer in Ermangelung eines mechanistischen Verständnisses der Prozesse, welche die Effizienz der BKP kontrollieren. Im Laufe der letzten zehn Jahre hat sich der Fokus zunehmend auf das Verständnis des Zusammenhangs zwischen Ökosystem-Strukturen und Export von organischer Materie verlagert. Dabei erhärten sich die Hinweise, dass regenerierende Systeme, welche charakteristisch für Regionen mit geringer Saisonalität und nährstoffarmen Bedingungen sind, einen effizienteren Export aufweisen als Systeme in Regionen mit hoher Saisonalität und durch anorganische Nährstoffe gespeisten Phytoplanktonblüten. Im Rahmen dieser Doktorarbeit wurde daher mit Experimenten in *in situ* Mesokosmen eine neuer Ansatz zur Untersuchung der Beziehung zwischen der Struktur von Planktongemeinschaften und export-relevanten Parametern verfolgt. In einem ersten Schritt wurden vier Mesokosmen-Studien, welche in arktischen, gemäßigten und subtropischen Regionen durchgeführt wurden, mit dem Ziel analysiert, Muster im Zeitversatz zwischen der Produktion und Sedimentation von organischer Materie zu finden. Dabei eignet sich der Mesokosmen-Ansatz besonders gut für eine derartige Analyse, da die Arbeit in einem geschlossenen System den Einfluss von lateraler Advektion ausschließt. Ergebnisse dieser Studie zeigen, dass der Zeitversatz negativ mit der Länge des Chlorophyll-Aufbaus in der Wassersäule korreliert. Dieser Zusammenhang ist mit hoher Wahrscheinlichkeit auf eine Verzögerung von Partikelaggregation und einer stärkeren Entkopplung von Produzenten und Konsumenten im Nahrungsnetz in Systemen mit rapiden Chlorophyll-Aufbau zurückzuführen. Weiterhin wurde unter Einbezug von Partikel-Sinkgeschwindigkeiten der Zeitversatz auf der Referenztiefe für Oberflächenexport (100 m) berechnet. Diese Kalkulation ergab, dass konventionelle Methoden (z.B. Sedimentfallen, Radioisotope) unter Umständen nicht ausreichend lange Integrationszeiträume haben um Exportraten akkurat einzuschätzen. Im Rahmen der zweiten und dritten Studie wurde ein *in situ* Mesokosmen-Experiment vor der Küste von Gran Canaria durchgeführt, in dessen Zuge die Planktongemeinschaft und export-relevante Parameter gleichzeitig untersucht wurden. Zu Beginn der Studie wurden die Mesokosmen mit verschiedenen Mengen an CO_2 angereichert, wodurch ein Gradient mit verschiedenen Versauerungs-Szenarien des Ozeans der Zukunft eingestellt wurde. Zusätzlich wurde nach

einer ausgedehnten oligotrophischen Phase ein natürliches Auftriebsereignis, welches typisch für diese Region ist, simuliert, indem nährstoffreiches Tiefenwasser gesammelt und zu allen Mesokosmen gleichermaßen zugegeben wurde. In dieser Studie wurde der Schwerpunkt auf den Zusammenhang zwischen Unterschieden in der Planktongemeinschaft und der Änderung der elementaren Zusammensetzung von partikulärer organischer Materie (POM) während des Sinkvorgangs gelegt. Aus den Ergebnissen dieser Analyse wird ersichtlich, dass in den zwei Mesokosmen mit höchsten CO_2 Konzentrationen sinkende POM weniger stark abgebaut wurde. Dies ist vor allem auf die wesentlich geringeren Abundanzen von Mikro- und Mesozooplankton zurückzuführen, was ihre wichtige Rolle in der Transformation von organischer Materie im Kontext der BKP unterstreicht. Das dritte Kapitel thematisiert den Zusammenhang zwischen Unterschieden in der Planktongemeinschaft, Sinkgeschwindigkeit von Partikeln und kohlenstoff-normalisierter Respirationsrate von sinkender POM. Der Wechsel von einer typisch oligotrophen Nahrungsnetz-Struktur hin zu einer durch anorganische Nährstoffe gespeisten Diatomeenblüte hatte substantielle Änderungen in der Sinkgeschwindigkeit von Partikeln zur Folge. Dies begründet sich einerseits durch Unterschiede im Anteil von ballastierenden Mineralien, und andererseits durch Änderungen in der Porosität von Partikeln. Des Weiteren wurden im Verlauf des Experiments starke Unterschiede in der kohlenstoff-normalisierter Respirationsrate gefunden, wobei maximale Raten sowohl zur Zeit einer schwachen Blüte von *Synechococcus*, als auch während der ausgeprägten Diatomeenblüte beobachtet wurden. Besonders niedrige Raten wurden hingegen in Phasen geringer Produktivität verzeichnet. Um Rückschlüsse auf den Tiefenexport von Kohlenstoff ziehen zu können, wurde weiterhin die Remineralisierungs-Längen-Skala (L) ausgerechnet. Im Großen und Ganzen bestätigen die Ergebnisse der dritten Studie das Konzept von geringeren Transfereffizienzen in opal-dominierten Regionen, verglichen mit oligotrophen Regionen, in welchen komplexere Nahrungsnetze und geringe Saisonalität zur Produktion von refraktärerer POM führen. Da solche Regionen vorwiegend von kleinen Phytoplanktonarten dominiert werden, ist Phytoplanktongröße ein verbreiteter Indikator für Transfereffizienz. Die hohen Werte für L während der Blüte von *Synechococcus*, welche in dieser Arbeit beobachtet wurden, deuten jedoch klar darauf hin, dass Faktoren wie die Abbaubarkeit und elementare Zusammensetzung von POM eine entscheidende Rolle spielen in der Kontrolle der Transfereffizient. Zusammenfassend hat die vorliegende Doktorarbeit Muster in dem Verhältnis zwischen Nahrungsnetz-Struktur und der Effizienz der BKP aufgezeigt, jüngste Konzepte bestätigt und erweitert. Außerdem verdeutlicht diese Arbeit, dass der methodische Ansatz von *in situ* Mesokosmenexperimenten einen wichtigen Beitrag in der Erforschung der BKP leisten kann und die Beantwortung von Fragen ermöglicht, welche mit herkömmlichen Methoden bisher nicht ohne weitere Annahmen möglich war.

Summary

The biological carbon pump (BCP) is a complex suite of processes responsible for transporting organic matter produced in the surface ocean to depth. As such, it is an important mechanism in controlling the sequestration of atmospheric carbon dioxide (CO_2) and its storage on time scales of decades to centuries. This receives special attention in light of the rising anthropogenic CO_2 emissions, which are unprecedented in the recent geological history of this planet. Despite its importance, we are still lacking a mechanistic understanding of the processes controlling the efficiency of the BCP. Over the past decade, the focus has increasingly shifted towards illuminating the effect of differences in ecosystem structure on organic matter export. In this respect, growing evidence suggests that recycling systems commonly found in regions with low seasonality and oligotrophic conditions are characterized by more efficient export compared to systems found in regions with strong seasonality and pronounced phytoplankton blooms that thrive on inorganic nutrients. Within the scope of this doctoral dissertation, *in situ* mesocosm were used as a new approach to study the relation between plankton community structure and export relevant parameters.

As a first step, four mesocosm studies conducted in arctic, temperate and subtropical regions were analyzed in order to identify patterns in the time lag between organic matter build-up and its sedimentation. Such an analysis is particularly suited for mesocosm experiments, since working in enclosed systems prevents the influence of lateral advection. Results of this study show that time lag is negatively correlated with the duration of chlorophyll a build-up, which is most likely explained by delayed aggregation of particles and a stronger decoupling between producers and grazers in systems where chlorophyll builds up rapidly, e.g. phytoplankton blooms. Using sinking velocity measurements, the surface time lag was then extrapolated to a depth of 100 m, which is commonly used as a reference depth for export flux measurements. The calculated time lag at this depth suggested that conventional methods (e.g. sediment traps, radioisotopes) may not have sufficiently long integration times to accurately estimate the export ratio.

Within the scope of the second and third study, a mesocosm experiment was conducted off the coast of Gran Canaria, during which the plankton community structure and export relevant parameters were monitored simultaneously. In order to simulate future ocean conditions, mesocosms were pertubated with different levels of CO_2 creating a gradient of ocean acidification scenarios. We further simulated a natural upwelling event, which is commonly observed in this area, by equally adding nutrient-rich deep water to all mesocosms. For the second study, emphasis was put on how changes in the plankton community structure influence the elemental stoichiometry of particulate organic matter during sinking. This analysis revealed that decomposition of sinking POM was less pro-

nounced in mesocosms with highest levels of pCO_2, which was most likely driven by much lower abundances of micro- and mesozooplankton grazers highlighting their substantial contribution to organic matter transformation in the context of the BCP.
The third study emphasized the relation between plankton community structure and particle sinking velocity, as well as carbon-specific respiration rates of sinking POM. The shift in food-web structure from one characteristic for oligotrophic conditions to a diatom bloom fueled by the addition of inorganic nutrients through deep-water was accompanied by substantial changes in sinking velocity, which we partly attributed to changes in ballasting mineral content and differences in particle porosity. We further observed profound differences in carbon-specific respiration rates over the course of the experiment, with maximum values during a small bloom of Synechococcus and the pronounced diatom bloom and minimal values during times of low productivity. Building on that, we calculated the remineralization length scale in order to estimate how the changes in food-web structure may affect deep carbon export. Overall, these results align with the concept that highly seasonal, opal-dominated regions are characterized by lower transfer efficiencies compared to regions where more complex food webs and low seasonality result in the production of more reworked and thus refractory particulate organic matter. Since oligotrophic regions are often dominated by small phytoplankton, the latter have been often associated with high transfer efficiencies. However, the comparably high values of L during a small bloom of *Synechococcus* observed in this work suggest that factors other than phytoplankton size, such as the degradability and elemental stoichiometry of POM, have a paramount control on T_{eff}.
In summary, this doctoral dissertation has revealed patterns in the relation between food-web structure changes and the efficiency of the BCP and circumstantiated recent concepts in this field of research. Furthermore, this work exemplifies that the methodological approach of utilizing *in situ* mesocosms can make a significant contribution to BCP research, for it allows answering questions that conventional methods have not been able to address.

1 — Introduction

1.1 The importance of the ocean in the global carbon cycle

The oceans hold the second largest pool of inorganic carbon on planet Earth, with a reservoir roughly 50 times larger than that of the atmosphere (Falkowski et al., 2000). The majority of this carbon is stored in the form of dissolved inorganic carbon (DIC) in the deep ocean, while only a small fraction is organically bound in the form of dissolved and particulate organic carbon (DOC, POC)(Fig. 1.1). With regards to CO_2, the surface ocean remains more or less in equilibrium with the atmosphere, and inorganic carbon is constantly exchanged in the form of carbon dioxide (CO_2) at the air-sea interface. By governing atmospheric CO_2 concentrations, the oceans thus hold a crucial role in controlling the Earth's climate – a feature that is only possible due to a steep gradient of DIC with depth.

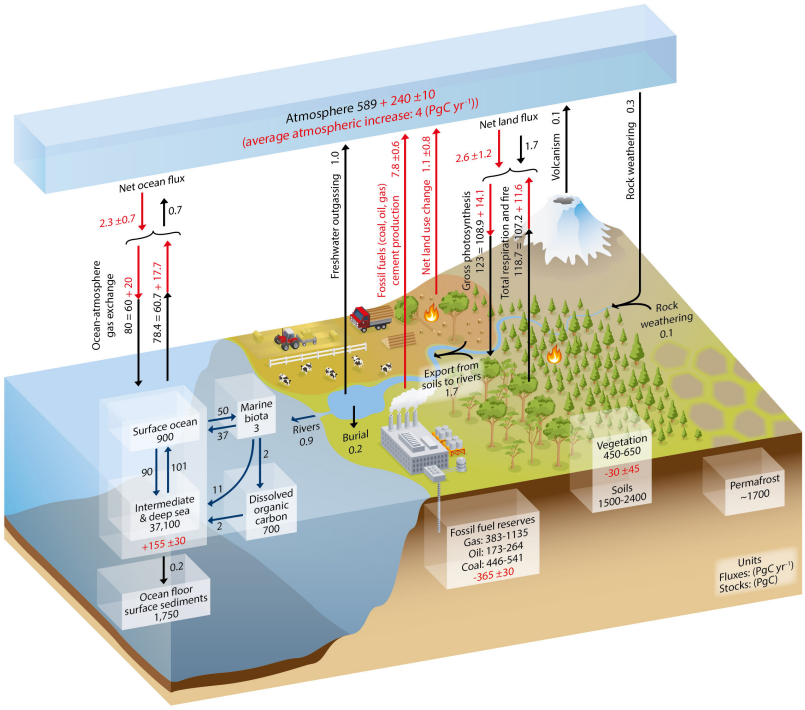

Figure 1.1: Schematic representation of the global carbon cycle. Black numbers within the boxes indicate the pre-industrial (before 1750) reservoir-sizes. Arrows and the corresponding numbers indicate the fluxes between reservoirs. Red numbers and arrows indicate changes in the period between 2000 and 2009. Red numbers in boxes indicate the cumulative changes over the industrial era (1750-2011). This Figure was taken from the IPCC assessment report 2013 (AR5 - WG1, Chapter 06).

The latter is maintained by two mechanisms: the solubility pump and the biological carbon pump (Volk and Hoffert, 1985). The solubility pump is a physical mechanism that operates on long time scales of hundreds of years. In principle, warm surface water drifts polewards and cools down, thereby increasing its uptake capacity for CO_2. As part of the thermohaline circulation some of the CO_2 enriched waters sink to depth at

high latitudes, which effectively prevents re-equilibration with the atmosphere for several hundred years. The efficiency of the solubility pump partly depends on global ocean circulation patterns and differences in seasonal and regional ocean ventilation. Although the contribution of the solubility pump to the oceanic DIC gradient is substantial (35%, Toggweiler et al. (2003b)), the biological carbon pump is the dominant mechanism in transporting carbon to depth (Toggweiler et al., 2003a).

1.1.1 The biological carbon pump

About half of the global primary production is contributed by marine phytoplankton every year (Field, 1998). These autotrophic organisms transform DIC and nutrients into DOC and POC, and form the base of the marine food web. The majority of this organic matter is rapidly respired in the surface and only a small fraction escapes the remineralization processes and is exported to depth. This biologically mediated transport of organic matter to the deep ocean is commonly referred to as the soft-tissue or organic carbon pump and functions through various modes of transport. The main pathway for the transport of organic matter to depth is the gravitational settling of POC (Hopkinson and Vallino, 2005; Passow and Carlson, 2012). First descriptions of this mechanism go back to the early 20th century when William Beebe observed sinking detritus and large flocks, later described as "marine snow" by Suzuki and Kato (1953). During the last decades, however, downwelling of DOC and the active transport of carbon by diurnal vertical migration (DVM) of zooplankton have been identified as potentially important additional transport mechanisms for carbon to depth. The relative contribution of these processes to the BCP is still poorly confined and varies regionally and over time. Estimates for DOC contribution to total export range from 9 to 20% in the North Atlantic (Carlson et al., 2010) and 20% on a global scale (Hansell and Carlson, 1998), while the active transport by DVM has been observed to account for up to 37% of total flux to depth below 300m in the Sargasso Sea (Steinberg et al., 2000).
Another important pathway that drives the vertical DIC gradient is the hard-tissue or carbonate pump. This mechanism describes the biologically mediated precipitation of CaCO3 by marine algae (coccolithophores) and heterotrophic protists (foraminifera) and its gravitational settling to depth. The relative strength of the organic and carbonate pump is described in the rain ratio (POC/PIC) and commonly ranges from 0.7 to 0.8 (Klaas and Archer, 2002). In this thesis, the organic carbon pump will be emphasized with particular focus on the gravitational settling of POC.
The depth to which organic carbon is transported before it is remineralized determines the timescale over which it is effectively prevented from re-equilibrating with the atmosphere. This depth is commonly referred to as the remineralization depth, or remineralization length scale (RLS)(Kwon et al., 2009; Passow and Carlson, 2012). Any carbon that was respired above the winter mixed layer (WML) is thus brought back to the surface within 1 to 10 years (Fig. 1.2). Carbon that sinks below the WML is, however, considered sequestered and eventually resurfaces on timescales corresponding to the thermohaline circulation (100-1000 years). In this thesis, we define the total amount of particulate organic carbon passing through the base of the euphotic zone (100m or 1% light level) as export flux or export production (EP), while carbon passing the WML depth (1000 m) as sequestration flux (SF).

1.2 Uncertainties in estimating the strength of the BCP

The BCP is generally described by its strength and efficiency, both of which are defined slightly different in the literature. Here, we define the strength of the BCP as the total amount of POC passing the euphotic zone depth. The efficiency of the BCP is defined by Buesseler and Boyd (2009) as the proportion of surface production that is exported to the deep ocean. As such, it can be further differentiated into the export efficiency (EP_{eff}), which is the fraction of surface primary production that is exported from the euphotic zone, and the transfer efficiency (T_{eff}) defined as the ratio of SF and EP.

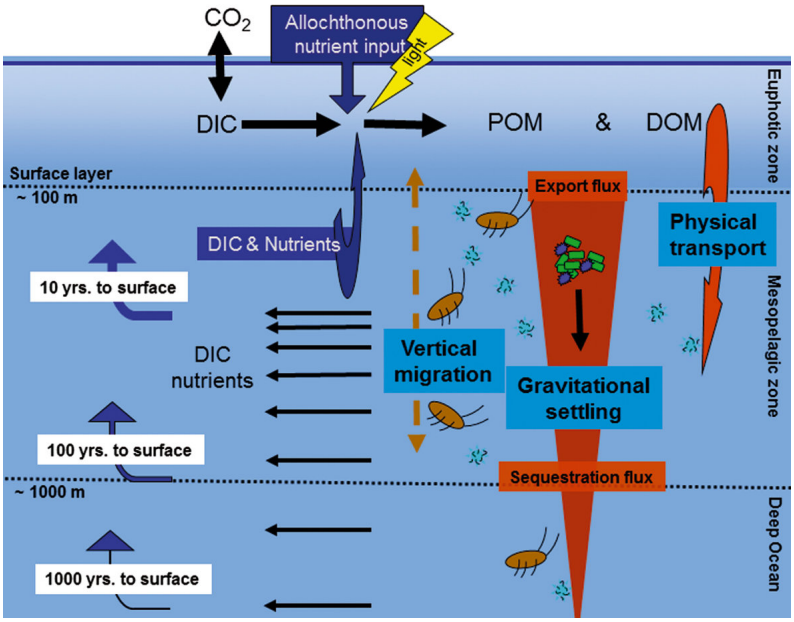

Figure 1.2: Schematic illustration of the BCP, adapted from Passow and Carlson (2012)

Current global estimates of the strength of the BCP vary significantly between 5 to >12 Gt C yr^{-1} (Falkowski, 1998; Boyd and Trull, 2007; Henson et al., 2011). This variability reflects our limited understanding of this important mechanism and results from differences in the methodological approaches used to quantifying the flux of organic carbon to depth. The latter can be estimated using a variety of different methods. These include direct measurements of particle fluxes with moored (Honjo et al., 1982; Lampitt and Antia, 1997; Karl et al., 2012) and neutrally buoyant sediment traps (Salter et al., 2007; Lampitt et al., 2008), or marine snow catchers (Riley et al., 2012; Belcher et al., 2017), and indirect estimates based on e.g. measurements of radioisotopes (Buesseler, 1998; van der Loeff et al., 2006; Le Moigne et al., 2013; Le Moigne et al., 2013a), nutrient uptake (Eppley and Peterson, 1979; Sanders et al., 2005), or oxygen utilization (Jenkins, 1982). Due to the fact that *in situ* estimates of particle export are logistically and financially demanding, only a sparse set of *in situ* data is available. The spatial and temporal coverage of these data is therefore rather limited. Ultimately, a key objective in BCP research is thus the estimation of export using correlations with parameters that can be

measured globally, e.g. via remote sensing (Siegel et al., 2016).
One of the first algorithms estimating global carbon export was published in the late 1970s by Eppley and Peterson (1979). This algorithm was built upon earlier work by Dugdale and Goering (1967) who defined total primary production (PP) as the sum of new production (NP) and regenerated production (RP). Based on these finding, Eppley and Peterson (1979) concluded that over sufficiently large scales of time and space, EP equals NP. The authors summarized this relation in the f-ratio:

$$f-\text{ratio} = \frac{\text{NP}}{\text{NP} + \text{RP}} \tag{1.1}$$

First applications of this algorithm resulted in comparably high estimates of global carbon export of approx. 21 Gt C yr^{-1} (Eppley and Peterson, 1979). This concept was subsequently adopted to include flux measurements from shallow sediment traps, resulting in the export ratio (Downs, 1989; Laws et al., 2000):

$$e-\text{ratio} = \frac{\text{EP}}{\text{PP}} \tag{1.2}$$

where EP was commonly measured at either 100m or the base of the euphotic zone. Using the linear relationship between the e-ratio and sea surface temperature (SST), Laws et al. (2000) re-estimated the global carbon export at 12 Gt C yr^{-1}. Another approach uses the difference in particle reactivity of radioisotopes and their decay products to quantify shallow POC export (Buesseler et al., 1992; van der Loeff et al., 2006; Le Moigne et al., 2013; Le Moigne et al., 2013a). Using this method in combination with ship-based new production measurements, the *ThE* ratio, named after the most commonly used isotopic tracer ^{234}Th, introduced by Buesseler (1998):

$$ThE\ \text{ratio} = \frac{\text{EP}}{\text{PP}} \tag{1.3}$$

where EP is determined based on the disequilibrium between the particle-reactive isotope ^{234}Th and its conservative mother atom ^{238}U. By combining the global database of particle flux measurements based on the thorium method and satellite derived PP and SST, Henson et al. (2011) estimated global carbon export at a much lower rate of 5 Gt C yr^{-1}. The wide range in global estimates of the strength of the BCP may partially be explained by uncertainties specific for each approach. For instance, the thorium method relies on the ratio between POC:^{234}Th, which varies regionally, with depth and depending on the sampling method (Buesseler et al., 2006). However, the most striking problem is that all global estimates are validated based on a small set of *in situ* flux measurements, with the assumption that these are representative for the entire oceanic realm and seasonal cycle. Furthermore, the relationship between PP and carbon export is more variable than previously assumed and current models fail to incorporate the needed complexity of the processes involved (Maiti et al., 2013; Le Moigne et al., 2016).
In order to reliably predict the strength of the BCP, it is thus important to 1) expand current *in situ* data sets of particle export, spanning over entire seasonal cycles and in regions that have so far been neglected, and 2) develop a complete and mechanistic understanding of processes driving the observed spatial and temporal variability in measurements of the BCP. This thesis will put emphasis on the latter.

1.3 What controls the efficiency of the BCP?

Particles formed in the surface ocean are major carriers of carbon to depth. During their gravitational sinking, these particles serve as an important microhabitat for heterotrophic life and are also subject to physical and chemical transformation processes. Due to these processes, a large fraction of the sinking particles is respired already in the surface ocean and the twilight zone, i.e. the mesopelagic below the euphotic zone and above the WML. Deep-moored and free-floating sediment traps were deployed in the North East Pacific Ocean during several international projects (e.g. VERTEX, JGOFS) in order to quantify this attenuation of particle flux. The resulting *in situ* POC profiles gave a first indication that flux attenuation is strongest in the surface and subsurface, while it decreases significantly with depth. Based on these data, Martin et al. (1987) developed an empirical equation of the flux attenuation, commonly known as the "Martin curve":

$$F_z = F_{z_0} * (\frac{z}{z_0})^{-b} \tag{1.4}$$

where F_z is the POC flux at depth z, F_{z_0} is the POC flux at any given reference depth z_0 and b is a coefficient describing the flux attenuation. Based on their deep sediment trap flux data, the authors calculated a single value for b (b=0.858), which was widely applied to predict carbon fluxes in the subsequent years. It has since been shown that flux attenuation is subject to spatial and temporal variability and that the parameterization with a single flux attenuation coefficient (b) does not account for this variability (Henson et al., 2012; Marsay et al., 2015). For instance, b values measured in the North Pacific range between 0.51 to 1.3 (Buesseler et al., 2007b), while measurements in the subtropical North Atlantic gyre and north-east Atlantic show b values of 0.83 (Helmke et al., 2010) and 1.7 (Lampitt et al., 2008), respectively. Understanding the mechanisms that control the flux attenuation has thus been a key objective in the post-JGOFS era. Ultimately, the magnitude of flux attenuation determines how much carbon is lost during the sinking process and therefore also determines the efficiency of the BCP. In principle, two main factors control the flux attenuation with depth: (1) the speed at which the produced organic matter sinks to depth, and (2) the degradation rate of sinking POC. Sinking velocity and remineralization rates, in turn, are controlled by a large variety of factors, which differ in their contribution with depth and on a regional and seasonal scale. These factors will be addressed in the following sections.

1.3.1 Aggregation and repackaging processes

Particle size has a paramount influence on sinking velocities and remineralization rates (Alldredge and Gotschalk, 1988; Ploug and Grossart, 2000). Hence, the formation of particles in the surface ocean is an important first step in the BCP. This formation of sinking particles is mediated by two independent pathways: The physical coagulation by marine phytoplankton and small particles (Jackson, 1990; Kiørboe et al., 1990), as well as biotic repackaging of organic matter into fecal pellets by grazers (Bishop et al., 1978; Turner, 2002).

The formation of particles by coagulation has been studied both *in situ* and to a large extent in laboratory experiments (Kiørboe et al., 1990; Kiørboe and Hansen, 1993; Engel,

2000). In principle, differences in turbulence shear and sinking velocity result in random collision of phytoplankton cells and particles. The collision rate and thus the potential for aggregation is enhanced when cell or particle abundance is large (e.g. during phytoplankton blooms; Logan et al. (1995)) and during periods of increased turbulence (e.g. wind or wave forcing). However, the coagulation of cells and particles also depends on whether they stick together upon collision (i.e. "stickiness" = coagulation efficiency (Jackson, 1990; Kiørboe et al., 1990)). The latter is largely controlled by the presence of particulate polysaccharides (Alldredge et al., 1993; Passow et al., 1994). These transparent exopolymer particles (TEPs) are very adhesive and often produced in large quantities during the end of phytoplankton blooms (Engel, 2000). Aggregate formation promoted by TEPs is commonly observed towards the end of phytoplankton blooms, particularly in diatoms with particle sizes among the largest reported in the marine realm. These loosely packed aggregates, or "marine snow", can reach diameters of several millimetres and are known to substantially contribute to surface export at high latitudes (Boyd and Newton, 1995; Martin et al., 2011).

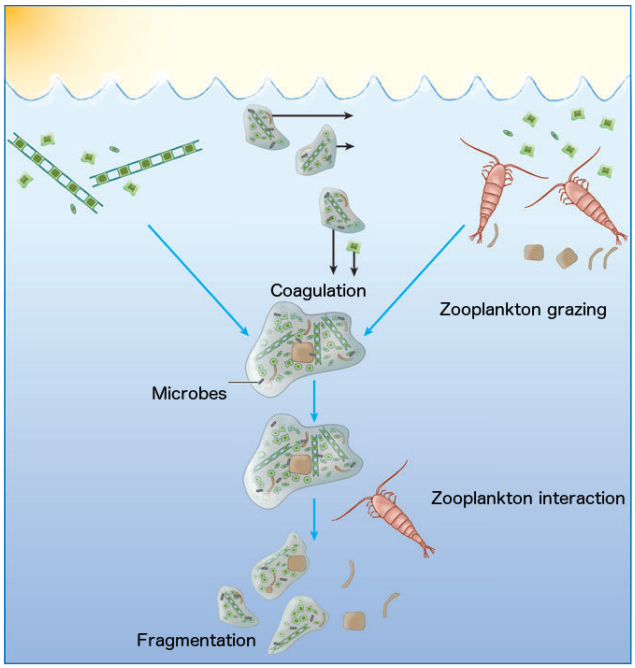

Figure 1.3: Schematic representation of processes governing the aggregation and disaggregation in the surface and subsurface ocean. Figure adapted from Burd and Jackson (2009)

The other pathway controlling particle formation in the surface ocean is packaging by zooplankton grazers. This process describes the ingestion of single cells or small particles and subsequent excretion in the form of aggregated fecal matter. Density and size of these pellets differs significantly among zooplankton groups and ranges from loosely packed, small "minipellets", mainly produced by heterotrophic dinoflagellates, ciliates and radiolarians (Gowing and Silver, 1985), up to elongated, densely packed pellets from large copepods and salps (Gleiber et al., 2012). The particularly high density of these pellets accelerates sinking speeds, which renders them an important player in the BCP (Turner, 2002).

However, zooplankton grazing on particles can also enhance fragmentation (Fig. 1.3), which in turn decreases the size and sinking velocity of those particles and may accelerate the substrate turnover in the upper mixed layer (Dilling and Alldredge, 2000; Iversen and Poulsen, 2007). Overall, our understanding of the processes that promote particle formation has increased over the past years (reviewed by Lam and Marchal (2015)). However, there are still numerous uncertainties, such as the observed aggregation without the facilitation of TEP or disaggregation with depth that need to be addressed in order to successfully parameterize these processes for biogeochemical models (Burd and Jackson, 2009).

1.3.2 The ballast hypothesis

While the formation of particles is primarily associated with surface ocean processes, repackaging by zooplankton (as described in the previous section) and mineral ballasting occur throughout the entire water column. The importance of ballast minerals in particle export has been heavily debated over the past two decades. This debate was initiated by the formulation of the "ballast ratio hypothesis" (Armstrong et al., 2009), suggesting that deep POC flux is determined by its association with ballast minerals, i.e. opal, $CaCO_3$ and lithogenic material. This hypothesis was based on the observation that POC and ballast minerals are strongly correlated in deep sediment traps (Armstrong et al., 2002). The authors concluded that this correlation is most likely due to a reduction in remineralization of mineral associated organic matter as well as a positive effect of minerals on sinking velocity of particles. Within the same year, two more studies specified this correlation showing that of the three dominant ballast minerals (i.e. $CaCO_3$, opal and lithogenic material) $CaCO_3$ exerts the dominant control on determining deep POC export (Francois et al., 2002; Klaas and Archer, 2002).
Another theory hypothesizes an inverse interpretation of the ballast ratio hypothesis, i.e. the flux of POC to depth determines ballast mineral fluxes and not vice versa (Passow, 2004; Passow and De La Rocha, 2006). This theory is based on the assumption that large, sticky particles needed to agglutinate ballast minerals are limiting in the surface and therefore the component that control export of ballast (De La Rocha and Passow, 2007). Furthermore, the authors found that artificially formed aggregates show increased fragmentation under increasing mineral load, which resulted in a reduction in particle size and thus slower sinking. These findings suggest that the effect of ballast minerals on the sinking velocity of particles can both be positive (increase in density) and negative (enhanced fragmentation) and is thus not straightforward (Hamm, 2002).
A theory that arose as part of the "ballast ratio hypothesis" stated that ballast minerals may exert a protective effect in sinking particulate matter against degradation processes (Armstrong et al., 2002; Engel et al., 2009). This theory was tested extensively in the laboratory and while particle sinking velocities increased substantially with mineral load, carbon-specific respiration rates did not change significantly (Ploug et al., 2008b,a; Iversen and Ploug, 2010). Contrastingly, Le Moigne et al. (2013b) observed a decrease in microzooplankton grazing on particles with increasing concentration of $CaCO_3$. There is currently no general consent on whether a protective effect of minerals may occur in the field. It has further been highlighted that the global correlations of ballasting minerals and POC at depth may be an artifact of spatial averaging and vary regionally as well as

over the course of the seasonal cycle (Passow and De La Rocha, 2006; Boyd and Trull, 2007). Using geographically weighted regression analysis, Wilson et al. (2012) confirmed that carrying coefficients of all three ballasting minerals are subject to substantial spatial variability. The authors concluded that a simple and globally applicable ballasting control on deep POC export does not exist and that, instead, pelagic ecosystem characteristics specific for certain biogeochemical provinces may be a more likely cause for the observed correlations in sediment trap records.
This conclusion is in agreement with several other studies who hypothesize that POC T_{eff} is not primarily dependent on ballasting minerals, but on upper ocean ecosystem structure (Francois et al., 2002; Lam and Bishop, 2007; Lam et al., 2011; Henson et al., 2012). In particular, these authors argue that regions with low seasonality, i.e. low latitudes, are characterized by low export, but high transfer efficiencies, compared to regions with high seasonality, where the opposite is observed. This theory builds on the premise that the complex food webs in regenerative systems export rather refractory organic matter, whereas the short food webs, characteristic for high latitudes, export labile, easy degradable matter.

1.3.3 Degradation processes and diel vertical migration (DVM) of zooplankton

The majority of POC degradation takes place in the upper ocean with substantial spatial variability (Suess, 1980; Martin et al., 1987; Buesseler et al., 2007a). Sinking aggregates are known to be hot spots for bacterial activity (Alldredge et al., 1986; Aristegui et al., 2009). Part of the sinking organic matter is solubilized by ecto-enzymatic hydrolysis of particle-attached bacteria (Karner and Herndl, 1992; Smith et al., 1992) and released in the form of DOM. The latter is then respired by free-living microbes (Cho and Azam, 1988; Ploug et al., 1999).
Another important process influencing the degradation of sinking POC is the fragmentation and respiration of particles by zooplankton [Lampitt et al., 1993; Steinberg, 1995; Kiørboe, 2000]. Similar to bacteria, zooplankton abundance is often much higher within and in close proximity to aggregates [Green and Dagg, 1997]. In addition to repackaging of particles into fecal pellets and the removal of sinking POC through respiration, zooplankton also influence the vertical transport of carbon by diel vertical migration (DVM). A first attempt in constructing a carbon budget of the twilight zone showed that mesopelagic POC flux was not sufficient to cover the carbon demand of bacteria and zooplankton at two contrasting stations in the Pacific Ocean [Steinberg et al., 2008]. The authors hypothesized that the required carbon is consumed by zooplankton in the surface and subsequently supplied to the mesopelagic through DVM. This has been recently revised by Giering et al. [2014] who found that 70-92% of respiration in the twilight zone is contributed by prokaryotes due to a tight synergy with zooplankton that feed on fast-sinking particles and thereby providing an otherwise unavailable source of carbon. Overall, we are just starting to understand the complex processes in the twilight zone and in particular the relative importance of bacterial and zooplankton-mediated degradation of sinking POC.

1.4 How to study the influence of plankton community structure on export relevant parameters?

Over the last two decades it has become evident that understanding how changes in plankton community structure may affect the efficiency of the BCP is an emerging field with a lot of potential for future research. Without a mechanistic understanding of this relationship, we will not be able to make accurate prediction on how the efficiency of carbon export to depth may change in the future. This is particularly important in consideration of the fact that ocean ecosystems are already affected by climate change.

1.4.1 Ocean acidification effects on plankton communities

Since the industrial revolution in the late 19th century, anthropogenic carbon emissions have gradually increased leading to atmospheric CO_2 concentrations, unprecedented in the recent geological history of the earth (Falkowski et al., 2000). As outlined above, the oceans function as a major sink for atmospheric CO_2 and thus play a crucial role in mitigating the effect of the increasing anthropogenic CO_2 emissions. Within the scope of this thesis, emphasize is put on the effects of ocean acidification (OA) on plankton community structure and how changes in the latter may effect the efficiency of the BCP. Upon dissolving in seawater, atmospheric CO_2 reacts with water molecules and forms a weak acid (H_2CO_3). This carbonic acid dissociates into hydrogen ions and bicarbonate resulting in a reduction of seawater pH and carbonate ion concentration. So far, our understanding of potential consequences of OA for marine organisms is primarily based on short-term, small volume incubations in the laboratory. Such experiments are invaluable, as the controlled environment allows for investigating direct physiological responses of single species or strains to OA. Over the last decade, we have thus improved our understanding on which groups may be more or less susceptible to future ocean conditions. Unfortunately, the acquired knowledge on the species level can often not be transferred to the community level where trophic interactions and competition are important factors (Riebesell and Gattuso, 2015).

1.4.2 Mesocosms: A tool to study the relation of changes in community structure and export relevant parameters

Studies on entire plankton communities under close-to-natural conditions are one important step towards reliable prediction of OA effects on marine ecosystems and biogeochemical cycles. Such studies are inherently challenging, as they require a sophisticated infrastructure and manpower, financial support and numerous participation of scientists with different expertise. Large-scale *in situ* mesocosms have proven to be a useful platform in this regard and a series of whole-community studies has already been conducted (Riebesell et al., 2013; Schulz et al., 2013; Paul et al., 2015; Bach et al., 2016a; Gazeau et al., 2016). While results from those studies are quite variable, it is evident that OA has the potential to alter the plankton community structure, which in turn affects biogeochemical element cycling (Knapp et al., 2016; Paul et al., 2015; Bach et al., 2016a; Hornick et al., 2017).

Mesocosms also offer great potential to study the relation between OA induced changes in community structure and export parameters, since working in a closed system eliminates the problem of lateral advection and allows for a clear assignment of sinking POM to the community it originates from. In a recent large scale mesocosm experiment, Bach et al. (2016b) investigated how changes in plankton community structure may influence the sinking velocity of sinking particulate matter. The authors found that the accelerating effect of ballasting minerals on sinking velocity was compensated by increasing particle porosity during a diatom bloom. Furthermore, they observed that communities dominated by picophytoplankton produced particles with overall lower porosity, leading to increasing particle sinking speeds. These results further strengthen the hypothesis that community structure exerts a major control on export efficiency, guiding the direction for future research.

1.5 Motivation of this work and thesis outline

Accurate predictions of the strength of the biological carbon pump require a thorough understanding of the processes controlling the flux attenuation with depth. The past decades have shown that without this mechanistic understanding, estimates will solely rely on a scarce set of observations, which in turn are heavily dependent on sampling time and location. Based on a growing body of evidence, several paradigms in BCP research were challenged and have to be re-evaluated. There is growing consensus in the community that carbon export is in fact closely coupled with the plankton community structure, involving community composition, trophic interactions and competition. However, finding export relevant patterns in this complex network is challenging and requires new methodological approaches.

Large-volume *in situ* mesocosm experiments have proven to be a useful tool in studying changes in plankton community structure and consequences for biogeochemical element cycling. The main goal of this thesis was to take advantage of this platform, monitoring changes in community structure and how these influence export relevant parameters over the course of the productive cycle.

1.5.1 Research focus of first-author publications

Within the scope of this doctoral dissertation, three first-author publications were prepared and are presented in the following chapters. In this section, an overview is given on the research focus of each publication and the contribution of the individual co-authors.

Publication I:
1) Investigating the relation between plankton community structure and the time lag between organic matter production and sedimentation.
2) Determining whether the range in time lag exceeds the integration time of conventional field methods.
3) Evaluating potential consequences for *e*-ratio estimates.

Publication II:
1) Evaluating how changes in the plankton community structure induced by OA and/or an artificial upwelling event, may influence the degradation of sinking POM.
2) Investigating the main drivers of this relation and how they change over the course of an *in situ* mesocosm experiment.

Publication III:
1) Identifying the key processes controling particle sinking velocity and carbon-specific respiration rates in the framework of an *in situ* mesocosm experiment.
2) Assessing how changes in plankton community structure may affect deep carbon export and whether current concepts in BCP research can be confirmed.

1.5.2 Declaration of contribution

Publication I:
Idea: Frederic Le Moigne
Analysis of data: Paul Stange
Preparation of manuscript: Paul Stange with comments from co-authors

Publication II:
Idea: Ulf Riebesell, Jan Taucher, Paul Stange
Experimental work: Paul Stange, Luana Krebs, Maria Alguéro-Muñiz, Henriette Horn, Jan Taucher, Alice Nauendorf
Analysis of data: Paul Stange
Preparation of manuscript: Paul Stange with comments from co-authors

Publication III:
Idea: Ulf Riebesell, Lennart Bach, Paul Stange
Experimental work: Paul Stange, Luana Krebs, Jan Taucher
Analysis of data: Paul Stange
Preparation of manuscript: Paul Stange with comments from co-authors

1.6 List of first-author publications

Publication I:
Stange, P., Bach, L.T., Le Moigne, F.A.C., Taucher, J., Boxhammer, T., and Riebesell, U.: Quantifying the time lag between organic matter production and export in the surface ocean: Implications for estimates of export efficiency. *Geophysical Research Letters*, 44, 268-276, 2017.

Publication II:
Stange, P., Taucher, J., Bach, L. T., Algueró-Muñiz, M., Horn, H. G., Krebs, L., Boxhammer, T., Nauendorf, A., and Riebesell, U.: Ocean acidification-induced restructuring of the plankton food web can influence the degradation of sinking particles. *Frontiers in Marine Sciences*, submitted.

Publication III:
Stange, P., Bach, L.T., Taucher, J., Achterberg, E.P., and Riebesell, U.: The influence of plankton community structure on particle sinking velocity and respiration rates. In preparation.

References

Alldredge, A. L., Cole, J. J., Caron, D. A., 1986. Production of heterotrophic bacteria inhabiting macroscopic organic aggregates (marine snow) from surface waters. *Limnology and Oceanography* 31 (1), 68–78.

Alldredge, A. L., Gotschalk, C., 1988. *In situ* settling behavior of marine snow. *Limnology and Oceanography* 33 (3), 339–351.

Alldredge, A. L., Passow, U., Logan, B. E., 1993. The abundance and significance of a class of large, transparent organic particles in the ocean. *Deep Sea Research Part I: Oceanographic Research Papers* 40 (6), 1131–1140.

Aristegui, J., Gasol, J. M., Duarte, C. M., Herndl, G. J., 2009. Microbial oceanography of the dark ocean's pelagic realm. *Limnology and Oceanography* 54 (5), 1501–1529.

Armstrong, R. A., Lee, C., Hedges, J. I., Honjo, S., Wakeham, S. G., 2002. A new, mechanistic model for organic carbon fluxes in the ocean based on the quantitative association of POC with ballast minerals. Deep-Sea Research Part II: Topical Studies in Oceanography 49, 219–236.

Armstrong, R. A., Peterson, M. L., Lee, C., Wakeham, S. G., 2009. Settling velocity spectra and the ballast ratio hypothesis. *Deep Sea Research Part II: Topical Studies in Oceanography* 56 (18), 1470–1478.

Bach, L. T., Boxhammer, T., Larsen, A., Hildebrandt, N., Schulz, K. G., Riebesell, U., 2016a. Influence of plankton community structure on the sinking velocity of marine aggregates. *Global Biogeochemical Cycles* , 1–21.

Bach, L. T., Taucher, J., Boxhammer, T., Ludwig, A., Achterberg, E. P., Algueró-Muñiz, M., Anderson, L. G., Bellworthy, J., Büdenbender, J., Czerny, J., Ericson, Y., Esposito, M., Fischer, M., Haunost, M., Hellemann, D., Horn, H. G., Hornick, T., Meyer, J., Sswat, M., Zark, M., Riebesell, U., 2016b. Influence of Ocean Acidification on a Natural Winter-to-Summer Plankton Succession: First Insights from a Long-Term Mesocosm Study Draw Attention to Periods of Low Nutrient Concentrations. *PloS One* 11 (8), e0159068.

Belcher, A., Manno, C., Ward, P., Henson, S. A., Sanders, R., Tarling, G. A., 2017. Copepod faecal pellet transfer through the meso- and bathypelagic layers in the Southern Ocean in spring. *Biogeosciences* 14 (6), 1511–1525.

Bishop, J. K., Ketten, D. R., Edmond, J. M., 1978. The chemistry, biology and vertical flux of particulate matter from the upper 400 m of the Cape Basin in the southeast Atlantic Ocean. Deep Sea Research 25 (12), 1121–1161.

Boyd, P., Newton, P., 1995. Evidence of the potential influence of planktonic community structure on the interannual variability of particulate organic carbon flux. *Deep Sea Research Part I: Oceanographic Research Papers* 42 (5), 619–639.

Boyd, P., Trull, T., 2007. Understanding the export of biogenic particles in oceanic waters: Is there consensus? *Progress in Oceanography* 72 (4), 276–312.

Buesseler, K., Benitez-Nelson, C., Moran, S., Burd, A., Charette, M., Cochran, J., Coppola, L., Fisher, N., Fowler, S., Gardner, W., Guo, L., Gustafsson, Ö., Lamborg, C., Masque, P., Miquel, J., Passow, U., Santschi, P., Savoye, N., Stewart, G., Trull, T., 2006. An assessment of particulate organic carbon to ^{234}Thorium ratios in the ocean and their impact on the application of ^{234}Th as a POC flux proxy. *Marine Chemistry* 100 (3-4), 213–233.

Buesseler, K. O., 1998. The decoupling of production and particulate export in the surface ocean. *Global Biogeochemical Cycles* 12 (2), 297.

Buesseler, K. O., Antia, A. N., Chen, M., Fowler, S. W., Gardner, W. D., Gustafsson, O., Harada, K., Michaels, A. F., Rutgers van der Loeff, M., Sarin, M., Steinberg, D. K., Trull, T., 2007a. An assessment of the use of sediment traps for estimating upper ocean particle fluxes. Journal of Marine Research 65 (3), 345–416.

Buesseler, K. O., Bacon, M. P., Kirk Cochran, J., Livingston, H. D., 1992. Carbon and nitrogen export during the JGOFS North Atlantic Bloom experiment estimated from ^{234}Th:^{238}U disequilibria. *Deep Sea Research Part A. Oceanographic Research Papers* 39 (7-8), 1115–1137.

Buesseler, K. O., Boyd, P. W., 2009. Shedding light on processes that control particle export and flux attenuation in the twilight zone of the open ocean. *Limnology and Oceanography* 54 (4), 1210–1232.

Buesseler, K. O., Lamborg, C. H., Boyd, P. W., Lam, P. J., Trull, T. W., Bidigare, R. R., Bishop, J. K. B., Casciotti, K. L., Dehairs, F., Elskens, M., Honda, M., Karl, D. M., Siegel, D. A., Silver, M. W., Steinberg, D. K., Valdes, J., Van Mooy, B., Wilson, S., 2007b. Revisiting Carbon Flux Through the Ocean's Twilight Zone. *Science* 316 (5824), 567–570.

Burd, A. B., Jackson, G. A., 2009. Particle Aggregation. *Annual Review of Marine Science* 1 (1), 65–90.

Carlson, C. A., Hansell, D. A., Nelson, N. B., Siegel, D. A., Smethie, W. M., Khatiwala, S., Meyers, M. M., Halewood, E., 2010. Dissolved organic carbon export and subsequent remineralization in the mesopelagic and bathypelagic realms of the North Atlantic basin. Deep-Sea Research Part II: Topical Studies in Oceanography 57 (16), 1433–1445.

Cho, B. C., Azam, F., 1988. Major role of bacteria in biogeochemical fluxes in the ocean's interior. *Nature* 332 (6163), 441–443.

De La Rocha, C. L., Passow, U., 2007. Factors influencing the sinking of POC and the efficiency of the biological carbon pump. *Deep Sea Research Part II: Topical Studies in Oceanography* 54 (5-7), 639–658.

Dilling, L., Alldredge, A. L., 2000. Fragmentation of marine snow by swimming macrozooplankton: A new process impacting carbon cycling in the sea. *Deep Sea Research Part I: Oceanographic Research Papers* 47 (7), 1227–1245.

Downs, J., 1989. Export of production in oceanic systems: information from phaeopigment carbon and nitrogen analyses. Ph.D. thesis, Univ. of Wash., Seattle.

Dugdale, R. C., Goering, J. J., 1967. Uptake of new and regenerated forms of nitrogen in primary productivity. *Limnology and Oceanography* 12, 196–206.

Engel, A., 2000. The role of transparent exopolymer particles (TEP) in the increase in apparent particle stickiness (alpha) during the decline of a diatom bloom. *Journal of Plankton Research* 22 (3), 485–497.

Engel, A., Abramson, L., Szlosek, J., Liu, Z., Stewart, G., Hirschberg, D., Lee, C., 2009. Investigating the effect of ballasting by CaCO3 in Emiliania huxleyi, II: Decomposition of particulate organic matter. *Deep Sea Research Part II: Topical Studies in Oceanography* 56 (18), 1408–1419.

Eppley, R. W., Peterson, B. J., 1979. Particulate organic matter flux and planktonic new production in the deep ocean. *Nature* 282, 677–680.

Falkowski, P., Scholes, R. J., Boyle, E., Canadell, J., Canfield, D., Elser, J., Gruber, N., Hibbard, K., Högberg, P., Linder, S., Mackenzie, F. T., Moore, B., Pedersen, T., Rosenthal, Y., Seitzinger, S., Smetacek, V., Steffen, W., 2000. The global carbon cycle: a test of our knowledge of earth as a system. *Science* 290 (October), 291–296.

Falkowski, P. G., 1998. Biogeochemical Controls and Feedbacks on Ocean Primary Production. *Science* 281, 200–206.

Field, C. B., 1998. Primary Production of the Biosphere: Integrating Terrestrial and Oceanic Components. *Science* 281 (5374), 237–240.

Francois, R., Honjo, S., Krishfield, R., Manganini, S., 2002. Factors controlling the flux of organic carbon to the bathypelagic zone of the ocean. *Global Biogeochemical Cycles* 16 (4), 34–1–34–20.

Gazeau, F., Sallon, A., Maugendre, L., Louis, J., Dellisanti, W., Gaubert, M., Lejeune, P., Gobert, S., Borges, A., Harlay, J., Champenois, W., Alliouane, S., Taillandier, V., Louis, F., Obolensky, G., Grisoni, J.-M., Guieu, C., 2016. First mesocosm experiments to study the impacts of ocean acidification on plankton communities in the NW Mediterranean Sea (MedSeA project). *Estuarine, Coastal and Shelf Science* 186, Part A, 11–29.

Gleiber, M., Steinberg, D., Ducklow, H., 2012. Time series of vertical flux of zooplankton fecal pellets on the continental shelf of the western Antarctic Peninsula. Marine Ecology Progress Series 471, 23–36.

Gowing, M. M., Silver, M. W., 1985. Minipellets: A new and abundant size class of marine fecal pellets. Journal of Marine Research 43 (2), 395–418.

Hamm, C. E., 2002. Interactive aggregation and sedimentation of diatoms and clay-sized lithogenic material. *Limnology and Oceanography* 47 (6), 1790–1795.

Hansell, D. A., Carlson, C. A., 1998. Net community production of dissolved organic carbon. *Global Biogeochemical Cycles* 12 (3), 443–453.

Helmke, P., Neuer, S., Lomas, M. W., Conte, M., Freudenthal, T., 2010. Cross-basin differences in particulate organic carbon export and flux attenuation in the subtropical North Atlantic gyre. *Deep Sea Research Part I: Oceanographic Research Papers* 57 (2), 213–227.

Henson, S. A., Sanders, R., Madsen, E., 2012. Global patterns in efficiency of particulate organic carbon export and transfer to the deep ocean. *Global Biogeochemical Cycles* 26 (1).

Henson, S. A., Sanders, R., Madsen, E., Morris, P. J., Le Moigne, F., Quartly, G. D., 2011. A reduced estimate of the strength of the ocean's biological carbon pump. *Geophysical Research Letters* 38 (4), 10–14.

Honjo, S., Manganini, S. J., Cole, J. J., 1982. Sedimentation of biogenic matter in the deep ocean. *Deep Sea Research Part A. Oceanographic Research Papers* 29 (5), 609–625.

Hopkinson, C. S., Vallino, J. J., 2005. Efficient export of carbon to the deep ocean through dissolved organic matter. *Nature* 433 (7022), 142–145.

Hornick, T., Bach, L. T., Crawfurd, K. J., Spilling, K., Achterberg, E. P., Woodhouse, J. N., Schulz, K. G., Brussaard, C. P. D., Riebesell, U., Grossart, H.-p., 2017. Ocean acidification impacts bacteria-phytoplankton coupling at low-nutrient conditions. *Biogeosciences* 14 (1), 1–15.

Iversen, M., Poulsen, L., 2007. Coprorhexy, coprophagy, and coprochaly in the copepods *Calanus helgolandicus*, *Pseudocalanus elongatus*, and *Oithona similis*. Marine Ecology Progress Series 350, 79–89.

Iversen, M. H., Ploug, H., 2010. Ballast minerals and the sinking carbon flux in the ocean: carbon-specific respiration rates and sinking velocity of marine snow aggregates. *Biogeosciences* 7 (9), 2613–2624.

Jackson, G. A., 1990. A model of the formation of marine algal flocs by physical coagulation processes. *Deep Sea Research Part A. Oceanographic Research Papers* 37 (8), 1197–1211.

Jenkins, W. J., 1982. Oxygen utilization rates in North Atlantic subtropical gyre and primary production in oligotrophic systems. *Nature* 300 (5889), 246–248.

Karl, D. M., Church, M. J., Dore, J. E., Letelier, R. M., Mahaffey, C., 2012. Predictable and efficient carbon sequestration in the North Pacific Ocean supported by symbiotic nitrogen fixation. *Proceedings of the National Academy of Sciences* 109 (6), 1842–1849.

Karner, M., Herndl, G. J., 1992. Extracellular enzymatic activity and secondary production in free-living and marine-snow-associated bacteria. Marine Biology 113 (2), 341–347.

Kiørboe, T., Andersen, K. P., Dam, H. G., 1990. Coagulation efficiency and aggregate formation in marine phytoplankton. Marine Biology 107 (2), 235–245.

Kiørboe, T., Hansen, J. L., 1993. Phytoplankton aggregate formation: observations of patterns and mechanisms of cell sticking and the significance of exopolymeric material. *Journal of Plankton Research* 15 (9), 993–1018.

Klaas, C., Archer, D., 2002. Association of sinking organic matter with various types of mineral ballast in the deep sea: Implications for the rain ratio. *Global Biogeochemical Cycles* 16 (4).

Knapp, A. N., Fawcett, S. E., Martínez-Garcia, A., Leblond, N., Moutin, T., Bonnet, S., 2016. Nitrogen isotopic evidence for a shift from nitrate- to diazotroph-fueled export production in the VAHINE mesocosm experiments. *Biogeosciences* 13 (16), 4645–4657.

Kwon, E. Y., Primeau, F., Sarmiento, J. L., 2009. The impact of remineralization depth on the air-sea carbon balance. *Nature Geoscience* 2 (9), 630–635.

Lam, P. J., Bishop, J. K. B., 2007. High biomass, low export regimes in the Southern Ocean. Deep-Sea Research Part II: Topical Studies in Oceanography 54, 601–638.

Lam, P. J., Doney, S. C., Bishop, J. K. B., 2011. The dynamic ocean biological pump: Insights from a global compilation of particulate organic carbon, $CaCO_3$, and opal concentration profiles from the mesopelagic. *Global Biogeochemical Cycles* 25 (3).

Lam, P. J., Marchal, O., 2015. Insights into particle cycling from thorium and particle data. *Annual Review of Marine Science* 7 (September 2014), 159–84.

Lampitt, R. S., Antia, a. N., 1997. Particle flux in deep seas: regional charactristics and temporal variability. *Deep Sea Research Part I: Oceanographic Research Papers* 44 (8), 1377–1403.

Lampitt, R. S., Boorman, B., Brown, L., Lucas, M., Salter, I., Sanders, R., Saw, K., Seeyave, S., Thomalla, S. J., Turnewitsch, R., 2008. Particle export from the euphotic zone: Estimates using a novel drifting sediment trap, ^{234}Th and new production. *Deep-Sea Research Part I: Oceanographic Research Papers* 55 (11), 1484–1502.

Laws, E. A., Falkowski, P. G., Smith, W. O., Ducklow, H., McCarthy, J. J., 2000. Temperature effects on export production in the open ocean. *Global Biogeochemical Cycles* 14 (4), 1231–1246.

Le Moigne, F. A. C., Gallinari, M., Laurenceau, E., De La Rocha, C. L., 2013a. Enhanced rates of particulate organic matter remineralization by microzooplankton are diminished by added ballast minerals. *Biogeosciences* 10 (9), 5755–5765.

Le Moigne, F. A. C., Henson, S. A., Cavan, E., Georges, C., Pabortsava, K., Achterberg, E. P., Ceballos-Romero, E., Zubkov, M., Sanders, R. J., 2016. What causes the inverse relationship between primary production and export efficiency in the Southern Ocean? *Geophysical Research Letters* 43 (9), 4457–4466.

Le Moigne, F. A. C., Henson, S. A., Sanders, R. J., Madsen, E., 2013b. Global database of surface ocean particulate organic carbon export fluxes diagnosed from the ^{234}Th technique. *Earth System Science Data* 5 (2), 295–304.

Le Moigne, F. A. C., Villa-Alfageme, M., Sanders, R., Marsay, C., Henson, S. A., García-Tenorio, R., 2013. Export of organic carbon and biominerals derived from 234Th and 210Po at the Porcupine Abyssal Plain. *Deep Sea Research Part I: Oceanographic Research Papers* 72, 88–101.

Logan, B. E., Passow, U., Alldredge, A. L., Grossartt, H.-P., Simont, M., 1995. Rapid formation and sedimentation of large aggregates is predictable from coagulation rates (half-lives) of transparent exopolymer particles (TEP). *Deep Sea Research Part II: Topical Studies in Oceanography* 42 (1), 203–214.

Maiti, K., Charette, M. A., Buesseler, K. O., Kahru, M., 2013. An inverse relationship between production and export efficiency in the Southern Ocean. *Geophysical Research Letters* 40 (8), 1557–1561.

Marsay, C. M., Sanders, R. J., Henson, S. a., Pabortsava, K., Achterberg, E. P., Lampitt, R. S., 2015. Attenuation of sinking particulate organic carbon flux through the mesopelagic ocean. *Proceedings of the National Academy of Sciences* 112 (4), 1089–1094.

Martin, J. H., Knauer, G. A., Karl, D. M., Broenkow, W. W., 1987. VERTEX: carbon cycling in the northeast Pacific. *Deep Sea Research Part A. Oceanographic Research Papers* 34 (2), 267–285.

Martin, P., Lampitt, R. S., Jane Perry, M., Sanders, R., Lee, C., D'Asaro, E., 2011. Export and mesopelagic particle flux during a North Atlantic spring diatom bloom. *Deep-Sea Research Part I: Oceanographic Research Papers* 58 (4), 338–349.

Passow, U., 2004. Switching perspectives: Do mineral fluxes determine particulate organic carbon fluxes or vice versa? Geochemistry, Geophysics, Geosystems 5 (4).

Passow, U., Alldredge, A. L., Logan, B. E., 1994. The role of particulate carbohydrate exudates in the flocculation of diatom blooms. *Deep Sea Research Part I: Oceanographic Research Papers* 41 (2), 335–357.

Passow, U., Carlson, C., 2012. The biological pump in a high CO2 world. Marine Ecology Progress Series 470 (2), 249–271.

Passow, U., De La Rocha, C. L., 2006. Accumulation of mineral ballast on organic aggregates. *Global Biogeochemical Cycles* 20 (1), 1–7.

Paul, A. J., Bach, L. T., Schulz, K. G., Boxhammer, T., Czerny, J., Achterberg, E. P., Hellemann, D., Trense, Y., Nausch, M., Sswat, M., Riebesell, U., 2015. Effect of elevated CO2 on organic matter pools and fluxes in a summer Baltic Sea plankton community. *Biogeosciences* 12 (20), 6181–6203.

Ploug, H., Grossart, H., Azam, F., Jørgensen, B., 1999. Photosynthesis, respiration, and carbon turnover in sinking marine snow from surface waters of Southern California Bight: Implications for the carbon cycle in the ocean. Marine Ecology Progress Series 179, 1–11.

Ploug, H., Grossart, H.-P., 2000. Bacterial growth and grazing on diatom aggregates: Respiratory carbon turnover as a function of aggregate size and sinking velocity. *Limnology and Oceanography* 45 (7), 1467–1475.

Ploug, H., Iversen, M. H., Fischer, G., 2008a. Ballast, sinking velocity, and apparent diffusivity within marine snow and zooplankton fecal pellets: Implications for substrate turnover by attached bacteria. *Limnology and Oceanography* 53 (5), 1878–1886.

Ploug, H., Iversen, M. H., Koski, M., Buitenhuis, E. T., 2008b. Production, oxygen respiration rates, and sinking velocity of copepod fecal pellets: Direct measurements of ballasting by opal and calcite. *Limnology and Oceanography* 53 (2), 469–476.

Riebesell, U., Czerny, J., von Bröckel, K., Boxhammer, T., Büdenbender, J., Deckelnick, M., Fischer, M., Hoffmann, D., Krug, S. A., Lentz, U., Ludwig, A., Muche, R., Schulz, K. G., 2013. Technical Note: A mobile sea-going mesocosm system - new opportunities for ocean change research. *Biogeosciences* 10 (3), 1835–1847.

Riebesell, U., Gattuso, J.-P., 2015. Lessons learned from ocean acidification research. *Nature* 5 (1), 12–14.

Riley, J. S., Sanders, R., Marsay, C., Le Moigne, F. A. C., Achterberg, E. P., Poulton, A. J., 2012. The relative contribution of fast and slow sinking particles to ocean carbon export. *Global Biogeochemical Cycles* 26 (1).

Salter, I., Lampitt, R. S., Sanders, R., Poulton, A., Kemp, A. E. S., Boorman, B., Saw, K., Pearce, R., 2007. Estimating carbon, silica and diatom export from a naturally fertilised phytoplankton bloom in the Southern Ocean using PELAGRA: A novel drifting sediment trap. Deep-Sea Research Part II: Topical Studies in Oceanography 54 (18-20), 2233–2259.

Sanders, R., Brown, L., Henson, S., Lucas, M., 2005. New production in the Irminger Basin during 2002. Journal of Marine Systems 55 (3-4), 291–310.

Schulz, K. G., Bellerby, R. G. J., Brussaard, C. P. D., Büdenbender, J., Czerny, J., Engel, A., Fischer, M., Koch-Klavsen, S., Krug, S. A., Lischka, S., Ludwig, A., Meyerhöfer, M., Nondal, G., Silyakova, A., Stuhr, A., Riebesell, U., 2013. Temporal biomass dynamics of an Arctic plankton bloom in response to increasing levels of atmospheric carbon dioxide. *Biogeosciences* 10 (1), 161–180.

Siegel, D. a., Buesseler, K. O., Behrenfeld, M. J., R, B.-N. C., Boss, E., Brzezinski, M. A., Burd, A., Carlson, C. A., DÂ´Asaro, E. A., Doney, S. C., Perry, M. J., Stanley, R. H., Steinberg, D. K., 2016. Prediction of the Export and Fate of Global Ocean Net Primary Production: The EXPORTS Science Plan. *Frontiers in Marine Science* 3 (22), 1–10.

Smith, D. C., Simon, M., Alldredge, A. L., Azam, F., 1992. Intense hydrolytic enzyme activity on marine aggregates and implications for rapid particle dissolution. *Nature* 359 (6391), 139–142.

Steinberg, D. K., Carlson, C. A., Bates, N. R., Goldthwait, S. A., Madin, L. P., Michaels, A. F., 2000. Zooplankton vertical migration and the active transport of dissolved organic and inorganic carbon in the Sargasso Sea. *Deep-Sea Research Part I: Oceanographic Research Papers* 47 (1), 137–158.

Suess, E., 1980. Particulate organic carbon flux in the oceans - surface productivity and oxygen utilization. *Nature* 288, 260–263.

Suzuki, N., Kato, K., 1953. Studies on suspended materials marine snow in the sea Part 1. Sources of marine snow. Bulletin of the Faculty of Fisheries of Hokkaido University 4, 132–135.

Toggweiler, J. R., Gnanadesikan, A., Carson, S., Murnane, R., Sarmiento, J. L., 2003a. Representation of the carbon cycle in box models and GCMs: 1. Solubility pump. *Global Biogeochemical Cycles* 17 (1).

Toggweiler, J. R., Murnane, R., Carson, S., Gnanadesikan, A., Sarmiento, J. L., 2003b. Representation of the carbon cycle in box models and GCMs, 2, Organic pump. *Global Biogeochemical Cycles* 17 (1), 1–10.

Turner, J. T., 2002. Zooplankton fecal pellets, marine snow and sinking phytoplankton blooms. Aquatic Microbial Ecology 27, 57–102.

van der Loeff, M. R., Sarin, M. M., Baskaran, M., Benitez-Nelson, C., Buesseler, K. O., Charette, M., Dai, M., Gustafsson, Ö., Masque, P., Morris, P. J., Orlandini, K., Rodriguez y Baena, A., Savoye, N., Schmidt, S., Turnewitsch, R., Vöge, I., Waples, J. T., 2006. A review of present techniques and methodological advances in analyzing ^{234}Th in aquatic systems. Marine Chemistry 100 (3-4), 190–212.

Volk, T., Hoffert, M. I., 1985. Ocean carbon pumps: Analysis of relative strengths and efficiencies in ocean-driven atmospheric CO_2 changes. In: Sundquist, E., Broecker, W. (Eds.), The Carbon Cycle and Atmospheric CO_2: Natural Variations Archean to Present. Vol. 32. American Geophysical Union, Washington, D. C., pp. 99–110.

Wilson, J. D., Barker, S., Ridgwell, A., 2012. Assessment of the spatial variability in particulate organic matter and mineral sinking fluxes in the ocean interior: Implications for the ballast hypothesis. *Global Biogeochemical Cycles* 26 (4).

2 — Manuscript I

Quantifying the time lag between organic matter production and export in the surface ocean: Implications for estimates of export efficiency.

Stange[1,*], P., **Bach**[1], L.T., **Le Moigne**[1], F.A.C., **Taucher**[1], J., **Boxhammer**[1], T., and **Riebesell**[1], U.

[1]Helmholtz Centre for Ocean Research Kiel (GEOMAR), Düsternbrooker Weg 20, 24105 Kiel, Germany
[*]corresponding author: pstange@geomar.de (P. Stange)

Geophysical Research Letters

AGU PUBLICATIONS

Geophysical Research Letters

RESEARCH LETTER
10.1002/2016GL070875

Key Points:
- We calculated time lags between peaks in chlorophyll a and organic matter sedimentation for four mesocosm studies in different regions
- Time lags varied between 2 to 15 days at the surface and increased with depth depending on sinking velocities
- Time lag correlated with chlorophyll *a* buildup rate, indicating a dependency of time lag on the plankton community structure

Supporting Information:
- Table S1

Correspondence to:
P. Stange,
pstange@geomar.de

Citation:
Stange, P., L. T. Bach, F. A. C. Le Moigne, J. Taucher, T. Boxhammer, and U. Riebesell (2017), Quantifying the time lag between organic matter production and export in the surface ocean: Implications for estimates of export efficiency, *Geophys. Res. Lett.*, *44*, 268–276, doi:10.1002/2016GL070875.

Received 17 AUG 2016
Accepted 16 DEC 2016
Accepted article online 17 DEC 2016
Published online 5 JAN 2017

Quantifying the time lag between organic matter production and export in the surface ocean: Implications for estimates of export efficiency

P. Stange[1], L. T. Bach[1], F. A. C. Le Moigne[1], J. Taucher[1], T. Boxhammer[1], and U. Riebesell[1]

[1]GEOMAR Helmholtz Centre for Ocean Research Kiel, Kiel, Germany

Abstract The ocean's potential to export carbon to depth partly depends on the fraction of primary production (PP) sinking out of the euphotic zone (i.e., the *e*-ratio). Measurements of PP and export flux are often performed simultaneously in the field, although there is a temporal delay between those parameters. Thus, resulting *e*-ratio estimates often incorrectly assume an instantaneous downward export of PP to export flux. Evaluating results from four mesocosm studies, we find that peaks in organic matter sedimentation lag chlorophyll *a* peaks by 2 to 15 days. We discuss the implications of these time lags (TLs) for current *e*-ratio estimates and evaluate potential controls of TL. Our analysis reveals a strong correlation between TL and the duration of chlorophyll *a* buildup, indicating a dependency of TL on plankton food web dynamics. This study is one step further toward time-corrected *e*-ratio estimates.

1. Introduction

About 50 Pg of carbon are fixed into organic matter (OM) by marine phytoplankton in the surface ocean every year [*Field*, 1998]. The majority of this OM is rapidly remineralized in the surface ocean, and only 5 to 12 Pg C per year are exported out of the euphotic zone [*Siegel et al.*, 2016], mainly in the form of sinking particles. The fraction of OM leaving the euphotic zone is increased by several processes, such as physically and biotically mediated particle aggregation [*Burd and Jackson*, 2009], as well as scavenging of ballasting minerals [*Armstrong et al.*, 2002; *Francois et al.*, 2002; *Klaas and Archer*, 2002]. However, particle reprocessing usually lasts hours to days. Thus, sinking OM reaches the bottom of the euphotic zone "long" after its formation in the surface and may take much longer to eventually reach the seafloor [*Deuser*, 1986]. Quantifying this time lag (TL) is challenging, as it requires tracing of OM from its production in the surface to the collection at depth.

Using outputs from a global biogeochemical model, *Henson et al.* [2015] recently calculated that the TL varies substantially throughout the oceans, with generally longer TLs at high compared to low latitudes. This variability was attributed to differences in seasonality. High latitudes are characterized by pulsed biomass formation during spring and late summer, commonly driven by large phytoplankton such as diatoms [*Martin et al.*, 2011]. The time it takes for single cells to aggregate into sinking particles results in delayed export fluxes. This delay can be intensified by a mismatch between phytoplankton and zooplankton due to the lag of repackaging into fecal pellets [*Lam and Bishop*, 2007; *Lam et al.*, 2011]. In contrast, at low latitudes shorter TLs may result from more constant primary production throughout the year and a tighter coupling between phytoplankton production and zooplankton grazing [*Henson et al.*, 2015].

Due to the scarcity of available time series data in large parts of the ocean, export flux and primary production (PP) are commonly measured during ship-based expeditions. However, due to logistic constraints these measurements are often conducted simultaneously, neglecting lateral advection and TL and thereby connecting PP values to collected organic matter that may have a different origin (Figure 1).

PP is commonly measured using ^{14}C or ^{18}O incubations [*Nielsen*, 1952; *Bender et al.*, 1987], fast repetition rate fluorometry, or O_2:Ar ratios [*Kolber and Falkowski*, 1992; *Kolber et al.*, 1998; *Martin et al.*, 2013]; all of which integrate over very short time scales of a few hours to 1 day. Export flux, however, is either directly measured with sediment traps or marine snow catchers [*Knauer et al.*, 1979; *Riley et al.*, 2012] or estimated from particle reactive radionuclides (e.g., ^{234}Th and ^{210}Po) [*Buesseler et al.*, 1992; *Cochran and Masqué*, 2003; *Le Moigne et al.*, 2013a]. These measurements integrate export flux over a few hours up to months [*Le Moigne et al.*, 2013b].

AGU Geophysical Research Letters 10.1002/2016GL070875

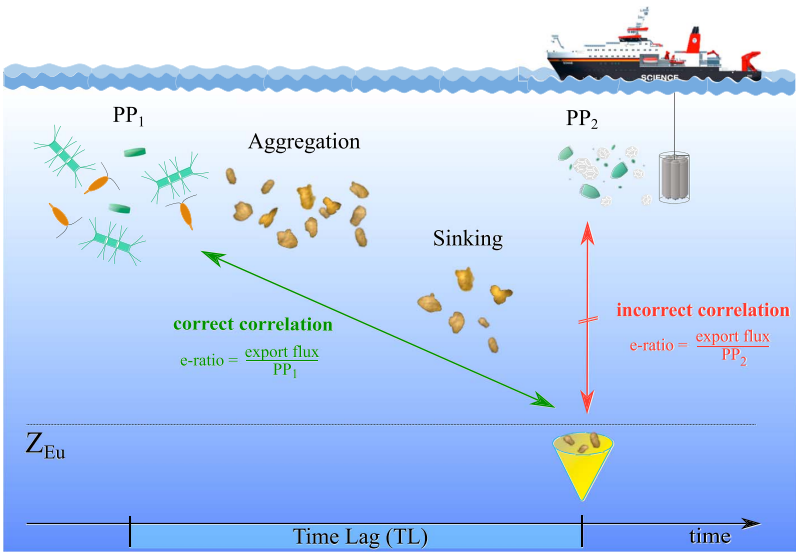

Figure 1. Conceptual figure illustrating the problem of in situ estimation of the export efficiency. Export flux is commonly correlated with simultaneous measurements of primary production (PP_2), which delivers incorrect *e*-ratio estimates (red). In order to correctly estimate the export efficiency of the system, collected material at depth has to be related to the primary production measurements conducted at the time of its production in the surface (PP_1). Accurate *e*-ratio estimates (green) thus have to account for both the time lag (TL) between PP and organic matter collection at depth and lateral advection of the latter on its way through the water column. This study emphasizes the importance of TL in *e*-ratio estimates and shows its range over different study sites.

Such *in situ* measurements of PP and export flux are subsequently used to estimate the efficiency with which organic carbon is exported from the euphotic zone, also referred to as export- or *e*-ratio:

$$e\text{-ratio} = \frac{\text{export flux}}{\text{PP}} \quad (1)$$

The *e*-ratio is thus based on the assumption that the material collected at depth originates from the measured surface PP. However, this is not necessarily the case when measurements are done simultaneously and integration time scales are insufficiently long (Figure 1). Accordingly, impossible *e*-ratio estimates greater than 1 [*Le Moigne et al.*, 2015] are commonly observed when neglecting TL. Lateral advection of organic matter is another factor that should also be taken into account but is not addressed in this study. The *e*-ratios will only provide the actual export efficiency of a system if the OM collected at export depth is traced back to the surface PP it originates from.

In this study we evaluated water column chlorophyll *a* concentrations and sedimentation of organic matter over time from four *in situ* mesocosm studies [*Riebesell et al.*, 2013] conducted in arctic (Kongsfjord, Svalbard), temperate (Gullmar Fjord, Sweden and Raunefjord, Norway), and subtropical regions (Gando Bay, Gran Canaria). We aimed to quantify the time it takes from peak surface production to peak sedimentation of sinking particles. Further, we assess potential controls that may drive differences in TL among the different study sites.

2. Methods

2.1. Experimental Design

In order to quantify TL we used the results of four mesocosm campaigns conducted between 2010 and 2014. All of these experiments focused on the effects of ocean acidification on plankton communities; however, we only included untreated (control) mesocosms in the analysis here. The four studies were conducted in Kongsfjord (Svalbard; 78.93667°N, 11.89333°E), Raunefjord (Norway; 60.265°N, 5.205°E), Gullmar Fjord

AGU Geophysical Research Letters 10.1002/2016GL070875

(Sweden; 58.26635°N, 11.47832°E), and Gando Bay (Gran Canaria, Spain; 27.92798°N, 15.36540°W). Further information on each experiment is given in Table S1 in the supporting information, and detailed descriptions regarding the experimental design are provided by *Schulz et al.* [2013] and *Bach et al.* [2016a, 2016b]. Experiments are henceforth referred to as SB_{2010}, N_{2011}, S_{2013}, and GC_{2014} as specified in Table S1.

The Kiel Off-Shore Mesocosms for Future Ocean Simulations (KOSMOS) were used in all of the experiments, which consist of a cylindrical polyurethane bag mounted in an 8 m long flotation frame [*Riebesell et al.*, 2013]. The bag ends in a 2 m long conical sediment trap with a collection cylinder attached to it [*Boxhammer et al.*, 2016]. The bottom of the cylinder is connected to the sea surface via a silicon tube that is used for vacuum sampling of sedimented matter. The sediment trap attachment to the mesocosm bags has been modified between SB_{2010} and N_{2011}, which did, however, not influence the trapping efficiency [*Riebesell et al.*, 2013]. Mesocosm lengths differed between experiments, ranging from 25 m in N_{2011} to 15 m in GC_{2014} (Table S1). Mesocosms were deployed following a similar protocol in each experiment as described by *Schulz et al.* [2013]. Temperature was measured with a hand-operated conductivity-temperature-depth (Sea and Sun Technology). Depth- and time-averaged temperatures for each campaign are given in Table S1.

2.2. Analysis of Surface Production

Samples for phytoplankton chlorophyll *a* (Chl *a*) analysis were taken every day (N_{2011}) or every other day (SB_{2010}, S_{2013}, and GC_{2014}) with an integrating water sampler (HydroBios), which automatically collects equal amounts of volume at each depth. Chl *a* samples were filtered on GF/F filters and immediately frozen at −80°C (described in detail by *Paul et al.* [2015]). Chl *a* concentrations were determined by reverse-phase high-performance liquid chromatography (HPLC). Filters from SB_{2010} and N_{2011} were analyzed using a WATERS HPLC with a Varian Microsorb-MV 100-3 C8 column [*Barlow et al.*, 1997], while filters from S_{2013} and GC_{2014} were analyzed with a Thermo Scientific HPLC Ultimate 3000 with an Eclipse XDB-C8 3.5 u 4.6 × 150 column [*Van Heukelem and Thomas*, 2001].

2.3. Sedimenting Organic Matter

Sediment trap samples were collected every other day, except for N_{2011}, where sampling was conducted daily following the methodology detailed in *Boxhammer et al.* [2016]. Briefly, samples were vacuum-pumped to the sea surface through a tube reaching down to the bottom of the collection cylinder of the sediment trap. The dense particle suspension was collected in 5 L glass bottles and transported unpoisoned to the land-based facilities within 1–3 h after collection. During GC_{2014}, samples were stored in large coolers (Coleman) throughout the sampling procedure due to higher air temperatures and the somewhat longer time (4–5 h) until processing. Subsequently, particles were concentrated by passive settling (SB_{2010} and N_{2011}), precipitation with the flocculant $FeCl_3$ (S_{2013}), or centrifugation (GC_{2014}). All approaches yield comparable results and are described by *Boxhammer et al.* [2016]. The resulting sediment pellets were stored at −20°C, freeze-dried, ground for homogenization, and then analyzed for total particulate carbon (TPC) with an elemental analyzer (Euro EA–CN, Hekatech) according to Sharp [*Sharp*, 1974]. Finally, TPC data were normalized by mesocosm volume.

2.4. Evaluation of Time Lag Between the Peaks of Chl *a* and OM Sedimentation

In order to quantify TL we identified the temporal difference of the peaks in water column Chl *a* (P_{Chl}) and peaks in sedimented total carbon (P_{Sed}) and extrapolated to 100 m as described in the next section. Chl *a* concentrations were used, as PP data were only available for two out of the four experiments and the low temporal resolution of these data did not allow for a precise determination of TL. C/Chl ratios did vary at the different locations, but Chl *a* concentrations were still the most reliable bloom indicator available. Phytoplankton blooms were identified using the threshold method [*Siegel et al.*, 2002; *Brody et al.*, 2013]. Briefly, median Chl *a* concentrations were calculated for each experiment and the first value equal to or above the median prior to the peak marks the bloom start date (BSD). The same method was applied to the sedimented total carbon concentrations to estimate mass flux initiation. The time from BSD to the peak in Chl *a* was evaluated for each mesocosm of the respective experiments and is hereafter referred to as duration of Chl *a* buildup. Note that we focused on inorganic nutrient-fueled phytoplankton blooms in this analysis of mesocosm data as we could only detect Chl *a* and subsequent sinking flux peaks in such settings. In later stages of the experiments OM production was often fueled by organic nutrients and resulted in smaller and more irregular pulses in OM sedimentation, thus making a precise assignment of peaks impossible.

AGU Geophysical Research Letters 10.1002/2016GL070875

2.5. Amplification of the Time Lag Between PP and Sinking Matter Flux With Depth

The range over which the time lag in the surface amplifies with depth primarily depends on how fast the organic matter sinks. Sinking velocity (SV) measurements were performed during each study except for the SB_{2010} experiment using the FlowCam method [*Bach et al*., 2012]. Briefly, a subsample of bulk material collected in the sediment trap is transferred to a sinking chamber, which is mounted in a modified version of the FlowCam (Fluid Imaging). Settling particles are recorded for ~20 min at *in situ* temperature of the mesocosms. This enables the characterization and tracking of individual particles in the size range of 40–400 μm, except for the last study (GC_{2014}), where we used a larger sinking chamber allowing for a larger particle size spectrum (40–1000 μm). Using this method, we measured size and SV of particles each day sediment trap samples were collected. From these measurements we get a correlation of sinking velocity to particle diameter. We use this correlation to calculate the SV for any given particle diameter:

$$\mathrm{SV}(\mathrm{N}_{2011}) = 0.04754 \times D + 1.5465 \quad (2)$$

$$\mathrm{SV}(\mathrm{S}_{2013}) = 0.054 \times D + 2.3 \quad (3)$$

$$\mathrm{SV}(\mathrm{GC2014}) = 0.07706 \times D + 21.15572 \quad (4)$$

where SV is the particle sinking velocity in $\mathrm{m\,d^{-1}}$ and D is the particle diameter in μm (equation (3) adopted from *Enke* [2014]). Using these equations, we then calculated the average SV of the particle size spectrum (100–1000 μm), which covers the size spectrum of particles responsible for the majority of mass flux [*Clegg and Whitfield*, 1990]. Several processes have been reported to influence the sinking velocity of particles both negatively and positively. Processes that accelerate particle sinking involve, e.g., bacterial remineralization, scavenging of ballasting minerals, and repackaging by grazers [*Armstrong et al*., 2002; *Francois et al*., 2002; *Klaas and Archer*, 2002; *Turner*, 2002; *Ploug et al*., 2008], while other processes decelerate particle sinking to depth, e.g., sinking through density gradients [*MacIntyre et al*., 1995; *Prairie et al*., 2013]. For our extrapolation of TL to 100 m we assumed a range of slow- to fast-sinking velocities based on the size versus sinking velocity relationship from the individual study sites (see above). It is important to note that we did not explicitly consider the variability of SV that is introduced through nonsize-related factors (e.g., ballast) in this extrapolation. However, we are confident that the uncertainty in SV generated through nonsize-related parameters is smaller than the range covered by the wide size spectrum. This confidence is based on observations in a previous study where maximum changes in SV due to changing excess density were within 30–40% of the total variance within a period of 4 weeks [*Bach et al*., 2016b].

We hereafter differentiate between the initial time lag (TL; time lag between peak Chl *a* and peak sedimentation of total carbon in the mesocosms) and the time lag at 100 m depth (TL_{100}; time lag between P_{Chl} and the point in time when sinking OM reaches 100 m water depth).

3. Results and Discussion

3.1. Observations of Time Lag Between Phytoplankton Blooms and Sedimentation From Several Mesocosm Studies

Table S1 lists the TL calculated for each mesocosm and location, as well as the concentrations of Chl *a* and TPC at P_{Chl} and P_{Sed}, respectively. Temporal development of Chl *a* concentrations and sedimentation of TPC are shown for each mesocosm in Figure 2. TLs varied between locations, ranging from 2 to 15 days, and to a lesser extent between replicate mesocosms (see Figure 3a). Error bars indicate the uncertainty associated with the identification of peaks in days, as Chl *a* concentrations and sedimentation were not measured on a daily basis in all experiments.

In the SB_{2010} experiment, Chl *a* concentration peaked at days 8 (Figure 2a) and 4 (Figure 2b) with 0.87 and $0.65\ \mu\mathrm{g\,L^{-1}}$, which led to a sedimentation of 1.01 and $0.54\ \mu\mathrm{mol\,kg^{-1}\ 48\,h^{-1}}$ TPC at day 16. Chl *a* buildup took 4 (M3) or 2 (M7) days. This experiment was characterized by comparatively long TLs of 8 (±2) and 12 (±2) days.

The N_{2011} experiment showed high peak Chl *a* concentrations of $3.92\ \mu\mathrm{g\,L^{-1}}$ at day 3 (Figure 2c). Using the threshold method, we determined that Chl *a* built up over 1 day, which does not reflect the observed data. This discrepancy results from the fact that Chl *a* concentrations stayed high after the P_{Chl} and did not return to low values as observed in the other experiments. This leads to relatively high median Chl *a* concentration, which in turn is used to determine the BSD. However, this discrepancy between observed and calculated

AGU Geophysical Research Letters 10.1002/2016GL070875

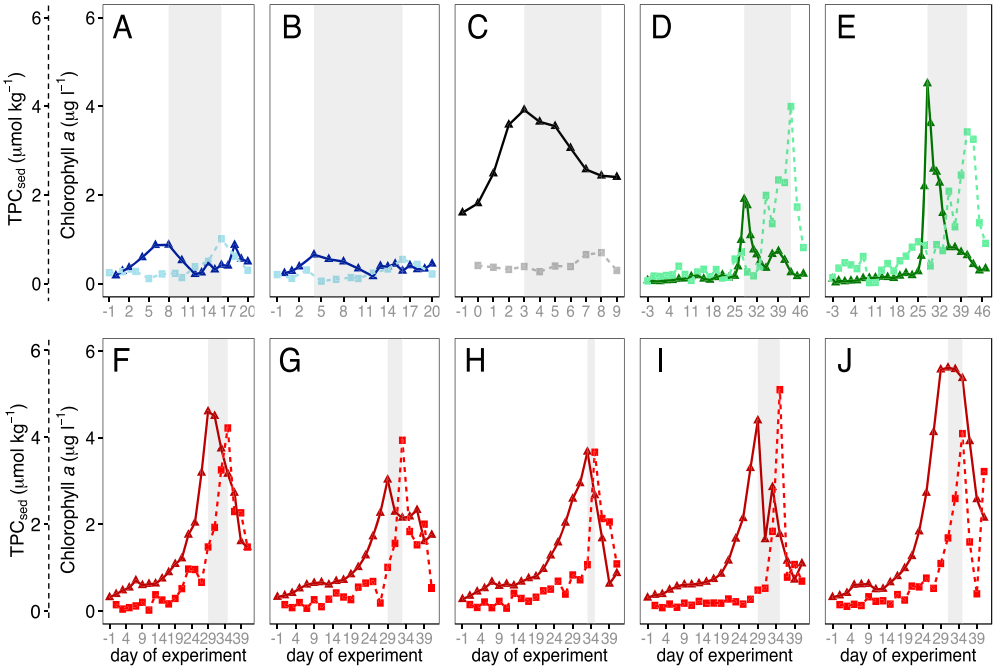

Figure 2. Chlorophyll *a* concentrations (solid lines) and organic matter concentrations (dashed lines), collected in the sediment traps during (a and b) SB_{2010}, (c) N_{2011}, (d and e) GC_{2014}, and (f–j) S_{2013}. The shaded areas indicate the time lag from Chl *a* peaks to sedimentation peaks. Note that OM concentrations are based on daily sampling for N_{2011} and every other day sampling for SB_{2010}, S_{2013}, and GC_{2014}. The colors differentiate the four sampling locations.

BSDs was only an issue for this particular mesocosm. For the other locations, the calculated BSD agreed well with the observations. Sedimentation of OM was rather low during N_{2011}, with a peak of 0.7 µmol kg^{-1} d^{-1} TPC on day 8. The observed TL during N_{2011} was 5 days. There was no uncertainty associated with the daily determination of TL during N_{2011}, as both Chl *a* concentrations and sediment fluxes were determined every day.

In S_{2013} (Figures 2f–2j), we observed the highest peak Chl *a* concentrations (4.61 (M1), 3.03 (M3), 3.67 (M5), 4.40 (M9), and 5.62 (M10) µg L^{-1}) and sinking fluxes (4.23, 3.94, 3.67, 5.11, and 4.1 µmol kg^{-1} 48 h^{-1} TPC). Although this study displayed some of the shortest TLs of all data sets (6, 4, 2, 6, and 4 ± 2 days), Chl *a* increased very slowly over 14 days. Due to the high number of replicates in this experiment ($n = 5$), we were able to get a better estimate of the variability of TL among replicates. We observed up to a threefold difference in TL between replicate mesocosms.

During GC_{2014} (Figures 2d and 2e), peak Chl *a* concentrations were high (1.91 (M1) and 4.51 (M9) µg L^{-1}) and they increased more rapidly (2 and 3 days) compared to S_{2013}. The sinking flux in this experiment showed a slower increase despite peaks being high (3.99 and 3.42 µmol kg^{-1} 48 h^{-1} TPC). We observed the longest TLs of 13 and 15 (±1) days in this experiment.

To estimate the amplification of TL between P_{Chl} and P_{Sed} up to 100 m water depth (TL_{100}; Figure 3b), we calculated average sinking velocities for N_{2011}, S_{2013}, and GC_{2014} using equations (2)–(4), respectively. For a particle size of 500 µm, this resulted in sinking velocities of 25.3 m d^{-1} (N_{2011}), 29.3 m d^{-1} (S_{2013}), and 59.7 m d^{-1} (GC_{2014}), which is well within the range expected for this size (see *Bach et al.* [2016b] for a detailed discussion). The considerably higher sinking velocities during GC_{2014} can be explained by two mechanisms: (1) the supply of Saharan dust to the mesocosms was likely higher during GC_{2014} compared to the other studies, both due to dust events commonly appearing during the period in which the GC_{2014} study took place and likely due to additional supply of volcanic sand from the islands as the mesocosms were positioned ~100–200 m downwind of a large headland. (2) Average water temperatures were higher during GC_{2014}, leading to a decrease in water viscosity with potential to increase sinking velocity [*Taucher et al.*, 2014].

AGU Geophysical Research Letters 10.1002/2016GL070875

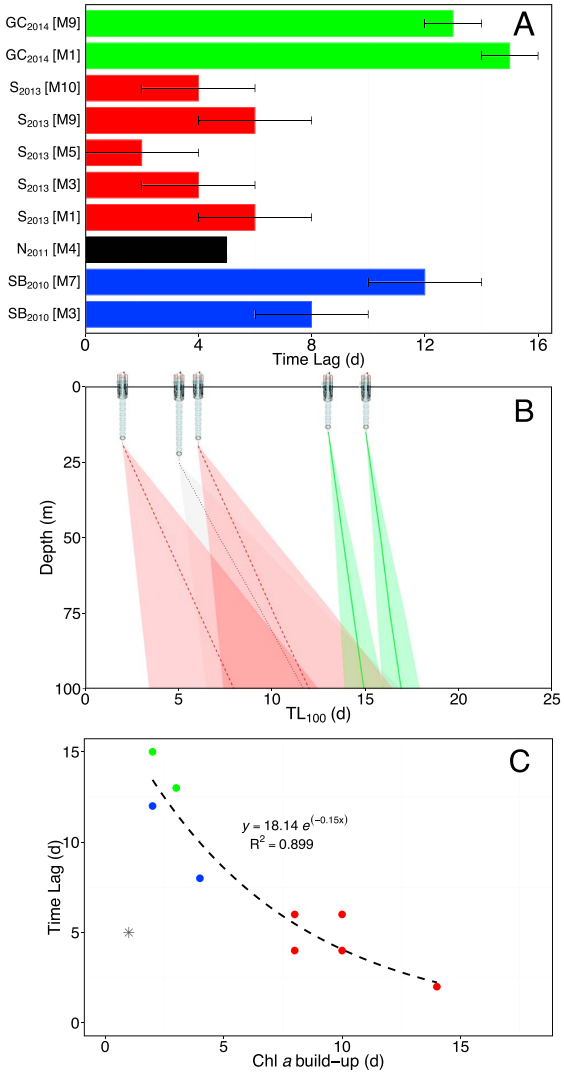

Figure 3. (a) Time lags in days between P_{Chl} and P_{Sed} (see section 2.4) of all mesocosms from SB_{2010} (M3 and M7; blue), N_{2011} (M4; black), S_{2013} (M1, M3, M5, and M9; red), and GC_{2014} (M1 and M9; green). The error bars indicate the uncertainty in days. (b) Amplification of time lag down to 100 m depth. SB_{2010} is absent due to missing sinking velocity data. Amplification of time lag for a range of particle sizes is indicated by shaded areas (upper limit = 100 μm, lower limit = 1000 μm, and line = mean). The colors represent the different experiments, and for ease of readability, only the mesocosms with longest and shortest TL were displayed (N_{2011} (M4) = black, S_{2013} (M1, M5) = red, and GC_{2014} (M1, M9) = green). (c) Correlation between TL and the duration of Chl *a* buildup. For the N_{2011} study, Chl *a* buildup determined with the threshold method did not match the observation and was excluded from the analysis (black asterisk; see section 3.1).

Due to higher sinking velocities in GC_{2014}, the mean TL_{100} (average of calculated TL_{100} for 100 μm and 1000 μm particle diameter) converges with those of the other experiments at depth. Thus, mean TL_{100} ranges from 8 to 17 days (see Figure 3b). However, the spread of TLs increases with depth as a function of minimum and maximum sinking velocities. Thus, locations with overall slower sinking velocities show a larger range at 100 m.

3.2. Importance of Time Lag in *e*-Ratio Estimates

This study revealed a relatively large range (2 to 15 days) in TL between surface production and particle collection in the sediment traps. TL amplifies with increasing depth depending on particle sinking velocities. At sea, measurements of PP and export flux are commonly performed on the same day and used to calculate the export efficiency of a given system. However, without the consideration of TL, the measured export flux is not connected to the surface production it originates from. Thus, resulting *e*-ratio estimates do not reflect the true export efficiency of the system and are less reliable the longer TL becomes (see Figure 1). This is likely to be more important in highly seasonal regions, such as the North Atlantic, the Arctic, and many coastal areas, where PP and export occur in a much more pulsed fashion relative to oligotrophic regions. In order to correctly connect PP to export flux, the OM produced in the surface would have to be traced and collected at depth. Unfortunately, conventional approaches are unable to resolve this connection or are limited by the duration of studies.

An alternative would be (1) to extend and more importantly (2) to synchronize the integration time of primary production and export flux estimates. The former has partly been implemented with the introduction of the ThE_i ratio, in which the time scale of satellite-derived estimates of PP were adapted to match thorium-derived estimates of export flux [*Henson et al.*, 2011; *Le Moigne et al.*, 2016]. Although this approach is still limited by the half-life time of thorium (approximately 24 days), it includes a potential

AGU Geophysical Research Letters 10.1002/2016GL070875

time lag within this time frame. Our results suggest that the integration time of the *ThEi* method would be sufficient to account for both the TL and TL_{100}. However, the large range of TL observed in our studies indicates that the amplification of TL at depth can occasionally exceed 1 month when TL is large and particle sinking velocities are low. Thus, the integration time of the *ThEi* approach may occasionally still be too small for accurate *e*-ratio estimations. It also has to be noted that this method does not account for lateral transport of sinking particulate matter, which remains an unsolved problem in *e*-ratio estimation in the field.

3.3. What Are Potential Controls on the Time Lag Between PP and Sinking Particle Production?

Ultimately, the aim is to adequately estimate the export efficiency of a given system. Thus, sampling for both PP and export flux have to integrate on adequate time scales or account for the TL. It is therefore crucial to identify and understand the underlying mechanisms that drive differences in this TL. In order to find mechanisms controlling the length of TL, we tested for potential correlations between TL and (1) duration of Chl *a* buildup (bloom start to Chl *a* peak), (2) temperature, and (3) mesocosm length.

A strong positive correlation was found between TL and duration of Chl *a* buildup ($y = 18.14e^{(-0.15x)}$, $r^2 = 0.899$, $p < 0.001$, $n = 9$; Figure 3c). A possible explanation for this correlation could be a dependency of TL on the dynamics between primary producers and grazers in the system. A rapid Chl *a* increase, as observed during the GC_{2014} and SB_{2010} experiments, leads to a stronger disequilibrium between primary producers and consumers. This may delay one of the major pathways of OM export, i.e., repackaging of phytoplankton OM into fecal pellets by grazers. This loss of the packaging function has previously been described as a potential mechanism to control export of particles to the mesopelagic [*Lam et al*., 2011]. Contrastingly, in systems with slow biomass buildup (e.g., S_{2013}), phytoplankton and grazer growth is likely to be more tightly coupled so that particle aggregation follows OM production with less delay. Indeed, *Henson et al*. [2015] reported long TLs at high-latitude regions characterized by pulsed surface production and short TLs in low-latitude regions characterized by more tightly coupled food webs.

The repackaging control on TL proposed above seems to be contradicted by the higher sinking speeds measured during GC_{2014}. However, as explained in section 3.1, we attribute these elevated sinking velocities to other factors (ballasting and low viscosity) so that this data set does not contradict the food web mechanism described above.

Another possible explanation for variable TLs could be that aggregation processes took longer in SB_{2010} and GC_{2014} due to differences in phytoplankton community composition. It has been shown that coagulation efficiency can vary substantially depending on phytoplankton species composition, nutritional status, and growth phase of the cells [*Kiørboe et al*., 1990; *Kiørboe and Hansen*, 1993; *Burd and Jackson*, 2009]. Unfortunately, we currently do not have enough understanding of the influence of these settings and their interaction on the rate of particle formation. Identifying which of these mechanisms (zooplankton repackaging or aggregation efficiency) is dominant in different plankton communities at specific times exceeds the scope of this study and will be addressed in future work.

We also found a weak positive correlation of TL and temperature ($y = 0.038x + 4.57$, $r^2 = 0.559$, $p = 0.013$, $n = 10$). These results contradict the finding of *Henson et al*. [2015], who observed larger TLs at high latitudes than at lower ones. However, we find a high variability in TLs even at the same temperature (average temperature in SB_{2010} and $S_{2013} = 3°C$; TL ranged between 2 and 12 days), suggesting that temperature may not be the controlling factor of the range in TL. A weak negative correlation was also found between TL and mesocosm length ($y = -0.97x + 24.9$, $r^2 = 0.488$, $p = 0.025$, $n = 10$) with longer TLs occurring in shorter mesocosms. This is counterintuitive and we conclude that this results from a coincidental co-correlation of length with food web structure rather than a true causal relation.

4. Conclusion

In this study we aimed to constrain the time lag between PP and export flux in different oceanic regions. We observed a relatively large range in TL of 2 to 15 days. The longest TLs were found in systems characterized by rapid Chl *a* increases. This illustrates that, when coupled with export flux measurements, instantaneous measurements of PP are insufficient to adequately estimate the export ratio and longer time scales must be considered. Our analysis further showed that the duration of TL correlates with the duration of Chl *a* buildup, indicating a strong coupling of TL with biological parameters, i.e., phytoplankton community composition

AGU Geophysical Research Letters 10.1002/2016GL070875

and/or food web dynamics. This study represents one step toward a time-corrected *e*-ratio (*e*-ratio$_{TC}$), which would portray a more accurate picture of differences in export efficiency among the ocean basins.

Acknowledgments
The authors thank the KOSMOS core team for the deployment and maintenance of the KOSMOS infrastructure during all experiments from 2010 to 2014. We also want to thank Kai Schulz, Matthias Fischer, and Alice Nauendorf for their contribution of chlorophyll data; Luana Krebs and Jana Meyer for assisting with the sediment trap sampling and processing during the Gran Canaria experiment; and Andrea Ludwig for managing the logistics on site. We are grateful to the crews of M/V *Esperanza*, R/V *Alkor* (AL376, AL406, and AL420), R/V *Håkan Mosby* (2011609), R/V *Heinke* (HE360), R/V *Poseidon* (POS463), and R/V *Hesperides* (29HE20140924) for the transportation, deployment, and recovery of the mesocosms. The mesocosm studies were funded by the Federal Ministry of Education and Research (BMBF) in the framework of the coordinated projects BIOACID II (FKZ 03F06550) and SOPRAN II (FKZ 03F0611), as well as by the European Union in the framework of the FP7 EU projects MESOAQUA (grant agreement 228224) and EPOCA (grant agreement 211384). Further financial support was provided by the Leibniz Award 2012, awarded to Ulf Riebesell by the German Science Foundation.

References

Armstrong, R. A., C. Lee, J. I. Hedges, S. Honjo, and S. G. Wakeham (2002), A new, mechanistic model for organic carbon fluxes in the ocean based on the quantitative association of POC with ballast minerals, *Deep. Res. Part II Top. Stud. Oceanogr.*, *49*, 219–236, doi:10.1016/S0967-0645(01)00101-1.

Bach, L. T., U. Riebesell, S. Sett, S. Febiri, P. Rzepka, and K. G. Schulz (2012), An approach for particle sinking velocity measurements in the 3–400 μm size range and considerations on the effect of temperature on sinking rates, *Mar. Biol.*, *159*(8), 1853–1864, doi:10.1007/s00227-012-1945-2.

Bach, L. T., et al. (2016a), Influence of ocean acidification on a natural winter-to-summer plankton succession: First insights from a long-term mesocosm study draw attention to periods of low nutrient concentrations, *PLoS One*, *11*(8), e0159068, doi:10.1371/journal.pone.0159068.

Bach, L. T., T. Boxhammer, A. Larsen, N. Hildebrandt, K. G. Schulz, and U. Riebesell (2016b), Influence of plankton community structure on the sinking velocity of marine aggregates, *Global Biogeochem. Cycles*, *30*, 1145–1165, doi:10.1002/2016GB005372.

Barlow, R., D. Cummings, and S. Gibb (1997), Improved resolution of mono- and divinyl chlorophylls *a* and *b* and zeaxanthin and lutein in phytoplankton extracts using reverse phase C-8 HPLC, *Mar. Ecol. Prog. Ser.*, *161*, 303–307, doi:10.3354/meps161303.

Bender, M., et al. (1987), A comparison of four methods for determining planktonic community production 1, *Limnol. Oceanogr.*, *32*(5), 1085–1098, doi:10.4319/lo.1987.32.5.1085.

Boxhammer, T., L. T. Bach, J. Czerny, and U. Riebesell (2016), Technical note: Sampling and processing of mesocosm sediment trap material for quantitative biogeochemical analysis, *Biogeosciences*, *13*(9), 2849–2858, doi:10.5194/bg-13-2849-2016.

Brody, S. R., M. S. Lozier, and J. P. Dunne (2013), A comparison of methods to determine phytoplankton bloom initiation, *J. Geophys. Res. Ocean*, *118*, 2345–2357, doi:10.1002/jgrc.20167.

Buesseler, K. O., M. P. Bacon, J. Kirk Cochran, and H. D. Livingston (1992), Carbon and nitrogen export during the JGOFS North Atlantic Bloom experiment estimated from ^{234}Th: ^{238}U disequilibria, *Deep Sea Res. Part A. Oceanogr. Res. Pap.*, *39*(7–8), 1115–1137, doi:10.1016/0198-0149(92)90060-7.

Burd, A. B., and G. A. Jackson (2009), Particle aggregation, *Annu. Rev. Mar. Sci.*, *1*(1), 65–90, doi:10.1146/annurev.marine.010908.163904.

Clegg, S. L., and M. Whitfield (1990), A generalized model for the scavenging of trace metals in the open ocean—I. Particle cycling, *Deep Sea Res. Part A. Oceanogr. Res. Pap.*, *37*(5), 809–832, doi:10.1016/0198-0149(90)90008-J.

Cochran, J. K., and P. Masqué (2003), Short-lived U/Th series radionuclides in the ocean: tracers for scavenging rates, export fluxes and particle dynamics, *Rev. Mineral. Geochem.*, *52*(1), 461–492, doi:10.2113/0520461.

Deuser, W. G. (1986), Seasonal and interannual variations in deep-water particle fluxes in the Sargasso Sea and their relation to surface hydrography, *Deep Sea Res. Part A, Oceanogr. Res. Pap.*, *33*(2), 225–246, doi:10.1016/0198-0149(86)90120-2.

Enke, G. (2014), Sinking flux of particulate organic matter and the special role of *Coscinodiscus wailesii*: A mesocosm experiment, Dresden Univ. of Technology, M.S. thesis, Dresden, Germany

Field, C. B. (1998), Primary production of the biosphere: Integrating terrestrial and oceanic components, *Science*, *281*(5374), 237–240, doi:10.1126/science.281.5374.237.

Francois, R., S. Honjo, R. Krishfield, and S. Manganini (2002), Factors controlling the flux of organic carbon to the bathypelagic zone of the ocean, *Global Biogeochem. Cycles*, *16*(4), 1087, doi:10.1029/2001GB001722.

Henson, S. A., R. Sanders, E. Madsen, P. J. Morris, F. Le Moigne, and G. D. Quartly (2011), A reduced estimate of the strength of the ocean's biological carbon pump, *Geophys. Res. Lett.*, *38*, L04606, doi:10.1029/2011GL046735.

Henson, S. A., A. Yool, and R. Sanders (2015), Variability in efficiency of particulate organic carbon export: A model study, *Global Biogeochem. Cycles*, *29*, 33–45, doi:10.1002/2014GB004965.

Kiørboe, T., and J. L. S. Hansen (1993), Phytoplankton aggregate formation: Observations of patterns and mechanisms of cell sticking and the significance of exopolymeric material, *J. Plankton Res.*, *15*(9), 993–1018, doi:10.1093/plankt/15.9.993.

Kiørboe, T., K. P. Andersen, and H. G. Dam (1990), Coagulation efficiency and aggregate formation in marine phytoplankton, *Mar. Biol.*, *107*(2), 235–245, doi:10.1007/BF01319822.

Klaas, C., and D. Archer (2002), Association of sinking organic matter with various types of mineral ballast in the deep sea: Implications for the rain ratio, *Global Biogeochem. Cycles*, *16*(4), 1116, doi:10.1029/2001GB001765.

Knauer, G. A., J. H. Martin, and K. W. Bruland (1979), Fluxes of particulate carbon, nitrogen, and phosphorus in the upper water column of the northeast Pacific, *Deep Sea Res. Part A. Oceanogr. Res. Pap.*, *26*(1), 97–108, doi:10.1016/0198-0149(79)90089-X.

Kolber, Z. S., and P. G. Falkowski (1992), Fast repetition rate (FRR) fluorometer for making *in situ* measurements of primary productivity, *OCEANS '92. Mastering the Oceans Through Technology. Proceedings.*, vol. 2, pp. 637–641, IEEE.

Kolber, Z. S., O. Prášil, and P. G. Falkowski (1998), Measurements of variable chlorophyll fluorescence using fast repetition rate techniques: Defining methodology and experimental protocols, *Biochim. Biophys. Acta Bioenerg.*, *1367*(1–3), 88–106, doi:10.1016/S0005-2728(98)00135-2.

Lam, P. J., and J. K. B. Bishop (2007), High biomass, low export regimes in the Southern Ocean, *Deep. Res. Part II Top. Stud. Oceanogr.*, *54*, 601–638, doi:10.1016/j.dsr2.2007.01.013.

Lam, P. J., S. C. Doney, and J. K. B. Bishop (2011), The dynamic ocean biological pump: Insights from a global compilation of particulate organic carbon, $CaCO_3$, and opal concentration profiles from the mesopelagic, *Global Biogeochem. Cycles*, *25*, GB3009, doi:10.1029/2010GB003868.

Le Moigne, F. A. C., M. Villa-Alfageme, R. J. Sanders, C. Marsay, S. Henson, and R. García-Tenorio (2013a), Export of organic carbon and biominerals derived from ^{234}Th and ^{210}Po at the Porcupine Abyssal Plain, *Deep Sea Res. Part I Oceanogr. Res. Pap.*, *72*, 88–101, doi:10.1016/j.dsr.2012.10.010.

Le Moigne, F. A. C., S. A. Henson, R. J. Sanders, and E. Madsen (2013b), Global database of surface ocean particulate organic carbon export fluxes diagnosed from the ^{234}Th technique, *Earth Syst. Sci. Data*, *5*(2), 295–304, doi:10.5194/essd-5-295-2013.

Le Moigne, F. A. C., et al. (2015), Carbon export efficiency and phytoplankton community composition in the Atlantic sector of the Arctic Ocean, *Deep Sea Res. Part I Oceanogr. Res. Pap.*, *120*, 3896–3912, doi:10.1002/2015JC010700.

Le Moigne, F. A. C., S. A. Henson, E. Cavan, C. Georges, K. Pabortsava, E. P. Achterberg, E. Ceballos-Romero, M. Zubkov, and R. J. Sanders (2016), What causes the inverse relationship between primary production and export efficiency in the Southern Ocean?, *Geophys. Res. Lett.*, *43*, 4457–4466, doi:10.1002/2016GL068480.

AGU Geophysical Research Letters 10.1002/2016GL070875

MacIntyre, S., A. L. Alldredge, and C. C. Gotschalk (1995), Accumulation of marines now at density discontinuities in the water column, *Limnol. Oceanogr.*, *40*(3), 449–468, doi:10.4319/lo.1995.40.3.0449.

Martin, P., R. S. Lampitt, M. Jane Perry, R. Sanders, C. Lee, and E. D'Asaro (2011), Export and mesopelagic particle flux during a North Atlantic spring diatom bloom, *Deep. Res. Part I Oceanogr. Res. Pap.*, *58*(4), 338–349, doi:10.1016/j.dsr.2011.01.006.

Martin, P., et al. (2013), Iron fertilization enhanced net community production but not downward particle flux during the Southern Ocean iron fertilization experiment LOHAFEX, *Global Biogeochem. Cycles*, *27*, 871–881, doi:10.1002/gbc.20077.

Nielsen, E. S. (1952), The use of radio-active carbon (C_{14}) for measuring organic production in the sea, *ICES J. Mar. Sci.*, *18*(2), 117–140, doi:10.1093/icesjms/18.2.117.

Paul, A. J., et al. (2015), Effect of elevated CO_2 on organic matter pools and fluxes in a summer Baltic Sea plankton community, *Biogeosciences*, *12*(20), 6181–6203, doi:10.5194/bg-12-6181-2015.

Ploug, H., M. H. Iversen, and G. Fischer (2008), Ballast, sinking velocity, and apparent diffusivity within marine snow and zooplankton fecal pellets: Implications for substrate turnover by attached bacteria, *Limnol. Oceanogr.*, *53*(5), 1878–1886, doi:10.4319/lo.2008.53.5.1878.

Prairie, J. C., K. Ziervogel, C. Arnosti, R. Camassa, C. Falcon, S. Khatri, R. M. McLaughlin, B. L. White, and S. Yu (2013), Delayed settling of marine snow at sharp density transitions driven by fluid entrainment and diffusion-limited retention, *Mar. Ecol. Prog. Ser.*, *487*, 185–200, doi:10.3354/meps10387.

Riebesell, U., et al. (2013), Technical note: A mobile sea-going mesocosm system—New opportunities for ocean change research, *Biogeosciences*, *10*(3), 1835–1847, doi:10.5194/bg-10-1835-2013.

Riley, J. S., R. Sanders, C. Marsay, F. A. C. Le Moigne, E. P. Achterberg, and A. J. Poulton (2012), The relative contribution of fast and slow sinking particles to ocean carbon export, *Global Biogeochem. Cycles*, *26*, GB1026, doi:10.1029/2011GB004085.

Schulz, K. G., et al. (2013), Temporal biomass dynamics of an Arctic plankton bloom in response to increasing levels of atmospheric carbon dioxide, *Biogeosciences*, *10*(1), 161–180, doi:10.5194/bg-10-161-2013.

Sharp, J. H. (1974), Improved analysis for "particulate" organic carbon and nitrogen from seawater, *Limnol. Oceanogr.*, *19*(6), 984–989, doi:10.4319/lo.1974.19.6.0984.

Siegel, D. A., S. C. Doney, and J. A. Yoder (2002), The North Atlantic spring phytoplankton bloom and sverdrup's critical depth hypothesis, *Science*, *296*(5568), 730–733, doi:10.1126/science.1069174.

Siegel, D. A., et al. (2016), Prediction of the export and fate of global ocean net primary production: The exports science plan, *Front. Mar. Sci.*, *3*(22), 1–10, doi:10.3389/fmars.2016.00022.

Taucher, J., L. T. Bach, U. Riebesell, and A. Oschlies (2014), The viscosity effect on marine particle flux: A climate relevant feedback mechanism, *Global Biogeochem. Cycles*, *28*, 415–422, doi:10.1002/2013GB004728.

Turner, J. T. (2002), Zooplankton fecal pellets, marine snow and sinking phytoplankton blooms, *Aquat. Microb. Ecol.*, *27*, 57–102, doi:10.3354/Ame027057.

Van Heukelem, L., and C. S. Thomas (2001), Computer-assisted high-performance liquid chromatography method development with applications to the isolation and analysis of phytoplankton pigments, *J. Chromatogr. A*, *910*(1), 31–49, doi:10.1016/S0378-4347(00)00603-4.

3 — Manuscript II

Ocean acidification-induced restructuring of the plankton food web can influence the degradation of sinking particles

Stange[1,*], P., **Taucher**[1], J., **Bach**[1], L.T., **Algueró-Muñiz**[2], M., **Horn**[2], H. G., **Krebs**[3], L., **Boxhammer**[1], T., **Nauendorf**[4], A., and **Riebesell**[1], U.

[1]Helmholtz Centre for Ocean Research Kiel (GEOMAR), Düsternbrooker Weg 20, 24105 Kiel, Germany
[2]Alfred Wegener Institute, Helmholtz Centre for Polar and Marine Research, Biologische Anstalt, Helgoland, 27483 Helgoland, Germany [3]Swiss Federal Institute of Technology, 8092 Zurich, Switzerland
[4]Leibniz Institute for Science and Mathematics Education, 24118 Kiel, Germany

[*]corresponding author: pstange@geomar.de (P. Stange)

submitted to *Frontiers in Marine Sciences*

3.1 Abstract

Ocean acidification (OA) is expected to alter plankton community structure in the future ocean. This, in turn, could change the composition of sinking organic matter and the efficiency of the biological carbon pump. So far, most OA experiments involving entire plankton communities have been conducted in meso- to eutrophic environments. However, recent studies suggest that OA effects may be more pronounced during prolonged periods of nutrient limitation. In this study, we investigated how OA-induced changes in low-nutrient adapted plankton communities of the subtropical North Atlantic Ocean may affect particulate organic matter (POM) standing stocks, POM fluxes, and POM stoichiometry. More specifically, we compared the elemental composition of POM suspended in the water column to the corresponding sinking material collected in sediment traps. Three weeks into the experiment, we simulated a natural upwelling event by adding nutrient-rich deep-water to all mesocosms, which induced a diatom-dominated phytoplankton bloom. Our results show that POM was more efficiently retained in the water column in the highest CO_2 treatment levels (>800 μatm pCO_2) subsequent to this bloom. We further observed significantly lower C:N and C:P ratios in post-bloom sedimented POM in the highest CO_2 treatments, suggesting that degradation processes were less pronounced. This trend is most likely explained by differences in micro- and mesozooplankton abundance during the bloom and post-bloom phase. Overall, this study shows that ocean acidification can indirectly alter POM fluxes and stoichiometry in subtropical environments through changes in plankton community structure.

3.2 Introduction

The increase in anthropogenic carbon dioxide (CO_2) emissions during the last century has led to atmospheric CO_2 concentrations that are unprecedented in the recent geological history (Stocker et al., 2013). About 25% of these emissions is taken up by the oceans each year (Le Quéré et al., 2016). While this dampens the atmospheric CO_2 increase, it also results in shifts in carbonate chemistry and a reduction of seawater pH, commonly referred to as ocean acidification (OA) (Caldeira and Wickett, 2003; Wolf-Gladrow et al., 1999). Estimates predict a 0.3 - 0.4 reduction in surface pH until the end of this century (Orr et al., 2005), which is expected to have significant impacts on physiological processes of marine biota (Doney et al., 2009).

Results from more than a decade of OA research have shown that responses differ substantially between marine organisms (Wittmann and Pörtner, 2013). While these studies helped in developing a principal understanding of how OA affects the physiology of single species, we are still largely lacking the understanding of how OA effects may manifest on the community level (Riebesell and Gattuso, 2015). Existing "whole community" studies show that both direct effects of OA on single species (Riebesell et al., 2017) and indirect effects through changes in plankton community structure (Bach et al., 2016; Fabricius et al., 2011; Gazeau et al., 2016; Hall-Spencer et al., 2008; Paul et al., 2015; Schulz et al., 2013) can significantly influence biogeochemical cycles in the ocean.

Mesocosm experiments with entire plankton communities allow us to investigate how OA induced changes in community structure may affect processes of biogeochemical cycles,

e.g. the production and quality of particulate organic matter (POM). Changes in elemental stoichiometry of POM have the potential to influence the partitioning of carbon between the ocean and atmosphere, which is particularly important in the context of climate change. In an *in situ* mesocosm experiment in a Norwegian fjord, Riebesell et al. (2007) observed increased carbon to nitrogen (C:N) ratios in POM under elevated levels of CO_2. The authors attributed these changes to an increase in carbon overconsumption in the dominant phytoplankton groups and outlined the possibility of a more efficient carbon pump under future ocean conditions once this carbon-enriched POM sinks out of the surface ocean. Using a global biogeochemical model, Oschlies et al. (2008) extrapolated these findings to the global ocean and found that the enhanced carbon export may lead to an expansion in suboxic water volume by up to 50% until the end of this century.
Recent mesocosm experiments showed that OA effects can be particularly pronounced during extended periods of low inorganic nutrient concentrations (Bach et al., 2016; Paul et al., 2015; Sala et al., 2015; Thomson et al., 2016). We therefore conducted an *in situ* mesocosm experiment in the eastern subtropical Atlantic Ocean off the coast of Gran Canaria (Canary Islands) – a region characterized by low concentrations of inorganic nutrients in particular during fall when the study took place (Arístegui et al., 2001). Halfway through the study we simulated an upwelling event of nutrient-rich water by adding collected deep-water to each mesocosm (see Taucher et al., accepted). Mesoscale upwelling events are naturally occurring frequently south of the Canary Islands, as this region is characterized by a distinct eddy-corridor (Sangrà et al., 2009). In this paper we address how OA induced changes in plankton community structure could influence the elemental composition and degradation of sinking POM.

3.3 Material and Methods

3.3.1 Experimental design

From September to December 2014 we conducted a pelagic *in situ* mesocosm study in Gando Bay (27° 55' 41" N, 15° 21' 55" W) off the coast of Gran Canaria (Canary Islands). We deployed nine "Kiel Off-Shore Mesocosms for Ocean Simulations" (KOSMOS, M1-M9), each consisting of a floatation frame and a mounted bag (2 m diameter) made of 1 mm thick thermoplastic polyurethane foil (Riebesell et al., 2013). Once deployed, the initially folded bags were lowered to a depth of 13 m and thereby filled with approximately 35 m^3 of seawater. The bags were sealed at the bottom and top with a net (mesh size of 3 mm) already before deployment in order to exclude unequally distributed nekton and large zooplankton (e.g. fish or jellyfish) from the experiment. The lowered bags were left open for 4 days to allow water exchange and ensure similar starting conditions in all mesocosms. Subsequently, the water bodies inside the mesocosms were enclosed by lifting the upper part of the bags above the sea surface, while divers simultaneously closed the bottom of each mesocosm with sediment traps. The collection cylinders of these traps were connected to silicon tubes, which were fixed to the floatation frames above sea surface (Boxhammer et al., 2016). Closing the mesocosms marked the start of the experiment on September 27, four days before the first CO_2 addition.
To simulate different OA scenarios, we added different amounts of CO_2-saturated seawa-

Mesocosm ID	Symbol	Water column pCO_2 [μatm]			Sediment trap pCO_2 [μatm]		
		Phase 1	Phase 2	Phase 3	Phase 1	Phase 2	Phase 3
M1		401	374	326	392	333	318
M9		406	343	297	382	292	299
M5		502	404	427	464	406	431
M3		636	493	546	578	536	533
M7		746	571	672	678	632	671
M4		800	620	710	729	697	682
M6		976	-	-	970	-	-
M2		1050	748	830	930	807	802
M8		1195	902	944	1080	940	897

Table 3.1: Average values for seawater pCO_2 for each experimental phase, defined in Sect. 3.4.1. pCO_2 values were calculated from the combination of TA and DIC using CO2SYS (Pierrot et al., 2006) with the carbonate dissociation constants (K1 and K2) of Lueker et al. (2000). A detailed description of the determination of the carbonate chemistry is given by Taucher et al., accepted.

ter to the mesocosms. In order to reduce the immediate stress response, the addition was conducted gradually in 4 consecutive steps. The first addition was performed on October 1 and marks the beginning of the experimental manipulation (day 0 = t0). Target concentrations were reached after the 4^{th} addition on October 7. Table 3.1 depicts the mean CO_2 concentrations in the respective mesocosms.

On October 23 (t22) approximately 85 m^3 of deep-water were collected with a deep-water collecting system (described in detail by Taucher et al., accepted) from 650 m depth, approximately 7.5 km northeast of the study site. The collector was moored adjacent to the mesocosms. During the night between t23 and t24, approximately 20% of each mesocosms' volume was removed and replaced by equivalent amounts of nutrient-rich deep-water. Exact mixing ratios were calculated based on previously determined mesocosm volumes and target nutrient concentrations (Taucher et al., accepted). In total, the study lasted 61 days with the last sampling on t55 and t57 for the water column and sediment trap, respectively.

Alongside the regular sampling routine, we dedicated extensive effort to continuous maintenance of each mesocosm, including cleaning of the mesocosm walls. While divers regularly cleaned the outside, a cleaning ring was used to wipe the inside of the walls every week (Riebesell et al., 2013). This procedure prohibits wall growth, except for the flange ring connecting the mesocosm to the sediment trap and the funnel of the sediment trap, which are too narrow to be cleaned with the ring. Cleaning of these parts was thus performed by divers inside the mesocosms on t56, after the last sampling of the water column.

3.3.2 Sampling procedure

3.3.2.1 Water column

Samples were taken every second day between 9 am and 12 pm. We used two sampling systems simultaneously: 1) an integrating water sampler (IWS, HYDRO-BIOS, Kiel) for parameters that are sensitive to gas exchange or contamination and require low amounts of sample volume (e.g. carbonate chemistry) and 2) a vacuum pumping system for parameters that require large amounts of sample volume (e.g. particulate matter)(Taucher et al., accepted). Both systems allowed for integrated sampling of the entire water column of each mesocosm from 0 to 13 m water depth. All water column parameters presented in this study are thus given as integrated values for each mesocosm on the respective sampling day. Sampling was conducted every second day except for the time directly after deep-water addition (t25 to t33), where samples were taken every day. Water collected with the pumping system was stored in 20 L carboys and transferred in a temperature-controlled room (set to *in situ* temperature) once they were transported back to the laboratory facilities. Carboys were always carefully mixed before withdrawing subsample volume in order to avoid sinking bias.
Additionally, net hauls were conducted on nine occasions during the 61 days experiment in order to estimate the abundance of mesozooplankton (e.g. copepods, appendicularians). Sampling frequency was restricted to one net haul every 4th sampling day in order to avoid overfishing. Samples were taken using an Apstein net (55 μm mesh size, 17 cm diameter opening) with a sampling volume of 295 L per haul. The net content was transferred into 500 mL Kautex bottles and immediately preserved with 4% formaldehyde buffered with sodium tetraborate solution until identification.
For the determination of microzooplankton abundances, 250 mL of unfiltered seawater was taken from the 20 L carboys and filled into brown glass bottles. Samples were preserved using acidic Lugol's solution (1-2% final concentration) and stored in the dark until enumeration with an inverse light microscope (Sect. 3.3.3.2).

3.3.2.2 Sediment trap

Sedimented POM was collected from each mesocosm every 48 hours starting at t-3. Sampling was always carried out before the water column samples were taken to avoid resuspension of sedimented matter. A detailed description of the sampling procedure is provided by Boxhammer et al. (2016). Briefly, sedimented material was pumped into 5 L Schott Duran glass bottles through the silicon tube connecting the collection cylinder of the sediment trap to the surface. All samples were collected within 0.5 to 1 hour and immediately stored in large coolers filled with seawater and additional cool packs for the remaining sampling procedure to avoid warming and minimize bacterial degradation of the material. Once collection was finished, sediment trap samples were transported to the land-based facilities and processed as described in Sect. 3.3.3.4.

3.3.3 Sample analysis

3.3.3.1 Chlorophyll *a* and phytoplankton pigments

Chlorophyll *a* and phytoplankton pigment concentrations were determined using reverse-phase high-performance liquid chromatography (HPLC). For this, we filtered up to 1.5 L of seawater onto glass fibre filters (nominal pore size of 0.7 μm, 25 mm diameter, Whatman) by gentle vacuum filtration (<200 mbar). During filtration, samples were covered with aluminium foil to reduce exposure to light. Pigments were extracted in acetone (90%) by homogenisation of the filters with glass beads in a cell mill. Samples were then centrifuged (10 min, 5200 rpm, 4 °C) and the supernatant was filtered through 0.2 μm PTFE filters (VWR International). Pigment concentrations were determined in the supernatant by reverse-phase high-performance liquid chromatography (HPLC; Thermo Scientific HPLC Ultimate 3000 with an Eclipse XDB-C8 3.5u 4.6 x 150 column (Van Heukelem and Thomas, 2001)). Contributions of individual phytoplankton groups to total chlorophyll a were then calculated using the software CHEMTAX (Mackey et al., 1996).

3.3.3.2 Zooplankton counts

Mesozooplankton was analysed quantitatively and taxonomically using a stereomicroscope (Olympus SZX9). Copepod abundances include copepodites as well as adults. Microzooplankton abundances were determined following the method described by Utermöhl (1931) using an inverted microscope (Zeiss Axiovert 25). Only the dominant groups of microzooplankton were counted, i.e. ciliates and heterotrophic dinoflagellates. A thorough description of the methodology will be provided by Algueró-Muñiz et al. (in prep.).

3.3.3.3 POM in water column samples

For the determination of total particulate carbon (TPC), as well as particulate organic carbon, nitrogen and phosphorous (POC, PON, POP), we took up to 1 L subsample from the 20 L carboys. Subsamples were filtered with a gentle vacuum (<200 mbar) onto combusted glass fibre filters (nominal pore size of 0.7 μm, 25 mm diameter, Whatman). Filters for the determination of TPC were dried at 60 °C over night and transferred into tin cups until analysis. Filters for POC and PON analysis were stored in combusted glass petri dishes at -20 °C, while POP filters were directly transferred into 40 mL glass bottles and frozen at -20 °C. POC/PON filters were fumed with hydrochloric acid (37%) for 2h before measurement in order to remove particulate inorganic carbon (PIC). Concentrations of TPC, POC and PON were determined using an elemental CN analyser (EuroEA) following Sharp (1974).
POP filters were placed in 40 mL of deionized water with oxidizing decomposition reagent ("Oxisolve", Merck) and autoclaved for 30 min in a pressure cooker to oxidize the particulate organic phosphorus to orthophosphate. After cooling, POP concentrations were determined by spectrophotometric analysis analogous to the method for dissolved inorganic phosphate, following Hansen and Koroleff (1999).

3.3.3.4 POM in sediment trap samples

Quantities of the sediment trap material suspended in the 5 L bottles (see Sect. 3.3.2.2) were determined gravimetrically after transport to the laboratory. Afterwards, we homogenized the suspended material in the sampling bottles by gently mixing, to take subsamples for a variety of parameters, which are not considered any further in this study. Total subsample volume was small (generally <10% of bulk sample volume). The remaining bulk sample was transferred stepwise into 800 mL beakers and centrifuged therein with 5236 x g for 10 minutes (6-16 KS centrifuge, SIGMA). The supernatant was then carefully decanted while the sedimented pellets were transferred into 110 mL centrifuge tubes. This procedure was repeated until the entire sample was centrifuged and transferred. For further compression, the 110 mL tubes were centrifuged a second time at 5039 x g for 10 minutes (3K12 centrifuge, SIGMA) and the suspension was decanted. The remaining pellets were immediately deep frozen at -20 °C and stored in small plastic screw cap cups. The decanted supernatant was visually inspected for translucency and discarded unless there were still large amounts of organic material present in the supernatant. Between t35 and t49 we observed strongly elevated sedimentation and sample volumes increased drastically. During this period, translucency of the supernatant decreased as a larger proportion of the suspended matter could not be concentrated by centrifugation. We therefore pipetted small subsamples of the homogenized supernatant onto glass fibre filters (nominal pore size of 0.7 μm, 25 mm diameter, Whatman). All filters were deep-frozen at -20 °C immediately after filtration for subsequent analysis of TPC, POC, PON, and POP as described for water column samples. In some cases the particle density of the original samples was too low for centrifugation to compress the sedimented matter into transferrable pellets (t21 to t33 for M2 and t31 to t33 for M8). In these cases we filtered subsamples of up to 100 mL for POM analysis of the entire samples as described for the supernatant at strongly elevated sedimentation.
The frozen centrifuge pellets were freeze-dried and ground to a very fine and homogenous powder as described in Boxhammer et al. (2016). This powder was then subsampled for the determination of TPC, POC, PON and POP. Duplicate subsamples of 2 mg were taken for the determination of TPC and transferred into tin cups. Additionally, two similar subsamples were transferred into silver cups and acidified before measurement to remove the inorganic carbon fraction (acidified for 1 hour with 1 M HCl and dried at 50 °C over night). All four subsamples were measured using an elemental analyser (Euro EA-CN, Hekatech), which was calibrated with acetanilide (C_8H_9NO) and soil standard (Hekatech, catalogue number HE33860101) prior to each measurement run. PIC was then calculated from total and organic carbon content. For the analysis of POP, subsamples of 2 mg were transferred into 40 mL glass vials and analysed similar to the water column samples, as described above. In this study, sediment trap data are presented as daily fluxes, which we calculated by dividing the sediment trap data of each sampling point (every 48 hours) by 2. Furthermore, the daily fluxes were normalized for mesocosm volume. Volume determination is described in the overview paper by Taucher et al. (accepted).

3.3.4 Estimating degradation of sinking particles based on stoichometry

Preferential remineralization of nitrogen and phosphorus over carbon is commonly observed in sinking POM, which leads to increasing elemental ratios (C:N, C:P) with depth (Sambrotto et al., 1993; Schneider et al., 2003; Thomas et al., 1999). We calculated the changes in elemental ratios between POM collected in the sediment trap and POM sampled from the water column and defined this ratio as the stoichiometry-based degradation index (SDI), as it gives an indication of the extent of degradation on sinking PM.

$$\mathrm{SDI_{CN}} = (\frac{\mathrm{C:N_{sink}}}{\mathrm{C:N_{susp}}}) \tag{3.1}$$

$$\mathrm{SDI_{CP}} = (\frac{\mathrm{C:P_{sink}}}{\mathrm{C:P_{susp}}}) \tag{3.2}$$

Here, a value of 1 indicates identical elemental ratios of POM suspended in the water column (e.g. $\mathrm{C:N_{susp}}$) and POM collected in the sediment trap (e.g. $\mathrm{C:N_{sink}}$), while values >1 denote higher C:N ratios in the sedimented POM compared to the water column, thus indicating preferential remineralization of nitrogen. Changes in stoichiometry were calculated on a daily basis. Hence, our calculation does not account for the time lag between POM production and sinking of POM to the sediment traps (Stange et al., 2017). The reason for this was that the time lag could only be accurately determined during the bloom, when clear peaks in biomass production and POM flux to the sediment traps were observed. It is unlikely that this time lag of approximately 10 days is representative for the entire experiment. We thus decided to calculate stoichiometry changes using the daily measurements. However, calculating this under the consideration of a 10-day time lag resulted in similar trends compared to the ones reported in this study.

3.3.5 Data analysis and statistical approach

To facilitate statistical analysis and a quantitative description of the data, we divided the dataset in three experimental phases based on the chlorophyll *a* development. A detailed description of the determination of the experimental phases is given in Sect. 3.4.1. We applied linear regression analysis to determine the relationship between average $p\mathrm{CO_2}$ and average response of the variables during each phase. Unfortunately, mesocosm 6 was irreparably damaged on t26 and thus excluded from the statistical analysis of phases II and III. Statistical analyses were undertaken using the software R, version 3.3.1 (R Core Team, 2013).

3.4 Results

3.4.1 Chlorophyll *a* and experimental phases

The experiment started in oligotrophic conditions, with very low concentrations of inorganic nutrients and chlorophyll a (Fig. 3.1A). Chlorophyll a concentration during phase I (t-3 to t24) averaged at approximately 0.1 μg $\mathrm{L^{-1}}$. On t24 we added nutrient-rich

deep-water to the mesocosms in order to simulate an eddy-induced upwelling event (for a detailed description of the deep-water addition see Taucher et al. (in review)). The deep-water addition increased inorganic nutrient concentrations to 3.15, 0.17, and 1.60 μmol L^{-1} for NO^{3-} + NO^{2-}, PO_4^{3-}, and $Si(OH)_4$, respectively. This stimulated the rapid development of a phytoplankton bloom in phase II (t25 to t35) with a peak in chlorophyll a at t28 (Fig. 3.1). The inorganic nutrients were quickly depleted and reached values close to detection limit between t28 and t30. After the peak on t28 chlorophyll a concentrations decreased rapidly in all mesocosms until they reached a minimum at t35. In the post-bloom phase (phase III, t37 to t55) inorganic nutrients and chlorophyll a concentrations remained low, except for the two mesocosms with highest CO_2, which displayed elevated chlorophyll a until the end of the experiment. Experimental phases were defined differently for the POM flux to the sediment traps, as described in Sect. 3.4.3.2.

3.4.2 Temporal dynamics in plankton community composition

Fig. 3.1 (B and C) show the development of cyanophytes and diatoms over the course of the experiment. We only focused on these groups since they had by far the largest contribution to total chlorophyll *a* concentrations during the respective experimental phases. During the oligotrophic phase I, (pico-)cyanobacteria (*Synechococcus* sp.) were the dominant phytoplankton group, with a contribution of 70 to 80% to total chlorophyll *a* (Fig. 3.5B). Abundances of this group increased towards t11 and decreased afterwards until the deep-water addition on t24. We observed a significant positive effect of pCO_2 on the abundance of cyanophytes during phase I ($p = 0.002$, $F=26.67$).
Following the deep-water addition on t24, the phytoplankton community underwent significant changes. Throughout phases II and III, large chain-forming diatoms, such as *Leptocylindrus* sp., *Guinardia* sp., and *Bacteriastrum* sp. dominated the phytoplankton community with a contribution to total chlorophyll *a* concentrations of 50 to 70% (Fig. 3.5B). While their overall abundance decreased towards the end of the experiment, diatoms were still the dominant phytoplankton group throughout phase III. This dominance was particularly pronounced in both high CO_2 mesocosms (M2 and M8, see Fig. 3.1B) and we observed a significant positive effect of pCO_2 on the abundance of diatoms during phase III ($p = 0.026$, $F = 8.71$). A detailed analysis of treatment effects on all phytoplankton groups is presented in Taucher et al. (in prep.).
Fig. 3.1 (B-D) shows the temporal development of micro- and mesozooplankton abundances in all mesocosms. For the purpose of this study, we only differentiated between copepods, appendicularians and microzooplankton. Abundances of copepods were constantly low throughout phase I of the experiment. Appendicularian abundances increased during phase I in all mesocosms, but declined again and reached a minimum right after deep-water addition. Phase II and III were characterized by higher abundances of both groups in all mesocosms, except in M2 and M8. While abundances of appendicularians in those two mesocosms remained low until the end of the experiment, copepod abundances increased from t50 to the last sampling day. Microzooplankton abundances were overall low during phase I of the experiment and started to increase in all mesocosms after t25, but remained comparably low in M2 and M8. A detailed analysis of CO_2 effects on meso- and microzooplankton is presented in Algueró-Muñiz et al. (in prep.).

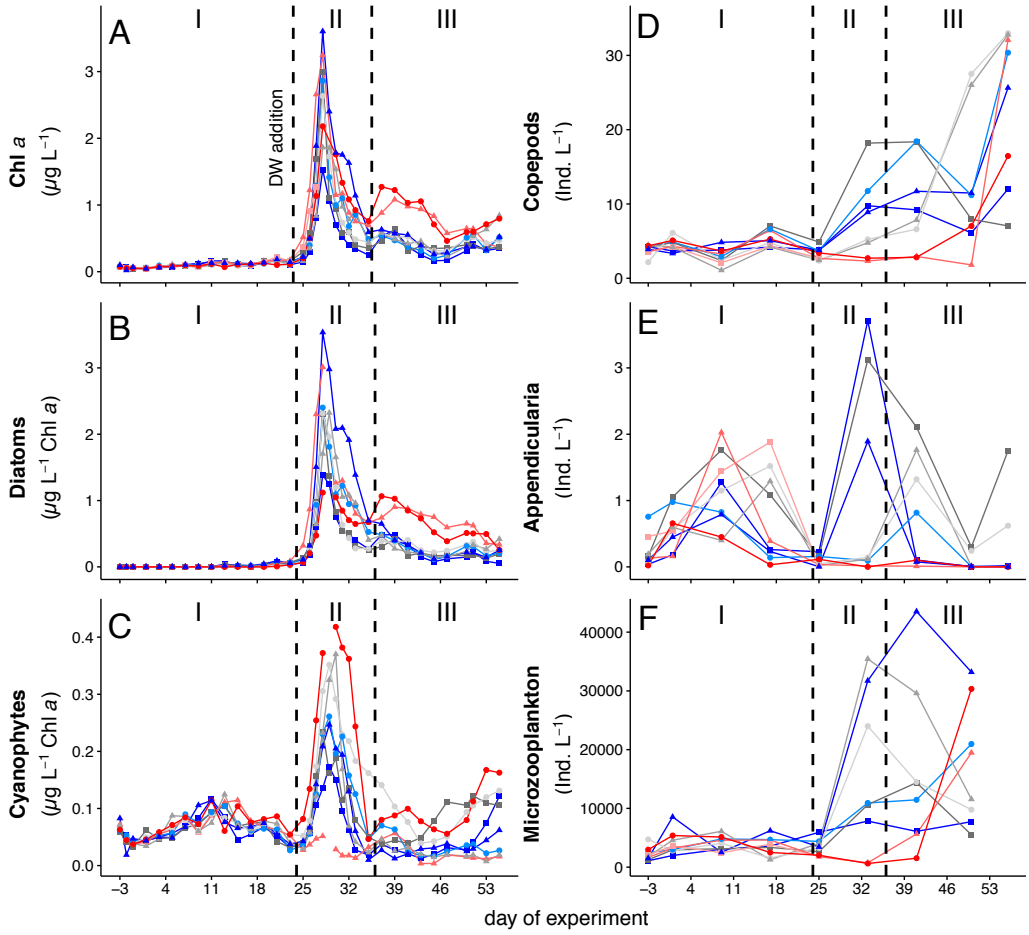

Figure 3.1: Development of **(A)** chlorophyll a concentrations. **(B)** abundances of diatoms, and **(C)** abundances of cyanophytes. **(D-F)** depict zooplankton abundances over the course of the experiment with **(B)** copepods, including both adult and all copepodite stages, **(C)** appendicularians, and **(D)** protozoan microzooplankton, mostly ciliates and heterotrophic dinoflagellates. The three different phases are indicated with I, II and III and separated by the dashed vertical lines. Note that the first dashed line also depicts the time of deep-water addition. Colours and symbols are described in Table 3.1.

3.4.3 Temporal dynamics of POM

3.4.3.1 Water column

The temporal development of POC, PON, and POP in the water column is shown in Fig. 3.2A-C. Water column POC and PON concentrations were only determined from t9 onwards as we did not have sufficient filtration volume during the first couple of days. Concentrations of all three parameters remained low from t9 onwards, but increased slightly towards the end of phase I (t17 to t23). With the addition of deep-water at t24, POM increased rapidly in the water column and peaked between t30 and t31 in all mesocosms. After the peak in phase II, most POM was retained in the water column and only slowly decreased during phase III. We observed a slight but significant negative effect of $p\mathrm{CO}_2$ on POP during phase I (Table 3.2), but this effect vanished during the subsequent phases. During phase III, concentrations of water column POC, PON and POP were elevated in the two highest CO_2 mesocosms (M2 and M8), but we did not detect an overall significant effect of $p\mathrm{CO}_2$.

3.4.3.2 Sediment trap

Peaks in POM sedimentation were temporally delayed to POM concentration peaks in the water column. Due to this delay we define experimental phases differently for the sediment trap material ($\mathrm{phase}_{\mathrm{sed}}$ I = t-3 to t33; $\mathrm{phase}_{\mathrm{sed}}$ II = t35 to t45; $\mathrm{phase}_{\mathrm{sed}}$ III = t47 to t55). Total POM fluxes to the sediment trap were low throughout $\mathrm{phase}_{\mathrm{sed}}$ I (Fig. 3.2D-F). The onset of increased POM fluxes to the sediment trap followed water column POM build-up with a temporal delay of approximately 10 days. After an initial peak in POM flux on t35 ($\mathrm{phase}_{\mathrm{sed}}$ II), we observed rather low sedimentation rates on t37. This changed again on t39, after which sedimentation rates stayed high until t43. M3 and M5 had the largest contribution to the initial peak on t35, while the remaining mesocosms showed highest sedimentation rates on t39 and t43. Rates decreased during the last $\mathrm{phase}_{\mathrm{sed}}$ (t45 to t55) but were still higher than in $\mathrm{phase}_{\mathrm{sed}}$ I. The two mesocosms with highest CO_2 concentrations (M2, M8) showed particularly low sedimentation rates during $\mathrm{phase}_{\mathrm{sed}}$ III. However, we did not detect a significant effect of $p\mathrm{CO}_2$ in the regression analysis (Table 3.2).
The analysis of filters taken due to low translucency of the supernatant during the period of high sedimentation (t35 to t49; described in Sect. 3.3.3.4) contributed generally less than 4% to the total concentration of the respective parameter and was thus neglected. The cleaning of the lowest segment of the mesocosms and sediment trap walls on the last day of the experiment (day 57) resulted in strongly elevated sedimentation rates since there was considerable growth of benthic autotrophs on this segment. (Fig. 3.6). We thus excluded this day from the analysis.

3.4.4 Dynamics in elemental stoichiometry

3.4.4.1 Water column

We observed higher ratios of C:N (POC:PON), N:P (PON:POP) and C:P (POC:POP) compared to Redfield proportions (C:N:P = 106:16:1) throughout almost the entire exper-

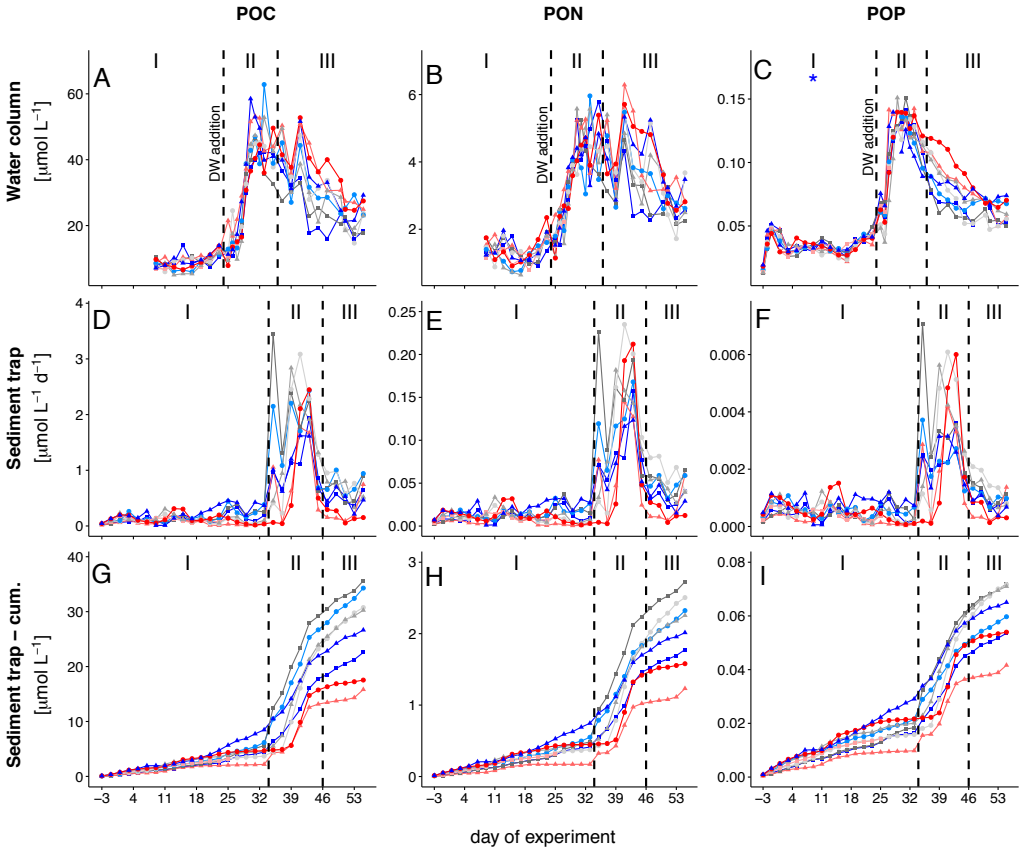

Figure 3.2: Temporal development of standing stocks and fluxes of total particulate carbon (TPC; **A, D** and **G**), nitrogen (TPN; **B, E** and **H**) and phosphorus (TPP; **C, F** and **I**). **(A - C)** and **(D - F)** depict POM concentrations from the water column and daily flux to the sediment trap, respectively. **(G - I)** show the cumulative flux of POM to the sediment trap. Coloured lines depict the different mesocosms. The three different phases are indicated with I, II and III and separated by the dashed vertical lines. Note that the first dashed line in **A - C** also depicts the time of deep-water addition. Colours and symbols are described in Table 3.1.

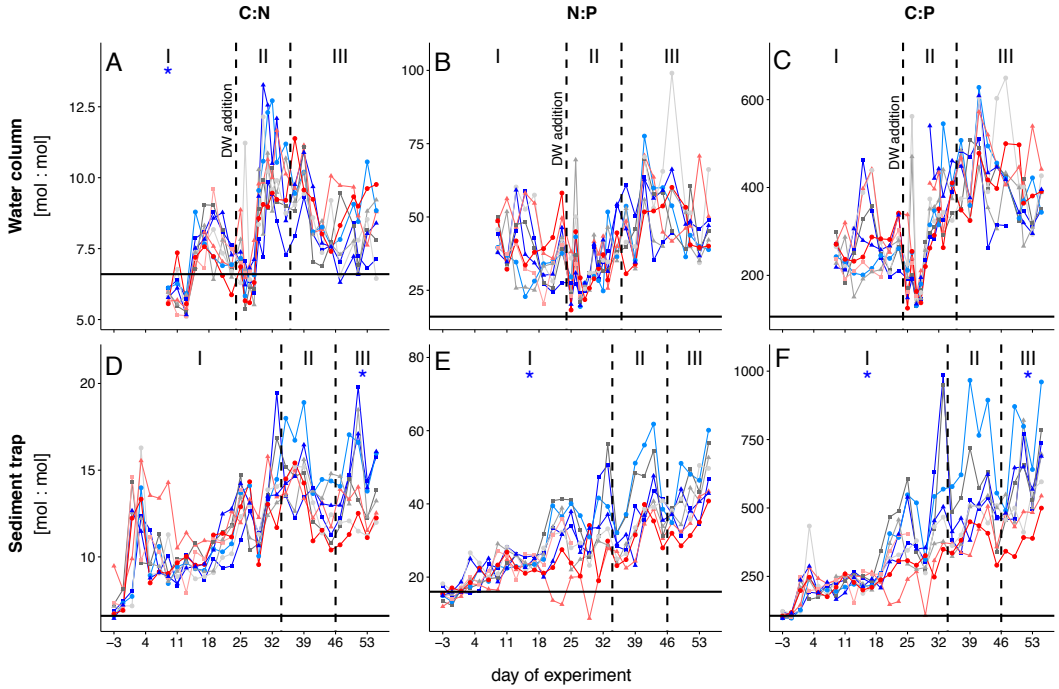

Figure 3.3: Temporal development of POM elemental stoichiometries in the water column **(A - C)** and the sediment trap samples **(D - F)**. Black horizontal lines indicate Redfield proportions for the respective elemental ratios (C:N = 6.6, N:P = 16, C:P = 106). Coloured lines depict the different mesocosms. The three different phases are indicated with I, II and III and separated by the dashed vertical lines. Note that the phases for water column and sediment trap POM have been defined differently (see section 3.1). Colours and symbols are described in Table 3.1.

iment (Fig. 3.3A-C). The only exceptions were C:N ratios during phase I (t9 to t13) and during the phytoplankton bloom right after the addition of deep-water (t25 to t28). We observed a small peak in C:N stoichiometry between t17 and t19 in all mesocosms. C:N ratios subsequently declined until the deep-water addition and stabilized close to Redfield proportions of approximately 6-7 from t25 to t28. C:N ratios increased profoundly directly after the bloom peak and nutrient depletion (t29 until t32). After this transient peak, C:N decreased towards the end of the experiment. Statistical analysis of C:N ratios averaged over the entire experiment did not reveal a significant effect of pCO_2. However, when we tested each phase individually, we observed a significantly negative effect of pCO_2 on C:N during phase I (see Table 3.2). We also found a borderline insignificant positive effect on C:N during phase III. However, the lack of significance was likely due to the effect being exclusively driven by both high CO_2 mesocosms instead of a linear relationship (see Fig. 3.7C).

Both N:P and C:P did not show a clear change during phase I. Similar to C:N, we observed minimum values for both ratios right after deep-water addition. While C:P also increased rapidly after t28 and stayed constant afterwards, N:P was characterized by a comparably slow and steady increase towards the end of the experiment. We neither observed significant treatment effects on C:P and N:P when averaged over the entire time, nor for any of the three phases individually.

3.4.4.2 Sediment trap

C:N and C:P ratios of sediment trap material were above Redfield and also higher than in water column POM (Fig. 3.3D and F). This difference was less pronounced in the N:P ratios (Fig. 3.3E). We observed a slow and steady increase in all ratios over the course of the experiment. After t19, the variability between mesocosms increased in N:P and C:P and stayed high until the end of the experiment. We observed a significant negative effect of pCO_2 on the C:N ratio in sedimented POM during phasesed III (see Table 3.2) as well as on N:P during phasesed I and C:P during phasessed I and III. These CO_2 effects were driven primarily by the very low values in the two highest CO_2 mesocosms (M2 and M8) (Fig. 3.3D-F).

3.4.5 Temporal development of the SDI

SDI_{CN} was above 1 in all mesocosms throughout the experiment, with only few exceptions (see Fig. 3.4A). This shows that C:N ratios in the sediment trap were higher compared to those in the water column for most of the time. There was no clear trend of SDI_{CN} over time, however, the ratio fluctuated in all mesocosms from the beginning up until t39 and stayed more or less constant after that. We observed a significant positive treatment effect of CO_2 on SDI_{CN} during phase I and a highly significant negative treatment effect during phase III (see Table 3.3).
SDI_{CP} did not strongly deviate from one during the majority of phase I except for the first two sampling days (Fig. 3.4B). SDI_{CP} increased during phase II and remained elevated throughout phase III except for mesocosms M4, M2 and M8. We observed significant negative CO_2 treatment effects on SDI_{CP} during phases II and III.

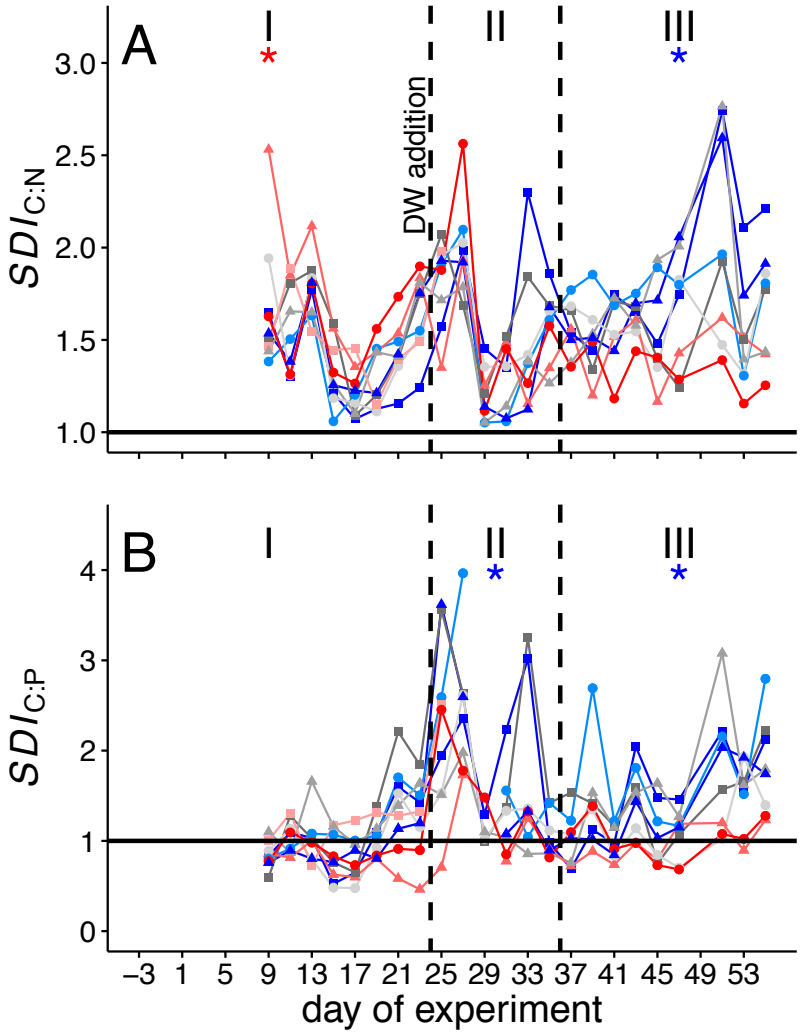

Figure 3.4: SDI (stoichiometry-based degradation index), depicting the relation between the elemental stoichiometries of the water column and sedimented POM. SDI was calculated on the base of **(A)** C:N and **(B)** C:P stoichiometry. The horizontal lines indicate a 1:1 relationship and thus equal stoichiometries in the sediment trap and water column POM. The dashed vertical lines indicate experimental phases for water column material. Colours and symbols are described in Table 3.1.

		Water column			Sediment trap		
	Phase	p	R^2	F	p	R^2	F
POC	I	0.943	0.000	0.006	0.062	0.414	4.942
	II	0.951	0.000	0.004	0.523	0.071	0.461
	III	0.110	0.369	3.503	0.274	0.195	1.45
PON	I	0.368	0.117	0.924	0.086	0.362	3.975
	II	0.568	0.057	0.365	0.815	0.009	0.059
	III	0.209	0.247	1.971	0.553	0.062	0.394
POP	I	**0.019 (-)**	0.569	9.268	0.279	0.164	1.372
	II	0.171	0.287	2.42	0.889	0.003	0.021
	III	0.151	0.311	2.702	0.616	0.045	0.280
C:N	I	**0.002 (-)**	0.759	22.09	0.605	0.040	0.293
	II	0.649	0.037	0.229	0.295	0.179	1.314
	III	0.075	0.436	4.641	**0.012 (-)**	0.682	12.85
N:P	I	0.218	0.208	1.833	**0.019 (-)**	0.571	9.321
	II	0.986	0.000	0.000	0.135	0.331	2.975
	III	0.857	0.006	0.035	0.287	0.185	1.362
C:P	I	0.539	0.056	0.417	**0.006 (-)**	0.684	15.12
	II	0.710	0.025	0.152	0.154	0.306	2.666
	III	0.353	0.145	1.015	**0.037 (-)**	0.545	7.186

Table 3.2: Statistical results from the linear regression analysis on response means over the respective phases. Mesocosm 6 was lost after phase I and was thus not considered in the analysis in phases II and III (df for phase I = 7, and for phases II and III = 6). Significant p values ($p < 0.05$) are highlighted in bold. We indicate the trend of the effect in brackets behind the p-value, with (+) indicating a positive and (-) and negative trend.

	Phase	p	R^2	F
SDI_{CN}	I	**0.037 (+)**	0.483	6.543
	II	0.847	0.007	0.041
	III	**0.002 (-)**	0.814	26.21
SDI_{CP}	I	0.366	0.118	0.936
	II	**0.047 (-)**	0.51	6.245
	III	**0.049 (-)**	0.503	6.061

Table 3.3: Statistical results from the linear regression analysis on response means of SDI over the respective phases. Mesocosm 6 was lost after phase I and was thus not considered in the analysis in phases II and III (df for phase I = 7, and for phases II and III = 6). Significant p values ($p < 0.05$) are highlighted in bold. We indicate the trend of the effect in brackets behind the p-value, with (+) indicating a positive and (-) and negative trend.

3.5 Discussion

3.5.1 Temporal development of POM standing stocks

CO_2-related differences in standing stocks and elemental composition of POM were detected primarily after the phytoplankton bloom in phase II and more pronounced during phase III (Figs. 3.2 and 3.3). In particular, we observed that in both mesocosms with highest pCO_2, post-bloom water column POM remained at high concentrations longer than in low and intermediate treatment levels. This led to less sedimentation of POC, PON and POP to the sediment trap during the study period under high pCO_2 (see the cumulative plots of sedimented matter in Fig. 3.2G-I). However, the CO_2 trend was not linear, but driven almost entirely by the two mesocosms with highest pCO_2 (M2 and M8, Fig. 3.7A,B). There are three possible explanations for the observed differences in post-bloom water column POM retention: Differences in 1) particle load with ballasting minerals, such as calcite, opal or lithogenic material, 2) grazing and thus repackaging by micro- and mesozooplankton, or 3) the rate of sinking particle formation (aggregation rate). PIC/POC and biogenic silica (BSi)/POC ratios (Fig. 3.8) did not give an indication for a lower ballasting effect in mesocosms M2 and M8 after the bloom and we have no reason to expect a differing supply of airborne lithogenic material to individual mesocosms. We thus conclude that the difference in POM retention was most likely driven by differences in food-web dynamics and/or aggregation processes. Indeed, abundances of the dominant groups of mesozooplankton, i.e. copepods and appendicularians, as well as microzooplankton abundances were particularly low in both high CO_2 mesocosms during phases II and III (Fig. 3.1D-F). The lower abundance of grazers in the highest CO_2 treatment levels may have resulted in reduced consumption and repackaging of POM, which in turn translated into a longer residence time of phytoplankton cells and aggregates in the water column.

The increased retention of water column POM in M2 and M8 may also be explained by lower aggregation rates. Differences in phytoplankton community composition, nutritional status and growth phase of the cells can profoundly influence the coagulation efficiency (Burd and Jackson, 2009; Kiørboe et al., 1990; Kiørboe and Hansen, 1993). However, measurements of the *in situ* particle size spectrum by Taucher et al. (in prep.) did not reveal CO_2 related differences for the start and rate of aggregate formation. We thus conclude that the increased retention of water column POM under elevated CO_2 is primarily driven by differences in zooplankton abundance.

3.5.2 Temporal development of element stoichiometry

Elemental ratios in water column POM were much higher than Redfield values for the majority of time during the experiment. This deviation is likely caused by very low concentrations of all major inorganic nutrients. Exceptions to this trend were observed in water column C:N ratios, which were substantially lower in the middle of phase I and right before the deep-water addition. We observed a small bloom of cyanophytes (mainly *Synechococcus* sp.) during phase I, with a peak in abundances around t11 (Fig. 3.1C). While nutrient concentrations were generally low throughout phase I (mean concentrations of NO^{3-} + NO^{2-} = 0.05 μmol L^{-1} and PO_4^{3-} = 0.03 μmol L^{-1}; Fig. 3.9), excess

phosphate was available during phase I (mean NO^{3-} + NO^{2-}/PO_4^{3-} = 2). *Synechococcus* has been shown to have particularly low intercellular C:N ratios during exponential growth (Bertilsson et al., 2003). Since this group dominated the phytoplankton community during phase I, it is likely that their C:N signature is reflected in the C:N ratios of water column POM. The small bloom of cyanophytes collapsed after t11 and water column C:N increased correspondingly in the following days. During this period, we observed a significantly negative effect of pCO_2 on water column C:N ratios (Fig. 3.3A). This effect again correlates well with the significantly higher abundances of cyanobacteria observed under elevated levels of CO_2 during that phase. With the addition of deep-water on t24, inorganic nutrient limitation was relieved for about four days. Consequently, C:N and C:P ratios of water column POM declined immediately after the addition on t24 and stayed low until t28 (Fig. 3.3A and C). C:N and C:P increased rapidly back to elevated values as soon as inorganic nutrients from deep-water addition were depleted. This indicates carbon overconsumption, a mechanism observed in many groups of marine phytoplankton, particularly in diatoms, under nutrient-deplete conditions (Riebesell et al., 2007; Toggweiler, 1993). Indeed, diatoms were the dominant phytoplankton group during the bloom in all mesocosms, with a contribution of $> 60\%$ to the total chlorophyll a concentrations (Taucher et al., accepted).
We observed a borderline insignificant effect ($p = 0.075$) of pCO_2 on the elemental stoichiometry of water column POM during phase III of the experiment. We argue that our analysis did not reveal a significant effect as the difference in C:N wasn't linear, but solely driven by both mesocosms with highest pCO_2 (Fig. 3.7C). This difference is likely caused by differences in phytoplankton community composition. Abundances of large diatoms were significantly increased in both mesocosms with highest pCO_2 during phase III (Fig. 3.1B) and they continued to increase even after the supplied nutrients were depleted on t28. The difference in abundance thus likely increased the magnitude of carbon overconsumption in the two highest CO_2 treatments, resulting in slightly higher C:N ratios in M2 and M8.

3.5.3 Influence of community structure on the degradation of sinking POM

SDI_{CN} and SDI_{CP} were larger than 1 for the majority of the experiment. This shows that elemental ratios of sedimented POM were overall elevated compared to those of POM suspended in the water column. A similar trend has also been observed to a lesser degree in a previous study (Czerny et al., 2013), and was interpreted as an indication for preferential remineralization of both N and P relative to C in sinking organic material (Sambrotto et al., 1993; Schneider et al., 2003; Thomas et al., 1999).
We observed a significant positive effect of pCO_2 on SDI_{CN} during phase I, suggesting that degradation processes were more pronounced under high CO_2 before the deep-water addition. This trend reversed during and after the bloom and a significant negative effect of pCO_2 was detected for SDI_{CP} during phase II and SDI_{CN} and SDI_{CP} during phase III. In order to identify the mechanisms responsible for the observed differences, we evaluated the processes, which have the potential to alter C:N and C:P stoichiometry in sinking POM. These include the degradation of POM by grazers (protozoans and metazoans) and bacteria.

Zooplankton grazers are known to assimilate nitrogen and phosphorus more efficiently than carbon in order to maintain homeostasis, i.e. keeping their elemental composition constant (Checkley and Entzeroth, 1985; Daly et al., 1999). The excess carbon is either respired, internally stored in lipid reservoirs (e.g. in overwintering copepods in the Arctic), or defecated, resulting in fecal pellets with substantially higher C:N ratios than sinking aggregates or marine phytoplankton (Daly et al., 1999; Gerber and Gerber, 1979; Small et al., 1983). Another pathway that has the potential to impact the stoichiometry of sinking POM is bacterial degradation. It has been shown that the rapid decrease of sinking particulate matter with depth is partly associated with degradation processes by particle-attached bacteria (Ploug and Grossart, 2000; Smith et al., 1992). However, production rates of free-living and particle-associated bacteria were not significantly different in the high CO_2 treatments throughout the experiment (T. Hornick, unpublished data). Furthermore, CO_2-related differences in zooplankton abundances between mesocosms only manifested during phase II and III (see Fig. 3.1). We can therefore only speculate that the higher SDI_{CN} under elevated levels of CO_2 during phase I is most likely related to differences in the quality of the sinking POM. Contrastingly, the significant negative effects of pCO_2 on SDI_{CN} and SDI_{CP} during phase II and III are indicative for slower degradation of sinking organic material, which correlates well with the lower abundances of micro- and mesozooplankton during these periods.
In an earlier study by Riebesell et al. (2007), increased consumption of dissolved inorganic carbon (DIC) with increasing levels of seawater pCO_2 was observed in an enclosed natural plankton community. The authors extrapolated these results and argued that this increased consumption may translate to enhanced carbon relative to nitrogen drawdown from the euphotic zone. In this study, we also observed slightly higher C:N ratios in water column POM in both mesocosms with highest pCO_2 (Fig. 3.3A), indicating that elevated levels of CO_2 may indeed promote carbon overconsumption. However, our results show that the degradation by micro- and mesozooplankton tightly controlled the fate of POM stoichiometry with depth, with the possibility to reverse CO_2 trends in elemental stoichiometry observed in the surface. We thus argue that changes in the elemental stoichiometry of suspended POM in the surface cannot be extrapolated to depth without estimating the degradation processes, which in turn are controlled by the plankton community structure.

3.6 Conclusion

In the present study, we show that OA induced changes in plankton community structure can significantly influence the degradation of sinking POM. We found that C:N ratios in suspended POM were slightly elevated after a diatom-dominated phytoplankton bloom in the two mesocosms with highest pCO_2, most likely due to enhanced carbon overconsumption. Yet, POM collected in the sediment traps showed significantly lower C:N ratios under high CO_2 conditions. This indicates that degradation of sinking matter was less pronounced under elevated levels of CO_2, which we mainly attribute to the lower abundances of micro- and mesozooplankton in those mesocosms during and after the phytoplankton bloom. These trends only manifested during post-bloom conditions, four weeks into the experiment, when differences in community structure were most pronounced. Our find-

ings underline that CO_2 induced changes in elemental stoichiometry of sinking POM are ultimately controlled by the plankton community structure. In particular, our results highlight the importance of micro- and mesozooplankton grazers on the transformation of sinking organic matter and we suggest that extrapolations of biogeochemical processes to global scales cannot be made without considering the entire planktonic food web.

References

Arístegui, J., Hernández-León, S., Montero, M. F., Gómez, M., 2001. The seasonal planktonic cycle in coastal waters of the Canary Islands. *Scientia Marina* 65 (S1), 51–58.

Bach, L. T., Taucher, J., Boxhammer, T., Ludwig, A., Achterberg, E. P., Algueró-Muñiz, M., Anderson, L. G., Bellworthy, J., Büdenbender, J., Czerny, J., Ericson, Y., Esposito, M., Fischer, M., Haunost, M., Hellemann, D., Horn, H. G., Hornick, T., Meyer, J., Sswat, M., Zark, M., Riebesell, U., 2016. Influence of Ocean Acidification on a Natural Winter-to-Summer Plankton Succession: First Insights from a Long-Term Mesocosm Study Draw Attention to Periods of Low Nutrient Concentrations. *PloS One* 11 (8), e0159068.

Bertilsson, S., Berglund, O., Karl, D. M., Chisholm, S. W., 2003. Elemental composition of marine *Prochlorococcus* and *Synechococcus*: Implications for the ecological stoichiometry of the sea. *Limnology and Oceanography* 48 (5), 1721–1731.

Boxhammer, T., Bach, L. T., Czerny, J., Riebesell, U., 2016. Technical note: Sampling and processing of mesocosm sediment trap material for quantitative biogeochemical analysis. *Biogeosciences* 13 (9), 2849–2858.

Burd, A. B., Jackson, G. A., 2009. Particle Aggregation. *Annual Review of Marine Science* 1 (1), 65–90.

Caldeira, K., Wickett, M. E., 2003. Oceanography: anthropogenic carbon and ocean pH. *Nature* 425 (6956), 365.

Checkley, D. M., Entzeroth, L. C., 1985. Elemental and isotopic fractionation of carbon and nitrogen by marine, planktonic copepods and implications to the marine nitrogen cycle. *Journal of Plankton Research* 7 (4), 553–568.

Czerny, J., Schulz, K. G., Boxhammer, T., Bellerby, R. G. J., Büdenbender, J., Engel, A., Krug, S. A., Ludwig, A., Nachtigall, K., Nondal, G., Niehoff, B., Silyakova, A., Riebesell, U., 2013. Implications of elevated CO2 on pelagic carbon fluxes in an Arctic mesocosm study - an elemental mass balance approach. *Biogeosciences* 10 (5), 3109–3125.

Daly, K. L., Wallace, D. W. R., Smith, W. O., Skoog, A., Lara, R., Gosselin, M., Falck, E., Yager, P. L., 1999. Non-Redfield carbon and nitrogen cycling in the Arctic: Effects of ecosystem structure and dynamics. Journal of Geophysical Research: Oceans 104 (C2), 3185–3199.

Doney, S. C., Fabry, V. J., Feely, R. A., Kleypas, J. A., 2009. Ocean acidification: The other CO2 problem. Ann. Rev. Mar. Sci. 1 (1), 169–192.

Fabricius, K. E., Langdon, C., Uthicke, S., Humphrey, C., Noonan, S., De'ath, G., Okazaki, R., Muehllehner, N., Glas, M. S., Lough, J. M., 2011. Losers and winners in coral reefs acclimatized to elevated carbon dioxide concentrations. *Nature Climate Change* 1 (3), 165–169.

Gazeau, F., Sallon, A., Maugendre, L., Louis, J., Dellisanti, W., Gaubert, M., Lejeune, P., Gobert, S., Borges, A., Harlay, J., Champenois, W., Alliouane, S., Taillandier, V., Louis, F., Obolensky, G., Grisoni, J.-M., Guieu, C., 2016. First mesocosm experiments to study the impacts of ocean acidification on plankton communities in the NW Mediterranean Sea (MedSeA project). *Estuarine, Coastal and Shelf Science* 186, Part A, 11–29.

Gerber, R. P., Gerber, M. B., 1979. Ingestion of natural particulate organic matter and subsequent assimilation, respiration and growth by tropical lagoon zooplankton. Marine Biology 52 (1), 33–43.

Hall-Spencer, J. M., Rodolfo-Metalpa, R., Martin, S., Ransome, E., Fine, M., Turner, S. M., Rowley, S. J., Tedesco, D., Buia, M.-C., 2008. Volcanic carbon dioxide vents show ecosystem effects of ocean acidification. *Nature* 454 (7200), 96–99.

Hansen, H., Koroleff, F., 1999. Determination of nutrients. In: Grasshoff, K., Kremling, K., Ehrhardt, M. (Eds.), Methods of Seawater Analysis. Wiley-VCH Verlag GmbH, Ch. 10, pp. 159–228.

Kiørboe, T., Andersen, K. P., Dam, H. G., 1990. Coagulation efficiency and aggregate formation in marine phytoplankton. Marine Biology 107 (2), 235–245.

Kiørboe, T., Hansen, J. L., 1993. Phytoplankton aggregate formation: observations of patterns and mechanisms of cell sticking and the significance of exopolymeric material. *Journal of Plankton Research* 15 (9), 993–1018.

Le Quéré, C., Buitenhuis, E. T., Moriarty, R., Alvain, S., Aumont, O., Bopp, L., Chollet, S., Enright, C., Franklin, D. J., Geider, R. J., Harrison, S. P., Hirst, A. G., Larsen, S., Legendre, L., Platt, T., Prentice, I. C., Rivkin, R. B., Sailley, S., Sathyendranath, S., Stephens, N., Vogt, M., Vallina, S. M., 2016. Role of zooplankton dynamics for Southern Ocean phytoplankton biomass and global biogeochemical cycles. *Biogeosciences* 13 (14), 4111–4133.

Lueker, T. J., Dickson, A. G., Keeling, C. D., 2000. Ocean pCO_2 calculated from dissolved inorganic carbon, alkalinity, and equations for K1 and K2: validation based on laboratory measurements of CO_2 in gas and seawater at equilibrium. *Marine Chemistry* 70 (1-3), 105–119.

Mackey, M., Mackey, D., Higgins, H., Wright, S., 1996. CHEMTAX - a program for estimating class abundances from chemical markers:application to HPLC measurements of phytoplankton. Marine Ecology Progress Series 144, 265–283.

Orr, J. C., Fabry, V. J., Aumont, O., Bopp, L., Doney, S. C., Feely, R. A., Gnanadesikan, A., Gruber, N., Ishida, A., Joos, F., Key, R. M., Lindsay, K., Maier-Reimer, E., Matear, R., Monfray, P., Mouchet, A., Najjar, R. G., Plattner, G.-K., Rodgers, K. B., Sabine, C. L., Sarmiento, J. L., Schlitzer, R., Slater, R. D., Totterdell, I. J., Weirig, M.-F., Yamanaka, Y., Yool, A., 2005. Anthropogenic ocean acidification over the twenty-first century and its impact on calcifying organisms. *Nature* 437 (7059), 681–686.

Oschlies, A., Schulz, K. G., Riebesell, U., Schmittner, A., 2008. Simulated 21st century's increase in oceanic suboxia by CO2-enhanced biotic carbon export. *Global Biogeochemical Cycles* 22 (4).

Paul, A. J., Bach, L. T., Schulz, K. G., Boxhammer, T., Czerny, J., Achterberg, E. P., Hellemann, D., Trense, Y., Nausch, M., Sswat, M., Riebesell, U., 2015. Effect of elevated CO2 on organic matter pools and fluxes in a summer Baltic Sea plankton community. *Biogeosciences* 12 (20), 6181–6203.

Pierrot, D., Lewis, E., Wallace, D. W. R., 2006. MS Excel Program Developed for CO_2 System Calculations. ORNL/CDIAC-105a.

Ploug, H., Grossart, H.-P., 2000. Bacterial growth and grazing on diatom aggregates: Respiratory carbon turnover as a function of aggregate size and sinking velocity. *Limnology and Oceanography* 45 (7), 1467–1475.

R Core Team, 2013. R: A Language and Environment for Statistical Computing.

Riebesell, U., Bach, L. T., Bellerby, R. G. J., Monsalve, J. R. B., Boxhammer, T., Czerny, J., Larsen, A., Ludwig, A., Schulz, K. G., 2017. Competitive fitness of a predominant pelagic calcifier impaired by ocean acidification. *Nature Geoscience* 10 (1), 19–23.

Riebesell, U., Czerny, J., von Bröckel, K., Boxhammer, T., Büdenbender, J., Deckelnick, M., Fischer, M., Hoffmann, D., Krug, S. A., Lentz, U., Ludwig, A., Muche, R., Schulz, K. G., 2013. Technical Note: A mobile sea-going mesocosm system - new opportunities for ocean change research. *Biogeosciences* 10 (3), 1835–1847.

Riebesell, U., Gattuso, J.-P., 2015. Lessons learned from ocean acidification research. *Nature* 5 (1), 12–14.

Riebesell, U., Schulz, K. G., Bellerby, R. G. J., Botros, M., Fritsche, P., Meyerhöfer, M., Neill, C., Nondal, G., Oschlies, A., Wohlers, J., Zöllner, E., 2007. Enhanced biological carbon consumption in a high CO_2 ocean. *Nature* 450 (7169), 545–8.

Sala, M. M., Aparicio, F. L., Balagué, V., Boras, J. A., Borrull, E., Cardelús, C., Cros, L., Gomes, A., López-Sanz, A., Malits, A., Martínez, R. A., Mestre, M., Movilla, J., Sarmento, H., Vázquez-Domínguez, E., Vaqué, D., Pinhassi, J., Calbet, A., Calvo, E., Gasol, J. M., Pelejero, C., Marrasé, C., 2015. Contrasting effects of ocean acidification on the microbial food web under different trophic conditions. *ICES Journal of Marine Science: Journal du Conseil* 73 (3), 670–679.

Sambrotto, R. N., Savidge, G., Robinson, C., Boyd, P., Takahashi, T., Karl, D. M., Langdon, C., Chipman, D., Marra, J., Codispoti, L., 1993. Elevated consumption of carbon relative to nitrogen in the surface ocean. *Nature* 363 (6426), 248–250.

Sangrà, P., Pascual, A., Rodríguez-Santana, Á., Machín, F., Mason, E., McWilliams, J. C., Pelegrí, J. L., Dong, C., Rubio, A., Arístegui, J., Marrero-Díaz, Á., Hernández-Guerra, A., Martínez-Marrero, A., Auladell, M., 2009. The Canary Eddy Corridor: A major pathway for long-lived eddies in the subtropical North Atlantic. *Deep-Sea Research Part I: Oceanographic Research Papers* 56 (12), 2100–2114.

Schneider, B., Schlitzer, R., Fischer, G., Nothig, E., 2003. Depth-dependent elemental compositions of particulate organic matter (POM) in the ocean. *Global Biogeochemical Cycles* 17 (2), 1032.

Schulz, K. G., Bellerby, R. G. J., Brussaard, C. P. D., Büdenbender, J., Czerny, J., Engel, A., Fischer, M., Koch-Klavsen, S., Krug, S. A., Lischka, S., Ludwig, A., Meyerhöfer, M., Nondal, G., Silyakova, A., Stuhr, A., Riebesell, U., 2013. Temporal biomass dynamics of an Arctic plankton bloom in response to increasing levels of atmospheric carbon dioxide. *Biogeosciences* 10 (1), 161–180.

Sharp, J. H., 1974. Improved analysis for particulate organic carbon and nitrogen from seawater. *Limnology and Oceanography* 19 (6), 984–989.

Small, L. F., Fowler, S. W., Moore, S. A., LaRosa, J., 1983. Dissolved and fecal pellet carbon and nitrogen release by zooplankton in tropical waters. Deep Sea Research Part A, Oceanographic Research Papers 30 (12), 1199–1220.

Smith, D. C., Simon, M., Alldredge, A. L., Azam, F., 1992. Intense hydrolytic enzyme activity on marine aggregates and implications for rapid particle dissolution. *Nature* 359 (6391), 139–142.

Stange, P., Bach, L. T., Le Moigne, F. A. C., Taucher, J., Boxhammer, T., Riebesell, U., 2017. Quantifying the time lag between organic matter production and export in the surface ocean: Implications for estimates of export efficiency. *Geophysical Research Letters* 44 (1), 268–276.

Stocker, T. F., Qin, D., Plattner, G.-K., Alexander, L. V., Allen, S. K., Bindoff, N. L., Bréon, F.-M., Church, J. A., Cubasch, U., Emori, S., Forster, P., Friedlingstein, P., Gillett, N., Gregory, J. M., Hartmann, D. L., Jansen, E., Kirtman, B., Knutti, R., KrishnaÂ Kumar, K., Lemke, P., Marotzke, J., Masson-Delmotte, V., Meehl, G. A., Mokhov, I. I., Piao, S., Ramaswamy, V., Randall, D., Rhein, M., Rojas, M., Sabine, C., Shindell, D., Talley, L. D., Vaughan, D. G., Xie, S.-P., 2013. Technical Summary. In: Stocker, T., Qin, D., Plattner, G.-K., Tignor, M., Allen, S., Boschung, J., Nauels, A., Xia, Y., Bex, V., Midgley, P. (Eds.), Climate Change 2013: The Physical Science Basis. Contribution of Working Group I to the Fifth Assessment Report of the Intergovernmental Panel on Climate Change. Cambridge University Press, Cambridge, pp. 33–115.

Thomas, H., Ittekkot, V., Osterroht, C., Schneider, B., 1999. Preferential recycling of nutrients-the ocean's way to increase new production and to pass nutrient limitation? *Limnology and Oceanography* 44 (8), 1999–2004.

Thomson, P., Davidson, A., Maher, L., 2016. Increasing CO2 changes community composition of pico- and nano-sized protists and prokaryotes at a coastal Antarctic site. Marine Ecology Progress Series 554, 51–69.

Toggweiler, J. R., 1993. Carbon overconsumption. *Nature* 363 (6426), 210–211.

Utermöhl, v. H., 1931. Neue wege in der quantitativen Erfassung des Planktons (mit besonderer Berücksichtigung des Ultraplanktons). *Verhandlungen der Internationalen Vereinigung für Theoretische und Angewandte Limnologie* 5, 567–596.

Van Heukelem, L., Thomas, C. S., 2001. Computer-assisted high-performance liquid chromatography method development with applications to the isolation and analysis of phytoplankton pigments. *Journal of Chromatography A* 910 (1), 31–49.

Wittmann, A. C., Pörtner, H.-O., 2013. Sensitivities of extant animal taxa to ocean acidification. *Nature Climate Change* 3 (11), 995–1001.

Wolf-Gladrow, D. a., Riebesell, U., Burkhardt, S., Bijma, J., 1999. Direct effects of CO2 concentration on growth and isotopic composition of marine plankton. Tellus 51B, 461–476.

3.7 Supplement

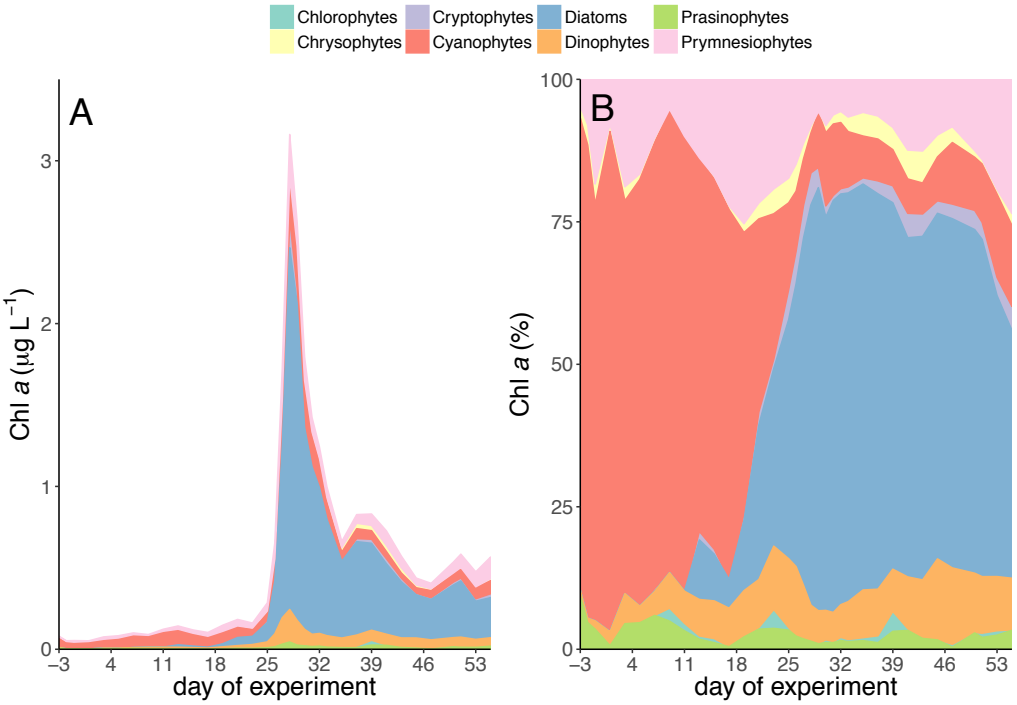

Figure 3.5: Contribution of individual phytoplankton groups to total chlorophyll a concentrations shown in **(A)** absolute concentrations and **(B)** relative contribution.

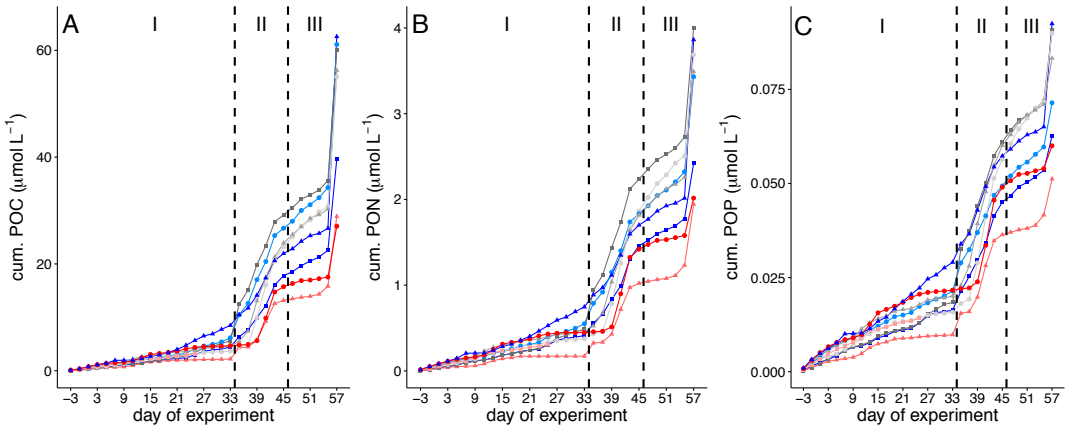

Figure 3.6: Cumulative fluxes of **(A)** TPC **(B)** TPN and **(C)** TPP to the sediment trap including t57.

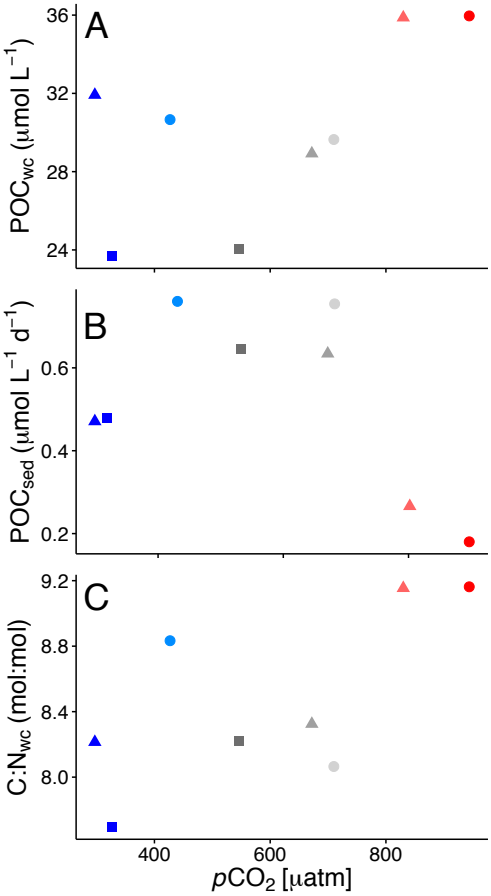

Figure 3.7: Mean values for phase III of **(A)** POC concentrations of the water column **(B)** POC fluxes to the sediment trap and **(C)** C:N ratios of water column POM. This figure emphasizes the non-linearity of the differences between mesocosms. Colours and symbols are described in Table 3.1.

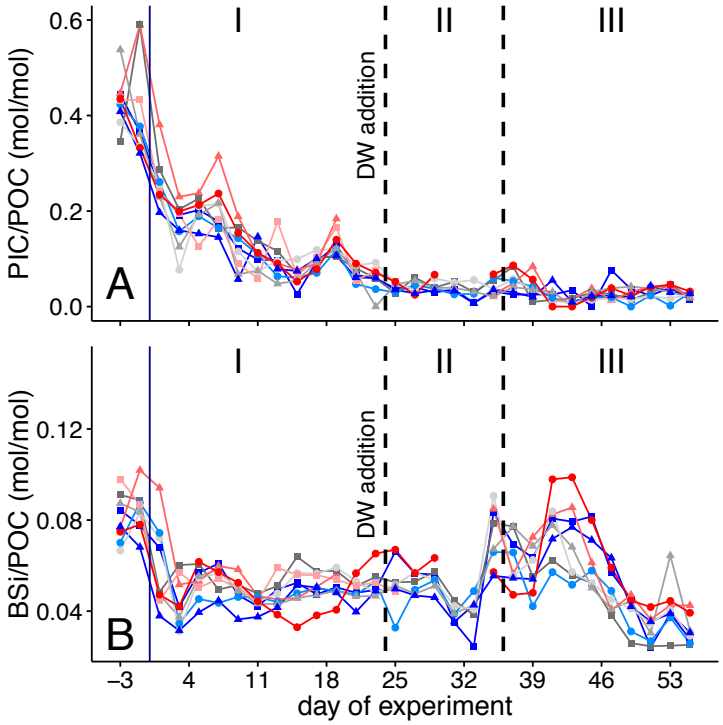

Figure 3.8: Contribution of **(A)** PIC to POC and **(B)** BSi to POC in the sediment trap samples. The blue vertical line depicts the first CO_2 addition. The two black, dashed vertical lines separate the phases. Colours and symbols are described in Table 3.1.

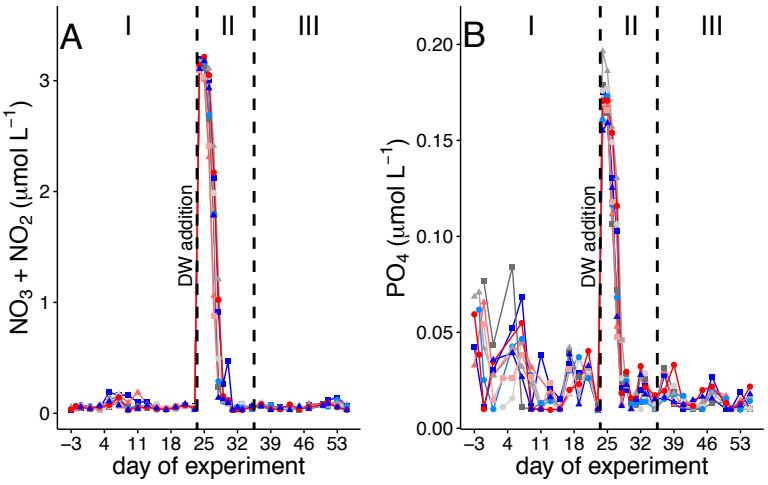

Figure 3.9: Inorganic nutrient concentrations over the course of the experiment with **(A)** NO^{3-} + NO^{2-}, **(B)** PO_4^{3-}.

4 — Manuscript III

The influence of plankton community structure on particle sinking velocity and respiration rates

Stange[1,*], P., **Bach**[1], L.T., **Taucher**[1], J., **Achterberg**[1], E.P., and **Riebesell**[1], U.

[1]Helmholtz Centre for Ocean Research Kiel (GEOMAR), Düsternbrooker Weg 20, 24105 Kiel, Germany

[*]corresponding author: pstange@geomar.de (P. Stange)

Manuscript in preparation

4.1 Abstract

The biological carbon pump (BCP) is the main pathway for photosynthetically fixed carbon from the surface ocean to depth. The fraction of sinking particulate organic matter reaching the deep ocean depends on the sinking velocity of particles and the remineralization rate, which in turn are determined to a large degree by the surface ocean plankton community. In fall 2014 we conducted an *in situ* mesocosm experiment in the subtropical North Atlantic Ocean in order to investigate the influence of plankton community structure on particle sinking and respiration rates. Conditions were oligotrophic during the first part of the study. After about 3 weeks, we added nutrient-rich deep water to all mesocosms stimulating a pronounced phytoplankton bloom dominated by large chain-forming diatoms. This shift in community structure was accompanied by a substantial decrease in particle sinking velocity, which we attribute to an increase in particle porosity during the diatom bloom. Furthermore, carbon-specific respiration was highest during a small bloom of Synechococcus at the beginning of the experiment and during the diatom bloom, while minimum values were observed during periods of low productivity. These results are in agreement with a growing body of literature that depict highly seasonal, diatom-dominated regions with lower transfer efficiencies (T_{eff}), opposed to regions where lower seasonality and more complex food webs result in the production of more refractory material. While oligotrophic regions are commonly dominated by small phytoplankton, the high respiration rates observed during the period of a *Synechococcus* bloom suggests that phytoplankton size may not be a suitable indicator for T_{eff}. Instead, other parameters, such as the degradability of particulate matter may have a paramount influence in controlling the efficiency of the BCP.

4.2 Introduction

The fixation of atmospheric carbon dioxide (CO_2) by marine phytoplankton in the surface ocean is an important sink for anthropogenic greenhouse gas emissions (Le Quéré et al., 2016; Sabine et al., 2004). The majority of the photosynthetically fixed organic matter is rapidly remineralized in the surface and only a small fraction is exported out of the euphotic zone. This transport of biologically bound carbon to depth is commonly referred to as the biological carbon pump (BCP; Volk and Hoffert (1985).

Observations based on sediment traps moored in the bathypelagic suggest that ballasting minerals often comprise a large proportion (<50%) of the mass of sinking particles (Honjo et al., 1982). These observations led to the hypothesis that ballast minerals determine deep POC flux, by protecting the sinking organic matter from degradation and increasing particle excess density and thus sinking velocity (Armstrong et al., 2002, 2009). Correlations of different ballast materials (calcium carbonate, opal and lithogenic material) with POC flux below 2000 m suggested that the most important carrier for organic carbon to depth is $CaCO_3$, due to its high density and abundance (Klaas and Archer, 2002). Even though the correlation for opal is not as strong, it has been shown that episodic diatom blooms can entail strong export events with high transfer efficiencies (ratio of deep export over shallow export, T_{eff}) (Buesseler and Boyd, 2009; Martin et al., 2011; Rynearson et al., 2013; Smetacek et al., 2012). These occasional deviations from global correlations

illustrate that spatial variability on T_{eff} is high and that factors, other than ballast, may be important drivers for the determination of deep carbon export. Using geographically weighted regression analysis, Wilson et al. (2012) confirmed that carrying coefficients of minerals are subject to substantial spatial variability, while global means were similar to ones reported by Klaas and Archer (2002). The findings by Wilson et al. (2012) suggest that the ballast effect by itself is insufficient in determining deep carbon export and they hypothesize that the spatial variability is most likely driven by differences in ecosystem characteristics. This is in agreement with results of other studies, which outline higher T_{eff} in regenerative systems that produce tightly packed, refractory particles, compared to productive systems that produce fluffy, labile aggregates (Francois et al., 2002; Henson et al., 2012; Lam et al., 2011).
Investigating the link between community structure and export parameters is challenging in the field and faces several problems, such as lateral advection or the time lag between surface production and export (Henson et al., 2015; Stange et al., 2017). *in situ* mesocosm experiments have been suggested as an important tool to link plankton community changes with export-relevant parameters (Sanders et al., 2014). Indeed, recent *in situ* mesocosm experiments have proven to be a useful tool in investigating the link between plankton community structure and biogeochemical cycling (Bach et al., 2016b; Gazeau et al., 2016; Knapp et al., 2016; Maugendre et al., 2017; Paul et al., 2015; Riebesell et al., 2007; Schulz et al., 2013). In a long-term *in situ* mesocosm experiment, Bach et al. (2016a) investigated the influence of changes in community structure on particle sinking velocity. They found that enhanced ballasting of particulate organic matter (POC) did not automatically lead to faster sinking of particles, but was rather controlled by changes in particle porosity, which in turn were driven by differences in the food-web structure. While these results strengthen the hypothesis that community structure is important in controlling organic matter export, the determination of POC remineralization is an essential next step in order to fully understand this relation.
We therefore conducted an *in situ* mesocosm experiment during which we closely monitored changes in plankton community structure, particle sinking velocity and degradation of particulate organic matter. The experiment was conducted from September and December 2014 in the oligotrophic Central Atlantic Ocean, off the coast of Gran Canaria. After approximately three weeks of nutrient limitation, we simulated a natural upwelling event by adding collected deep water to each mesocosm. This stimulated a diatom-dominated phytoplankton bloom, which collapsed shortly after its peak.

4.3 Material and Methods

4.3.1 Experimental set-up

On September 29th 2014, we deployed nine units of the "Kiel Off-Shore Mesocosms for Future Ocean Simulations" (KOSMOS, M1-M9; Riebesell et al. (2013)) in Gando Bay, Gran Canaria (27° 55' 41" N, 15° 21' 55" W). The mesocosms consisted of an 8 m high floatation frame, which was equipped with a cylindrical bag, made of transparent polyurethane (13 m long, 2 m in diameter). Each bag was equipped with a 2 m long, funnel-shaped sediment trap. A collection cylinder was attached to the bottom of each sediment trap

Mesocosm ID	Symbol	pCO_2 [μatm] Phase 1 (t-3 - t24)	Phase 2 (t25 - t35)	Phase 3 (t37 - t55)
M1		401	374	326
M9		406	343	297
M5		502	404	427
M3		636	493	546
M7		746	571	672
M4		800	620	710
M6		976	-	-
M2		1050	748	830
M8		1195	902	944

Table 4.1: Average values for seawater pCO_2 for each experimental phase. pCO_2 values were calculated from the combination of TA and DIC using CO2SYS (Pierrot et al., 2006) with the carbonate dissociation constants (K1 and K2) of Lueker et al. (2000). A detailed description of the determination of the carbonate chemistry is given by Taucher et al., accepted.

and connected to the surface through a silicon tube (1 cm in diameter)(Boxhammer et al., 2016).
The mesocosm bags, initially folded for ease of transportation and to avoid damage, were lowered and thereby filled with approx. 35 m^3 of surrounding seawater immediately after deployment. The upper and lower openings of the bags were covered with meshes (3 mm mesh size) during the lowering process, in order to exclude nekton, large zooplankton and debris from the enclosed water mass. The mesocosms were left floating for 4 days to allow rinsing of the mesocosm walls and to ensure homogenous mixing of the water column inside the bags. On the 27th September, divers removed the meshes from the openings and attached the sediment traps to the bottom of the mesocosms. Enclosure of the water columns on day -4 (t-4) marked the beginning of the experiment. The first sediment trap sampling was performed on the next day (t-3) and continued every other day after that. The last regular sampling of the sediment traps was on the 25th November (t55).
Between t0 and t6, seven of the nine mesocosm units were incrementally enriched with CO_2 aerated seawater until they reached target CO_2 concentrations. A detailed protocol of the procedure is described in Taucher et al. (accepted).

4.3.2 Sampling and processing of water column parameters

Samples for the determination of chlorophyll *a* concentrations and particulate organic carbon (POC) were taken every other day between 09:00 A.M. and 12:00 P.M. Samples were taken with a vacuum pumping system, which collects equal amounts of water from

each depth of the mesocosms (0-13m). Samples were stored in 20 L carboys and transferred in a temperature-controlled room (set to 15 °C) immediately after arriving at the laboratory facilities. Carboys were carefully mixed before subsamples for the individual measurements were taken. Subsamples for chlorophyll *a* and POC were filtered with a gentle vacuum (<200 mbar) on glass fibre filters. Chlorophyll *a* samples were immediately frozen at -80 °C and later analysed using reverse-phase high-performance liquid chromatography (HPLC) following Van Heukelem and Thomas (2001). POC filters were immediately frozen at -20 °C after filtration, stored in glass petri dishes and fumed in hydrochloric acid (37%) for 2 h before measurement. POC concentrations were determined using an elemental analyser (EuroEA) following Sharp (1974). Flow cytometry subsamples were taken directly from the 20 L carboys and measured within 3 h using an Accuri C6 flowcytometer. Gates were set based on the forward scatter or red fluorescence signals except for the *Synechococcus* group where the orange instead of the red fluorescence signal was used to distinguish them from bulk phytoplankton. The size of different phytoplankton groups was determined by fractionation with a variety of polycarbonate filters (0.2, 0.8, 2, 3, 5, 8 μm) following Veldhuis and Kraay (2000). We distinguished between picoeukaryotes (Pico; 0.2-2 μm), *Synechococcus*-like autotrophs (Synecho; 0.6-2 μm), small nanoautotrophs (Nano I; 2-5 μm), larger nanoautotrophs (Nano II; 5-8 μm) and microautotrophs (Micro; >8 μm). We further calculated the contribution of these different phytoplankton groups to total fluorescence, and then the ratio of groups smaller 2 μm (PICO) to groups larger 2 μm (NANO). For the determination of microzooplankton abundance, unfiltered subsamples of 250 mL volume were taken from the 20 L carboys and transferred into brown glass bottles. Subsamples were preserved with acidic Lugol's solution (1-2% final concentration) and kept in the dark until measurement. Abundances of the major groups, i.e. ciliates and heterotrophic dinoflagellates, were determined following Utermöhl (1931) using an inverse light microscope (Zeiss Axiovert 25). Samples for the determination of mesozooplankton abundance were collected on nine occasions throughout the experiment with an Apstein net (55 μm mesh size, 17 cm diameter opening).

4.3.3 Sampling and processing of sedimented POM

Sedimented particulate matter was collected every other day between 08:00 and 09:00 A.M. Samples were collected by attaching a weak vacuum to the hose that connects the collection cylinder of the sediment trap to the surface. We collected the sedimented matter in 5 L Schott Duran glass bottles, which were subsequently stored in large coolers (Coleman) filled with seawater for the remaining sampling process. Back onshore, quantities of the sediment trap samples were determined gravimetrically. Afterwards, we homogenized the samples by gently shaking them and subsequently transferring 60 mL subsamples with a serological pipette into screw cap plastic cups for the determination of sinking velocity and oxygen consumption. The remaining particle suspension was concentrated by centrifugation, freeze-dried and ground in order to get an homogenous powder for further biogeochemical analysis. For a detailed description of the process see Boxhammer et al. (2016). The powder was then analyzed for biogeochemical parameters, including total particulate carbon, nitrogen and phosphorous (TPC, TPN, TPP), particulate organic carbon (POC), biogenic silica (BSi) and aluminum as a tracer for lithogenic material.

For the determination of TPC, TPN and POC, duplicate subsamples (2 mg) of the sediment powder were transferred into tin (TPC, TPN) and silver cups (POC). POC subsamples were acidified for 1 hour with 1 M HCl and dried at 50 °C over night. Measurements were done using an elemental analyzer (Euro EA-CN, Hekatech), which was calibrated with acetanilide (C_8H_9NO) and soil standard (Hekatech, catalogue number HE33860101) prior to each measurement run. Particulate inorganic carbon (PIC) was calculated by subtraction of POC from TPC. For the analysis of BSi, subsamples of 1 mg were transferred into 40 mL plastic vials and heated for 135 minutes with NaOH (0.1 M) at 85 °C. Subsequently, samples were neutralized using H_2SO_4 (0.05 M) and analyzed by spectrophotometry following Hansen and Koroleff (1999).

4.3.4 Sampling of water for oxygen consumption measurements

Water samples for oxygen consumption measurements were collected with an integrated water sampler (IWS, Hydro-Bios). Samples for oxygen measurements were directly filled headspace-free into the incubation bottles (250 mL, Schott Duran) on board of the sampling boats. The bottles were kept in dark plastic boxes, covered with aluminum foil. Similar to the sediment trap samples, these boxes were also stored in large coolers for the remaining sampling process to avoid heating. Upon arrival in the laboratory, all bottles were kept in a dark water bath at *in situ* temperature for at least 2 h to ensure homogenous temperatures at the start of the incubation.

4.3.5 Measurement of oxygen consumption rates

We measured oxygen consumption in sinking particulate matter during nine incubations over the course of the experiment (t11, t19, t23, t29, t33, t37, t41, t47 and t53). Incubations were conducted in the dark and lasted 33-35 hours. Oxygen consumption was monitored using non-invasive oxygen sensitive micro sensor spots (PreSens, Germany) that were calibrated at air saturation and anoxic conditions. The PSt6 sensor spots have a measurement range of 0 - 1.8 mg/L dissolved oxygen, a resolution of ± 0.02 μmol at 2.8 μmol and a response time of $<$40 s. The sensors were mounted with silicon glue into 250 mL square glass bottles (Duran Group Inc., Mainz, Germany). Oxygen measurements were done using a handheld optical oxygen meter (Fibox 4, PreSens, Germany).
For each incubation, seven bottles were filled with unfiltered seawater from each mesocosm as described in Sect. 4.3.4. We then added 1 - 3 mL, (depending on the density of the organic matter) of the particulate matter collected in the sediment trap of the respective mesocosm on that day to four bottles. The three remaining bottles were incubated without the addition of sedimented matter and used as blanks. Additionally, three bottles were filled with unfiltered seawater from the Atlantic Ocean, collected next to the mesocosms and sterile filtered seawater (0.2 μm pore size), respectively, as procedural controls. Each incubation thus constituted of 69 bottles (7 bottles x 9 mesocosms + 3 x filtered seawater + 3 x Atlantic). Bottles were placed on a slowly rotating plankton wheel and incubated at *in situ* temperature of 20 °C for up to 39 hours.
Oxygen measurements were performed 6-7 times during each incubation. The first measurement was always conducted immediately after the addition of particulate matter to the replicate bottles. The second measurement was taken approx. 2 h after the first,

ensuring complete mixing of the water and stable and reliable oxygen measurements. Subsequent measurements were performed in 8 hour intervals. The Fibox4 handheld oxygen meter automatically corrects for salinity and temperature. We used the daily average salinity determined with a CTD on the day of incubation. Temperature was measured in a dummy bottle that was treated similar to the incubation bottles.

4.3.6 Calculation of carbon-specific respiration rates

After the incubation, the entire content of the bottles was filtered on combusted glass fibre filters (pore size 0.7, GF/F, Whatman). All filters were fumed with hydrochloric acid (37%) for 2 h to remove inorganic carbon and dried at 50 °C over night. POC was then determined as described in Sect. 4.3.3. We calculated the oxygen consumption in each bottle using the slope between the individual oxygen measurements, described in Sect. 4.3.5. We only considered time points when the decline in oxygen was linear, but the slope was always calculated from 3 or more individual measurements. Mean blank-slopes were subtracted from each replicate bottle. Respiration rates were normalized using the POC measurements from each bottle. Carbon-specific respiration rates were then calculated assuming a respiratory quotient of 1 mol O_2 : 1 mol CO_2.

4.3.7 Measurement of sinking velocity and particle properties

Sinking velocity was measured following a modified approach of the method described in Bach et al. (2012). In brief, the sediment trap subsample was transferred into a settling chamber (1x1 cm), which is mounted in a modified version of the FlowCam. We used a larger settling chamber compared to Bach et al. (2012), in order to enable the measurement of larger particles and decrease wall effects. Sinking particles were recorded individually at *in situ* temperatures of 20 °C for approx. 20 minutes. The settling chamber was additionally ventilated by a small fan to avoid convection through temperature differences.. After the recording process, we evaluated the data with the MATLAB script provided by Bach et al. (2012) to evaluate the sinking velocity of each recorded particle, discarding particles that were out of focus or did not sink in a straight line. Additionally to the sinking velocity, the imaging software of the FlowCam also recorded a number of optical parameters, describing the shape and color of the measured particles. These include the particle size as equivalent spherical diameter (ESD) and the particle intensity. The latter is defined as the average grayscale value of the pixels making up a particle and can range from 0 to 255. High intensities depict very bright particles, which can be indicative for holes or in general very loosely packed matter. On the other hand, low intensities are characteristic for dense and tightly packed particles. For the analysis of sinking velocity and particle properties, all particles were grouped into 6 classes according to their ESD (40 - 90 μm, 80 - 130 μm, 120 - 180 μm, 170 - 260 μm, 240 - 400 μmand 380 - 1000 μm). The overlap between classes was necessary in order to avoid exclusion of particles exactly on the border.

4.3.8 Calculation of the remineralization length scale

The remineralization length scale L (m^{-1}) was calculated by dividing the carbon-specific respiration rate with the particle sinking velocity. L therefore gives an estimation on how much carbon is respired per meter. Sinking velocities were calculated based on the sinking velocity vs. particle size relationship acquired with the FlowCam method (Sect. 4.3.7) and the mean *in situ* particle size of each mesocosm and day. The latter was based on measurements of the *in situ* particle size spectrum using the submersible camera system KielVision (Taucher et al., in prep). This was done because our sinking velocity measurements are a qualitative measure and do not necessarily reflect the size distribution of particles in the mesocosms.

4.3.9 Data analysis

The temporal changes in POC flux, ballasting mineral load, sinking velocity and particle properties were analyzed using the daily averages of all mesocosms. Unfortunately, Mesocosm 6 was irreparably damaged on t26 and thus excluded from the statistical analysis of phases II and III. Curve-fitting was done using the curve-fitting toolbox (MATLAB). Statistical analyses were undertaken using the software R, version 3.3.1(R Core Team, 2013).

4.4 Results

4.4.1 Temporal development of chlorophyll *a*, suspended and sedimented POC and experimental phases

The experiment started in oligotrophic conditions, with concentrations of all inorganic nutrients close to detection limit (data presented in Taucher et al., (accepted)). Chlorophyll *a* concentrations were correspondingly low during this period and averaged at approximately 0.1 μg L^{-1} (Fig. 4.1A). On t24, deep-water was added to all mesocosms, which increased inorganic nutrient concentrations to 3.15, 0.17, and 1.60 μmol L^{-1} for NO^{3-}+NO^{2-}, PO_4^{3-}, and $Si(OH)_4$, respectively. This stimulated a phytoplankton bloom with peak chlorophyll *a* concentrations of 2.61 μg L^{-1} on t28. Biomass formation increased correspondingly with a slight delay of about 1-2 days (Fig. 4.1B). While chlorophyll *a* concentrations decreased within a few days after the peak, water column POC remained elevated compared to pre-bloom conditions until the end of the experiment. We defined three experimental phases based on chlorophyll *a* concentrations: Phase I (t-3 to t24), Phase II (t25 to t35), and Phase III (t37 to t55). We observed a strong temporal delay between POC build-up in the water column and its sedimentation to the sediment traps (Fig. 4.1C). We therefore defined experimental phases differently for sediment trap based parameters. The first $phase_{sed}$ (t-3 to t33) was characterized by very low sedimentation of POC to the sediment trap (see Fig. 4.1C). During $phase_{sed}$ II (t35 - t45), the majority of organic matter produced during the phytoplankton bloom sank out, leading to the highest POC sedimentation rates of the experiment. Throughout $phase_{sed}$ III (t47 - t55), sedimentation rates were low again, but still larger compared to those observed during $phase_{sed}$ I. We observed clear differences between mesocosms with respect to the time of

peak sedimentation during $phase_{sed}$ II. M3 and M5 peaked earliest, while sedimentation rates of the other mesocosms increased more steadily until a peaks between t39 and t43.

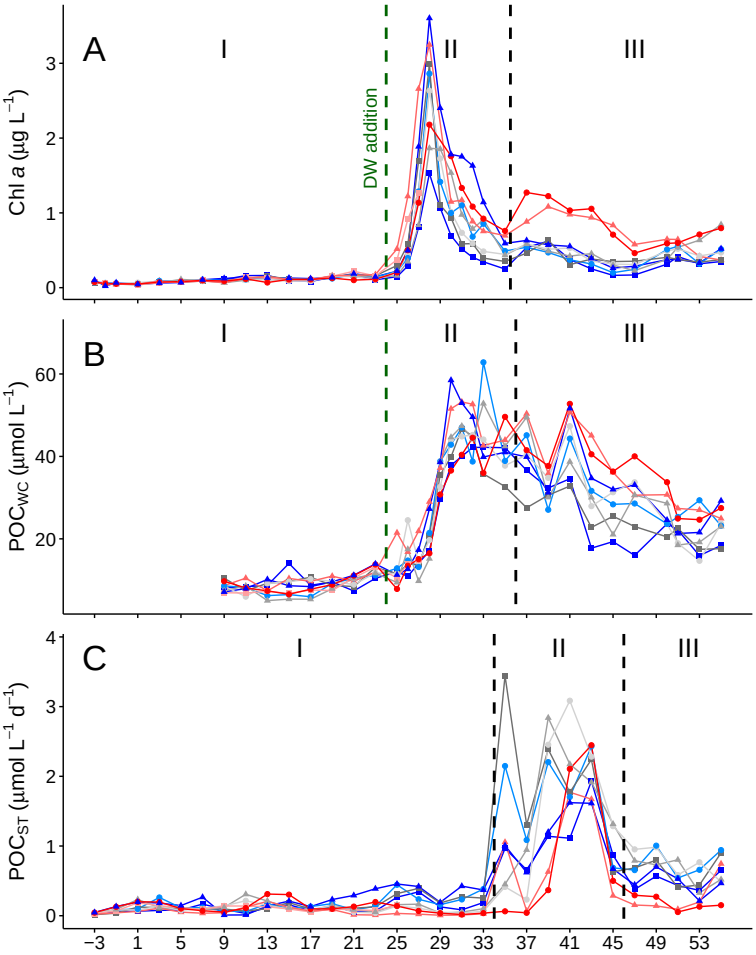

Figure 4.1: Temporal development of **(A)** chlorophyll a concentrations, **(B)** water column POC concentrations and **(C)** sedimented POC from the sediment traps. The three different phases indicated with I, II and III and separated by the dashed vertical lines differ for the water column and sediment trap, as described in Sect. 4.4.1. Colours and symbols are given in Table 4.1.

4.4.2 Plankton community composition

During the oligotrophic phase of the experiment, the phytoplankton community was dominated by picophytoplankton, with overall little contribution of nano- and microphytoplankton. A bloom of (pico-) cyanobacteria (*Synechococcus* sp.; 0.6 - 2 μm) developed during this phase, with a peak in abundances around t11 (Fig. 4.2). This is reflected by relatively high pico/nano ratios of up to 2 at t11. *Synechococcus* abundances declined towards the end of phase I, and we observed increasing abundances of picoeukaryotes (0.2 - 2 μm) between t13 - t23. The phytoplankton community underwent a significant change after the addition of nutrient-rich deep-water on t24. We observed substantial increases in abundance of all size classes, microphytoplankton (>10 μm), and large chain-forming

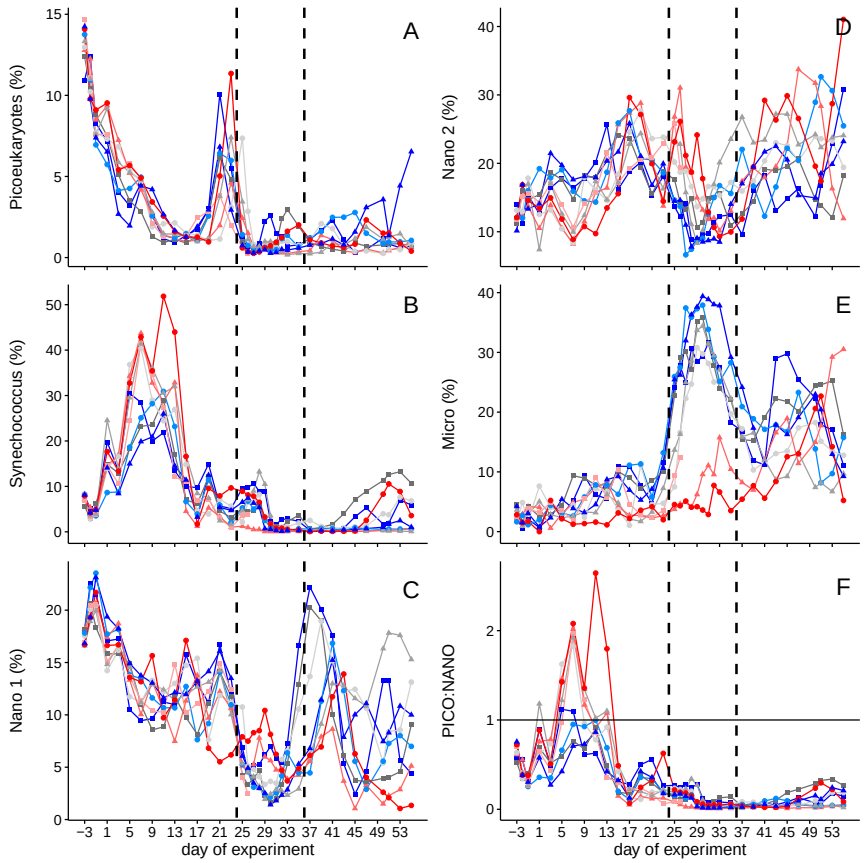

Figure 4.2: Phytoplankton community composition based on flow cytometry measurements and given in contribution to total fluorescence in (%) by **(A)** picoeukaryotes, **(B)** *Synechococcus*, **(C)** Nano 1 (2 - 5 μm), **(D)** Nano 2 (5 - 8 μm), **(E)** Micro (>8 μm), **(F)** the ratio of PICO:NANO, as described in Sect. 4.3.2. The dashed vertical lines indicate the experimental phases, described in Sect. 4.4.1. Colours and symbols are given in Table 4.1.

diatoms (*Leptocylindrus* sp., *Guinardia* sp., and *Bacteriastrum* sp.) started to dominate the community in terms of contribution to chlorophyll *a* and biomass. Other groups that contributed to a lesser extend to chlorophyll *a* concentrations were dinoflagellates and prymnesiophytes (mostly *Phaeocystis* sp.). Correspondingly, pico/nano ratios decreased towards the peak of the bloom on t28. During the beginning of phase III, microphytoplankton was still the biomass-dominanting group. However, we observed increasing abundances in both groups of nanophytoplankton (NANO I (2 - 5 μm) and NANO II (5 - 8 μm)) after t37 and again towards the end of the experiment. Similarly, abundances of *Synechococcus* sp. increased as well, but not equally in all mesocosms. Micro- and mesozooplankton concentrations were low throughout phase I, except for the group of appendicularians, where we observed intermediate abundances of 1000 - 3000 individuals per m^3. We observed a substantial increase in abundances of all zooplankton groups in most mesocosms with a short temporal delay to the phytoplankton bloom. During the post-bloom phase, grazer abundances continued to increase further, except for appendicularians.

4.4.3 Contribution of mineral ballast to sinking POM

We observed a very high contribution of PIC to the sinking POM at the beginning of the experiment (45% on t-3, Fig. 4.3A). This contribution decreased throughout phase^{sed} I and stayed more or less constant after t25. While the overall trend of PIC/POC during phase^{sed} I was declining, we observed a small peak around t19. This peak coincided with a local dust event, which occurred between t16 and t22 and was estimated with a total dry deposition of 230 mg m^{-2} of Saharan dust in the study area (D. Gelado-Caballero, pers. comm.). BSi/POC ratios indicate that the contribution of biogenic silica to the sinking POM was comparatively low throughout the experiment, with highest contributions at the start of the experiment and during the phase of highest mass flux (Fig. 4.3B). While PIC was the dominant ballasting mineral in the beginning of the experiment, BSi became more important during the period of highest mass flux.

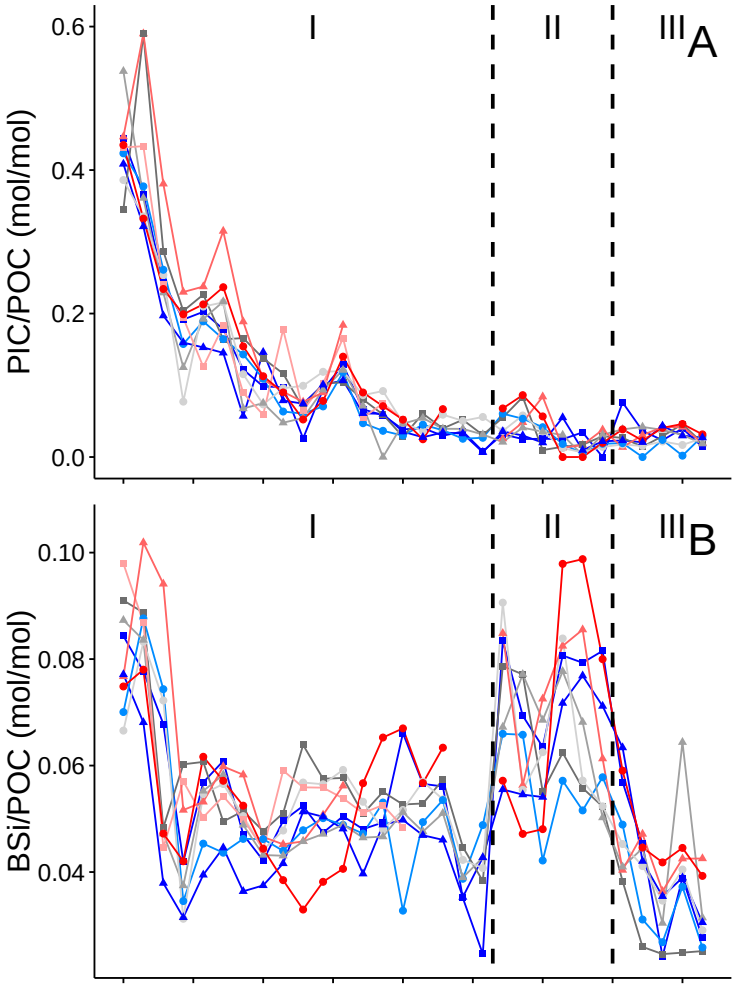

Figure 4.3: Molar ratios of **(A)** PIC to POC and **(B)** BSI to POC depicting the contribution of ballast minerals to the organic matter flux in the sediment traps. The dashed vertical lines indicate the experimental phases, described in Sect. 4.4.1. Colours and symbols are given in Table 4.1.

4.4.4 Sinking velocity and particle properties

We observed very large sinking velocities in almost all mesocosms on the first two sampling days (Fig. 4A-F). For the remainder of phase^{sed} I, mean sinking velocities of smaller particles (<120 μm) followed a slightly different trend than larger (>120 μm) particles. The former showed more or less constant sinking velocities for phasesed I, with only a slight maximum around t24. However, mean sinking velocities of larger particles fluctuated more pronounced, with larger values around t5/t7 and t21/t23 and minimum values around t15. Mean sinking velocities of all size classes decreased towards the end of phase^{sed} I and continued decreasing throughout phase^{sed} II. Lowest sinking velocities of the entire experiment were observed just at the end of phase^{sed} II, after which they increased again in all size classes. Particle intensity (a proxy for porosity) constantly increased in the small size classes during phase^{sed} I, but remained more constant in particles >240 μm(Fig. 4.4G-L). During phase^{sed} II, particle intensity increased drastically in larger particles (>240 μm) and plateaued towards the end of the phase in all size classes. Subsequently, particle intensity declined until the end of the experiment. Mean particle sizes in the respective size classes did not change considerably over the course of the experiment. Average sizes in ESD were 59 (40 - 90 μm), 101 (80 - 130 μm), 145 (120 - 180 μm), 208 (170 - 260 μm), 305 (240 - 400 μm) and 532 (380 - 1000 μm).

4.4.5 Carbon-specific respiration rates

We determined carbon-specific respiration rates R_c in nine incubation experiments throughout the experiment, starting on t11. R_c averaged at approximately 0.08 d^{-1} on t11 and decreased throughout phase$_{sed}$ I with minimum mean rates of 0.03 d^{-1} on t33 (Fig 4.5C). Although the overall trend suggested declining respiration throughout phase$_{sed}$ I, we observed a small peak on t29 in mesocosms M1, M5, M7 and M9. During phase$_{sed}$ II, mean R_c increased until t41 and subsequently declined until the end of the experiment. We do not show the standard deviation between replicate measurements in the plot, in order to improve the visibility. The agreement between the four replicate measurements was quite good, with an average standard deviation of 20% of the mean rate measurement.

4.4.6 *In situ* particle sizes and remineralization length scales

We observed a small peak in mean *in situ* particle size during the middle of phase$_{sed}$ I (t11).Mean particle size decreased again After this small peak until t19 and stayed low until t33. Corresponding with the increased mass flux to the sediment traps, particle sizes increased in all mesocosms during phase$_{sed}$ II, but decreased again in phase$_{sed}$ III. Sinking velocities of the mean *in situ* particle sizes were comparably high during phase$_{sed}$ I, but decrease constantly after the deep-water addition. L decreased on average from 0.0025 m^{-1} (t11) to 0.0008 m^{-1} (t33) throughout phase$_{sed}$ 1 (Fig. 4.5D). The comparably high value of M9 on t11 is caused by a combination of low sinking speeds and rather high carbon-specific respiration rates. We observed increasing variability in L between mesocosms on t29, which was mainly driven by very low values for mesocosms 2 and 8. The coinciding decrease in sinking velocities and increase in carbon-specific remineralization rates resulted in increasing L in phase$_{sed}$ II. After the peak in average L on t41, L constantly declined

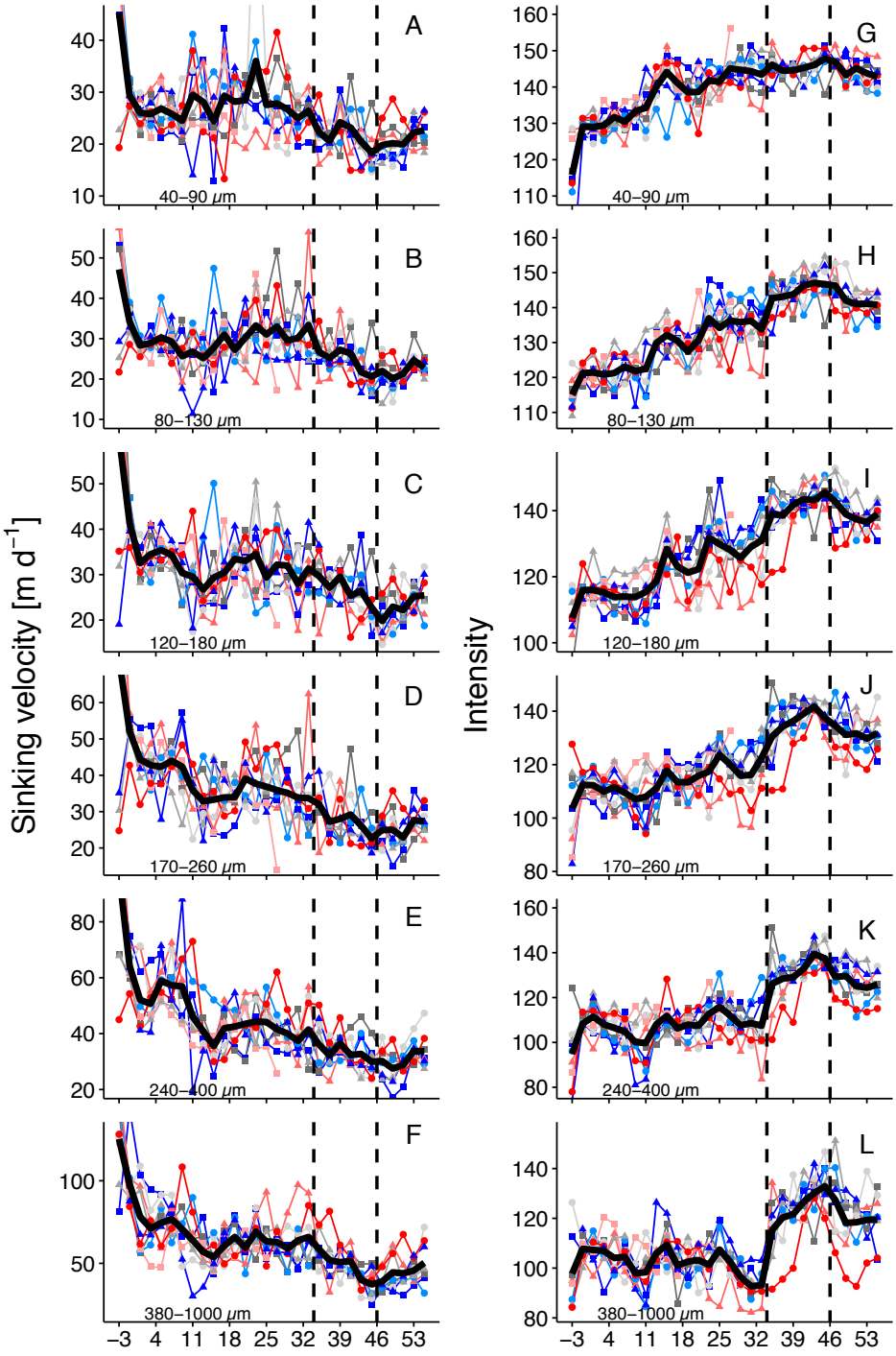

Figure 4.4: Temporal development of **(A-F)** sinking velocity of particles and their Intensity **(G-L)** averaged for each size class, defined in Sect. 4.3.7. The dashed vertical lines indicate the experimental phases, described in Sect. 4.4.1. Colours and symbols are given in Table 4.1.

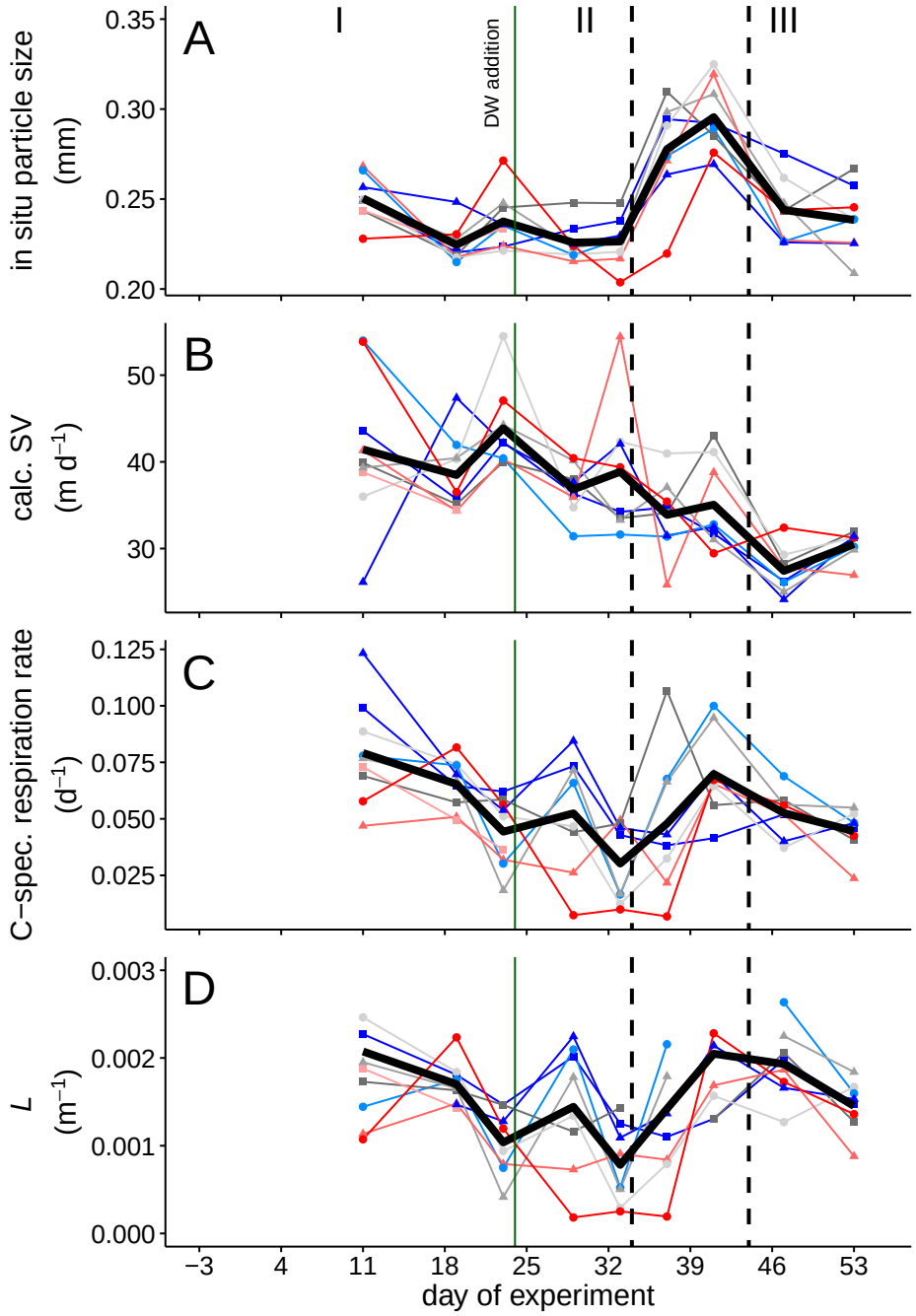

Figure 4.5: Temporal development of **(A)** *in situ* particle size spectrum measured with the *in situ* camera system KielVision **(B)** the calculated sinking velocity of the mean *in situ* particle size **(C)** measured carbon-specific respiration rate and **(D)** the calculated remineralization length scale L. The dashed vertical lines indicate the experimental phases, described in Sect. 4.4.1. Colours and symbols are given in Table 4.1.

towards the end of the experiment.

4.5 Discussion

4.5.1 The temporal development of sinking velocity

$Phase_{sed}$ I was characterized by low nutrient concentrations and a dominant contribution of picophytoplankton (mostly *Synechococcus* sp.) to total chlorophyll *a* concentrations (Fig. 4.1B). The latter formed a small bloom, which peaked around t11. Furthermore, PIC contributed largely to sinking POM during the first days of the experiment, but this contribution decreased rapidly towards the middle of $phase_{sed}$ I (>60% PIC on t-3; <10% on t15)(Fig. 4.3A). We observed unusually high sinking speeds during the first sampling day in all size classes, except for M7, M8 and M9. We did not find a conclusive explanation for this trend in other parameters and assume that these high sinking speeds were at least partly influenced by the closure of the mesocosms rather than driven by particle properties or mineral ballasting. However, mean sinking velocities were still comparably high after the first sampling day and decreased substantially until t15 in particles >120 μm. This indicates that $CaCO_3$ ballasting exerted a strong control on the sinking speeds of larger particles. This high contribution of $CaCO_3$ to POM during the first days of the experiment was partly due to the presence of calcifying phytoplankton (coccolithophores) and protists (foraminifera), as well as deposition of lithogenic material. Abundances of coccolithophores were rather low at the beginning of the experiment and increased slightly towards the middle of phasesed I (600 cells/L averaged over all mesocosms on t17, Wanchun Guan, unpublished data). Microscopic counts of foraminifera in sediment trap samples indicate that their contribution to sedimented POM was particularly high on t11 (S. Lischka, unpublished data), which is reflected in a small peak in PIC/POC ratios of sediment trap material and sinking velocity. Furthermore, a considerable part of PIC may have been deposited to the mesocosms by airborne lithogenic material. The latter likely originated from a large headland, which was located 100 - 200 m north of the mesocosm deployment site. As the main winds were north-westerly trade winds we expect a considerable input of dust originating from the headland. In addition, a common weather phenomenon called "Calima", which is characterized by strong north-easterly winds and known to transport Saharan dust from the African mainland to the Canary Islands. Depending on its specific origin, this Saharan dust has been shown to transport carbonate-rich compounds to the North East Atlantic Ocean (Moreno et al., 2006). We observed particularly strong winds during the first phase of the experiment, with maximum total dry deposition of dust between t16 and t22 of approx. 230 mg m^{-2} (D. Gelado-Caballero, pers. comm.). The addition of nutrient-rich deep-water on t24 had profound impacts on the plankton community composition, resulting in a shift from a pico-dominated regenerative food web, towards one, which was dominated by nano- and microplankton (mostly diatoms), characteristic for new production. The majority of the corresponding POM flux started to arrive in the sediment traps on t35, approx. 11 days after the deep-water addition. During this time, opal was the most important ballast mineral, with a contribution of up to 10% to POM (Fig. 4.3B). However, despite the increase in opal ballasting, we observed a constant decrease of sinking velocities in

all particle size classes after the deep-water addition. This decrease was particularly pronounced on t35, when sedimentation rates increased drastically. The discrepancy between increased opal ballasting and slower sinking of POM may to some extent be explained by an increase in particle porosity after the deep-water addition. In this study, we used particle intensity as a measure for the porosity of sinking aggregates (detailed explanation in 4.3.7). High values of intensity thus depict loosely packed aggregates and are indicative for high particle porosity. We observed a substantial increase in particle intensity on t35 in almost all particle size classes (Fig. 4.4G-L). Higher particle porosity may have thus compensated the increase in ballasting and resulted in decelerated sinking of particles. This is further supported by our visual inspections of sedimented POM, which showed that POM collected in the sediment traps before t35 was characterized by individually recognizable particles, while POM collected after t35 was a dense suspension of fluffy material. These observations agree well with results of a recent mesocosm study in a Norwegian fjord, where we observed exactly the same pattern - i.e. decreasing particle sinking velocities during the transition from a recycling food web to a diatom-dominated food web fueled by new nutrients (Bach et al., 2016a). Similar to the dataset presented here for the subtropical Atlantic, particle porosity also increased in the Norway study during the food-web transition. In both cases we attribute the drop in sinking velocity to an increase in aggregate porosity which cause a decrease in excess density. During $phase_{sed}$ III, particle porosity decreased again which was accompanied by increasing sinking velocities in all size classes. While the phytoplankton community was still dominated by diatoms (50 - 60% of total chlorophyll *a* concentrations), abundances of copepods and ciliates increased towards the end of the experiment (Algueró-Muñiz, in prep.). It is likely that the increase in grazer abundance resulted in stronger repackaging of POM, which in turn decreased the porosity of particles and accelerated their sinking speed. Microscopic counts of foraminifera in the sediment traps also indicate that more individuals sank out during this phase. However, PIC/POC ratios did not change much towards the end of the experiment so that the increase in sinking velocity cannot be explained by $CaCO_3$ ballasting during $phase_{sed}$ III. Overall, results of this and previous studies show that while the influence of plankton community composition on the sinking velocity of particles is complex, some overarching patterns are apparent: First, ballasting by $CaCO_3$ can exert a strong positive effect on particle sinking velocity. Second, the negative effect of opal ballasting on particle sinking velocity is often overcompensated by an increase in particle porosity. Third, pico-dominated food webs promote faster sinking compared to nano- and micro dominated food webs. In order to better illustrate the third point, we first calculated the contribution of all phytoplankton groups to total fluorescence, and then the ratio of groups smaller 2 μm (PICO) to groups larger 2 μm (NANO). We subsequently correlated this ratio with the average sinking velocity and intensity of all mesocosms on each day. We found a negative correlation for the PICO:NANO ratio and particle intensity and a positive correlation for sinking velocity over all particle size classes (Fig. 4.6S). These findings are in excellent agreement with the results by (Bach et al., 2016a) and confirm that communities dominated by larger phytoplankton groups produce particles with higher porosity and slower sinking speeds.

4.5.2 Temporal development of carbon-specific respiration rates

Overall, values for R_c observed in this experiment are on the lower end of the spectrum of R_c measured in a variety of aggregates in the laboratory. For instance, R_c measurements in diatom-aggregates produced by different species ranged between 0.05 and 0.11 d^{-1}, while R_c ranged between 0.08 to 0.21 d^{-1} in fecal pellets (Ploug et al., 2008; Ploug and Grossart, 2000). The slightly lower R_c measured in this experiment may have been caused by respiration of DOC. The addition of sediment slurry to the incubation bottles certainly also introduced DOC, which contributed to the decrease in oxygen during the incubation, but was not measured and accounted for at the end. We observed increased respiration during the periods of increased productivity, with two peaks in R_c on t11 and t41. The first peak on t11 corresponds well with the small bloom of *Synechococcus* that formed during the middle of $phase_{sed}$ I (Fig. 4.2B). The corresponding sedimented POM was characterized by overall lower C:N ratios, which may have been caused by lower intrinsic C:N ratios of *Synechococcus* (Bertilsson et al., 2003), or by less pronounced reworking of sinking matter during this time. After t11, abundances of *Synechococcus* declined again and C:N ratios of sedimented POM increased steadily until t33. This suggested that POM was more efficiently recycled in the water column and decreased in nutritional value, resulting in a constant decrease of R_c. Corresponding to the increase in mass flux, R_c increased from t37 to t41. This increase was most likely due to a higher availability of labile organic matter produced during the phytoplankton bloom, e.g. in the form of transparent exopolymer particles (TEP), which was likely caused by a stronger decoupling between grazer abundance and phytoplankton growth and thus less reworking of POM after the deep water addition. Aggregates formed by diatoms are especially rich in TEP and considered hotspots for microbial degradation (Alldredge et al., 1993; Ploug and Grossart, 2000). The measured TEP concentrations in the water column increased significantly during the diatom bloom in the water column (Fig. 4.7S) suggesting that the sedimented POM that originated from this bloom was also enriched in TEP. We further observed minimum values for R_c in times of low productivity, while R_c was generally higher in POM that originated from the pico- and microphytoplankton-dominated blooms. These findings support the general view that regions with high productivity are characterized by higher remineralization of sinking particles due to the production of more highly labile POM (Arístegui et al., 2005; Francois et al., 2002; Henson et al., 2012).

4.5.3 Changes in the remineralization length scale of POC in relation to community structure

The temporal development of L was similar to the development of R_c, with highest values during the bloom of *Synechococcus* (t11) and the diatom bloom (t41), as well as a minimum during times of low productivity (t33). This exemplifies that while ballast minerals may occasionally have an influence on the efficiency of organic matter export, the underlying control is exerted by the ecosystem structure. This emphasizes the point that the presence or absence of biominerals should instead be interpreted as an indicator for certain food-web structures.

The change in L from minimum values on t33 to a maximum on t41 further supports the hypothesis that regions dominated by diatoms are characterized by low T_{eff}, while T_{eff} is

high in regions that are characterized by low seasonality and increased recycling of organic matter (Francois et al., 2002; Henson et al., 2012; Lam et al., 2011). However, our results also suggest that the inverse correlation between phytoplankton size and T_{eff} used within this mindset does not hold true and other factors, such as the elemental composition of sinking POM or the "compactness" of aggregates may be more important in determining T_{eff}. This aligns well with a recent study by Mouw et al. (2016) who found lower T_{eff} in productive regions and high T_{eff} in oligotrophic regions, but when parsed by dominant size class, periods dominated by small phytoplankton were characterized by low T_{eff} and vice versa.

4.6 Conclusion

Understanding the relation between ecosystem structure and export relevant parameters has received increasing attention over the past decade. However, simultaneous measurements of these parameters are challenging in the field. We therefore conducted an *in situ* mesocosm experiment and closely monitored the plankton community structure, sinking velocity of particles and carbon-specific respiration of sinking POM. Our results reveal that sinking velocity was largest during periods when small phytoplankton dominated the food web and it decreased substantially after deep-water addition, when a pronounced diatom bloom developed. This temporal development is partially explained by a shift in biomineral content from $CaCO_3$ to opal, as well as an increase in particle porosity during the diatom bloom. The latter was most likely caused by the production of fluffy, TEP-rich aggregates. Carbon-specific respiration rates were highest during a small bloom of *Synechococcus* at the beginning of the experiment and during the diatom bloom and comparably low during times of low productivity. We further calculated the remineralization length scale (L) in order to evaluate the efficiency of the BCP with respect to different food-web structures. These results support the concept that productive regions dominated by diatoms are less efficient in transferring carbon to the deep ocean compared to regions characterized by pronounced recycling. However, the comparably high values of L during a small bloom of *Synechococcus* suggests that other factors than phytoplankton size, such as degradability and elemental stoichiometry of POM, have a paramount control on T_{eff}.

References

Alldredge, A. L., Passow, U., Logan, B. E., 1993. The abundance and significance of a class of large, transparent organic particles in the ocean. *Deep Sea Research Part I: Oceanographic Research Papers* 40 (6), 1131–1140.

Arístegui, J., Agustí, S., Middelburg, J. J., Duarte, C. M., 2005. Respiration in the mesopelagic and bathypelagic zones of the oceans. In: Respiration in Aquatic Ecosystems. Vol. 118. Oxford University Press, pp. 181–205.

Armstrong, R. A., Lee, C., Hedges, J. I., Honjo, S., Wakeham, S. G., 2002. A new, mechanistic model for organic carbon fluxes in the ocean based on the quantitative association of POC with ballast minerals. Deep-Sea Research Part II: Topical Studies in Oceanography 49, 219–236.

Armstrong, R. A., Peterson, M. L., Lee, C., Wakeham, S. G., 2009. Settling velocity spectra and the ballast ratio hypothesis. *Deep Sea Research Part II: Topical Studies in Oceanography* 56 (18), 1470–1478.

Bach, L. T., Boxhammer, T., Larsen, A., Hildebrandt, N., Schulz, K. G., Riebesell, U., 2016a. Influence of plankton community structure on the sinking velocity of marine aggregates. *Global Biogeochemical Cycles* , 1–21.

Bach, L. T., Riebesell, U., Sett, S., Febiri, S., Rzepka, P., Schulz, K. G., 2012. An approach for particle sinking velocity measurements in the 3-400 μm size range and considerations on the effect of temperature on sinking rates. *Marine Biology* 159 (8), 1853–1864.

Bach, L. T., Taucher, J., Boxhammer, T., Ludwig, A., Achterberg, E. P., Algueró-Muñiz, M., Anderson, L. G., Bellworthy, J., Büdenbender, J., Czerny, J., Ericson, Y., Esposito, M., Fischer, M., Haunost, M., Hellemann, D., Horn, H. G., Hornick, T., Meyer, J., Sswat, M., Zark, M., Riebesell, U., 2016b. Influence of Ocean Acidification on a Natural Winter-to-Summer Plankton Succession: First Insights from a Long-Term Mesocosm Study Draw Attention to Periods of Low Nutrient Concentrations. *PloS One* 11 (8), e0159068.

Bertilsson, S., Berglund, O., Karl, D. M., Chisholm, S. W., 2003. Elemental composition of marine *Prochlorococcus* and *Synechococcus*: Implications for the ecological stoichiometry of the sea. *Limnology and Oceanography* 48 (5), 1721–1731.

Boxhammer, T., Bach, L. T., Czerny, J., Riebesell, U., 2016. Technical note: Sampling and processing of mesocosm sediment trap material for quantitative biogeochemical analysis. *Biogeosciences* 13 (9), 2849–2858.

Buesseler, K. O., Boyd, P. W., 2009. Shedding light on processes that control particle export and flux attenuation in the twilight zone of the open ocean. *Limnology and Oceanography* 54 (4), 1210–1232.

Francois, R., Honjo, S., Krishfield, R., Manganini, S., 2002. Factors controlling the flux of organic carbon to the bathypelagic zone of the ocean. *Global Biogeochemical Cycles* 16 (4), 34–1–34–20.

Gazeau, F., Sallon, A., Maugendre, L., Louis, J., Dellisanti, W., Gaubert, M., Lejeune, P., Gobert, S., Borges, A., Harlay, J., Champenois, W., Alliouane, S., Taillandier, V., Louis, F., Obolensky, G., Grisoni, J.-M., Guieu, C., 2016. First mesocosm experiments to study the impacts of ocean acidification on plankton communities in the NW Mediterranean Sea (MedSeA project). *Estuarine, Coastal and Shelf Science* 186, Part A, 11–29.

Hansen, H., Koroleff, F., 1999. Determination of nutrients. In: Grasshoff, K., Kremling, K., Ehrhardt, M. (Eds.), Methods of Seawater Analysis. Wiley-VCH Verlag GmbH, Ch. 10, pp. 159–228.

Henson, S. A., Sanders, R., Madsen, E., 2012. Global patterns in efficiency of particulate organic carbon export and transfer to the deep ocean. *Global Biogeochemical Cycles* 26 (1).

Henson, S. A., Yool, A., Sanders, R., 2015. Variability in efficiency of particulate organic carbon export: A model study. *Global Biogeochemical Cycles* 29 (1), 33–45.

Honjo, S., Manganini, S. J., Cole, J. J., 1982. Sedimentation of biogenic matter in the deep ocean. *Deep Sea Research Part A. Oceanographic Research Papers* 29 (5), 609–625.

Klaas, C., Archer, D., 2002. Association of sinking organic matter with various types of mineral ballast in the deep sea: Implications for the rain ratio. *Global Biogeochemical Cycles* 16 (4).

Knapp, A. N., Fawcett, S. E., Martínez-Garcia, A., Leblond, N., Moutin, T., Bonnet, S., 2016. Nitrogen isotopic evidence for a shift from nitrate- to diazotroph-fueled export production in the VAHINE mesocosm experiments. *Biogeosciences* 13 (16), 4645–4657.

Lam, P. J., Doney, S. C., Bishop, J. K. B., 2011. The dynamic ocean biological pump: Insights from a global compilation of particulate organic carbon, $CaCO_3$, and opal concentration profiles from the mesopelagic. *Global Biogeochemical Cycles* 25 (3).

Le Quéré, C., Buitenhuis, E. T., Moriarty, R., Alvain, S., Aumont, O., Bopp, L., Chollet, S., Enright, C., Franklin, D. J., Geider, R. J., Harrison, S. P., Hirst, A. G., Larsen, S., Legendre, L., Platt, T., Prentice, I. C., Rivkin, R. B., Sailley, S., Sathyendranath, S., Stephens, N., Vogt, M., Vallina, S. M., 2016. Role of zooplankton dynamics for Southern Ocean phytoplankton biomass and global biogeochemical cycles. *Biogeosciences* 13 (14), 4111–4133.

Lueker, T. J., Dickson, A. G., Keeling, C. D., 2000. Ocean pCO_2 calculated from dissolved inorganic carbon, alkalinity, and equations for K1 and K2: validation based on laboratory measurements of CO_2 in gas and seawater at equilibrium. *Marine Chemistry* 70 (1-3), 105–119.

Martin, P., Lampitt, R. S., Jane Perry, M., Sanders, R., Lee, C., D'Asaro, E., 2011. Export and mesopelagic particle flux during a North Atlantic spring diatom bloom. *Deep-Sea Research Part I: Oceanographic Research Papers* 58 (4), 338–349.

Maugendre, L., Guieu, C., Gattuso, J.-P., Gazeau, F., 2017. Ocean acidification in the Mediterranean Sea: pelagic mesocosm experiments. A synthesis. *Estuarine, Coastal and Shelf Science* 186, Part A, 1–10.

Moreno, T., Querol, X., Castillo, S., Alastuey, A., Cuevas, E., Herrmann, L., Mounkaila, M., Elvira, J., Gibbons, W., 2006. Geochemical variations in aeolian mineral particles from the Sahara-Sahel Dust Corridor. *Chemosphere* 65 (2), 261–270.

Mouw, C. B., Barnett, A., McKinley, G. A., Gloege, L., Pilcher, D., 2016. Phytoplankton size impact on export flux in the global ocean. *Global Biogeochemical Cycles* 30 (10), 1542–1562.

Paul, A. J., Bach, L. T., Schulz, K. G., Boxhammer, T., Czerny, J., Achterberg, E. P., Hellemann, D., Trense, Y., Nausch, M., Sswat, M., Riebesell, U., 2015. Effect of elevated CO2 on organic matter pools and fluxes in a summer Baltic Sea plankton community. *Biogeosciences* 12 (20), 6181–6203.

Pierrot, D., Lewis, E., Wallace, D. W. R., 2006. MS Excel Program Developed for CO_2 System Calculations. ORNL/CDIAC-105a.

Ploug, H., Grossart, H.-P., 2000. Bacterial growth and grazing on diatom aggregates: Respiratory carbon turnover as a function of aggregate size and sinking velocity. *Limnology and Oceanography* 45 (7), 1467–1475.

Ploug, H., Iversen, M. H., Koski, M., Buitenhuis, E. T., 2008. Production, oxygen respiration rates, and sinking velocity of copepod fecal pellets: Direct measurements of ballasting by opal and calcite. *Limnology and Oceanography* 53 (2), 469–476.

R Core Team, 2013. R: A Language and Environment for Statistical Computing.

Riebesell, U., Czerny, J., von Bröckel, K., Boxhammer, T., Büdenbender, J., Deckelnick, M., Fischer, M., Hoffmann, D., Krug, S. A., Lentz, U., Ludwig, A., Muche, R., Schulz, K. G., 2013. Technical Note: A mobile sea-going mesocosm system - new opportunities for ocean change research. *Biogeosciences* 10 (3), 1835–1847.

Riebesell, U., Schulz, K. G., Bellerby, R. G. J., Botros, M., Fritsche, P., Meyerhöfer, M., Neill, C., Nondal, G., Oschlies, A., Wohlers, J., Zöllner, E., 2007. Enhanced biological carbon consumption in a high CO_2 ocean. *Nature* 450 (7169), 545–8.

Rynearson, T. A., Richardson, K., Lampitt, R. S., Sieracki, M. E., Poulton, A. J., Lyngsgaard, M. M., Perry, M. J., 2013. Major contribution of diatom resting spores to vertical flux in the sub-polar North Atlantic. *Deep-Sea Research Part I: Oceanographic Research Papers* 82, 60–71.

Sabine, C. L., Feely, R. A., Gruber, N., Key, R. M., Lee, K., Bullister, J. L., Wanninkhof, R., Wong, C. S., Wallace, D. W. R., Tilbrook, B., Millero, F. J., Peng, T.-H., Kozyr, A., Ono, T., Rios, A. F., 2004. The oceanic sink for anthropogenic CO_2. *Science* 305 (5682), 367–71.

Sanders, R., Henson, S. a., Koski, M., De La Rocha, C. L., Painter, S. C., Poulton, A. J., Riley, J., Salihoglu, B., Visser, A., Yool, A., Bellerby, R., Martin, A. P., 2014. The Biological Carbon Pump in the North Atlantic. *Progress in Oceanography* 129, 200–218.

Schulz, K. G., Bellerby, R. G. J., Brussaard, C. P. D., Büdenbender, J., Czerny, J., Engel, A., Fischer, M., Koch-Klavsen, S., Krug, S. A., Lischka, S., Ludwig, A., Meyerhöfer, M., Nondal, G., Silyakova, A., Stuhr, A., Riebesell, U., 2013. Temporal biomass dynamics of an Arctic plankton bloom in response to increasing levels of atmospheric carbon dioxide. *Biogeosciences* 10 (1), 161–180.

Sharp, J. H., 1974. Improved analysis for particulate organic carbon and nitrogen from seawater. *Limnology and Oceanography* 19 (6), 984–989.

Smetacek, V., Klaas, C., Strass, V. H., Assmy, P., Montresor, M., Cisewski, B., Savoye, N., Webb, A., D'Ovidio, F., Arrieta, J. M., Bathmann, U., Bellerby, R., Berg, G. M., Croot, P., Gonzalez, S., Henjes, J., Herndl, G. J., Hoffmann, L. J., Leach, H., Losch, M., Mills, M. M., Neill, C., Peeken, I., Röttgers, R., Sachs, O., Sauter, E., Schmidt, M. M., Schwarz, J., Terbrüggen, A., Wolf-Gladrow, D., 2012. Deep carbon export from a Southern Ocean iron-fertilized diatom bloom. *Nature* 487 (7407), 313–319.

Stange, P., Bach, L. T., Le Moigne, F. A. C., Taucher, J., Boxhammer, T., Riebesell, U., 2017. Quantifying the time lag between organic matter production and export in the surface ocean: Implications for estimates of export efficiency. *Geophysical Research Letters* 44 (1), 268–276.

Utermöhl, v. H., 1931. Neue wege in der quantitativen Erfassung des Planktons (mit besonderer Berücksichtigung des Ultraplanktons). *Verhandlungen der Internationalen Vereinigung für Theoretische und Angewandte Limnologie* 5, 567–596.

Van Heukelem, L., Thomas, C. S., 2001. Computer-assisted high-performance liquid chromatography method development with applications to the isolation and analysis of phytoplankton pigments. *Journal of Chromatography A* 910 (1), 31–49.

Veldhuis, M. J., Kraay, G. W., 2000. Application of flow cytometry in marine phytoplankton research: current applications and future perspectives. *Scientia Marina* 64 (2), 121–134.

Volk, T., Hoffert, M. I., 1985. Ocean carbon pumps: Analysis of relative strengths and efficiencies in ocean-driven atmospheric CO_2 changes. In: Sundquist, E., Broecker, W. (Eds.), The Carbon Cycle and Atmospheric CO_2: Natural Variations Archean to Present. Vol. 32. American Geophysical Union, Washington, D. C., pp. 99–110.

Wilson, J. D., Barker, S., Ridgwell, A., 2012. Assessment of the spatial variability in particulate organic matter and mineral sinking fluxes in the ocean interior: Implications for the ballast hypothesis. *Global Biogeochemical Cycles* 26 (4).

4.7 Supplement

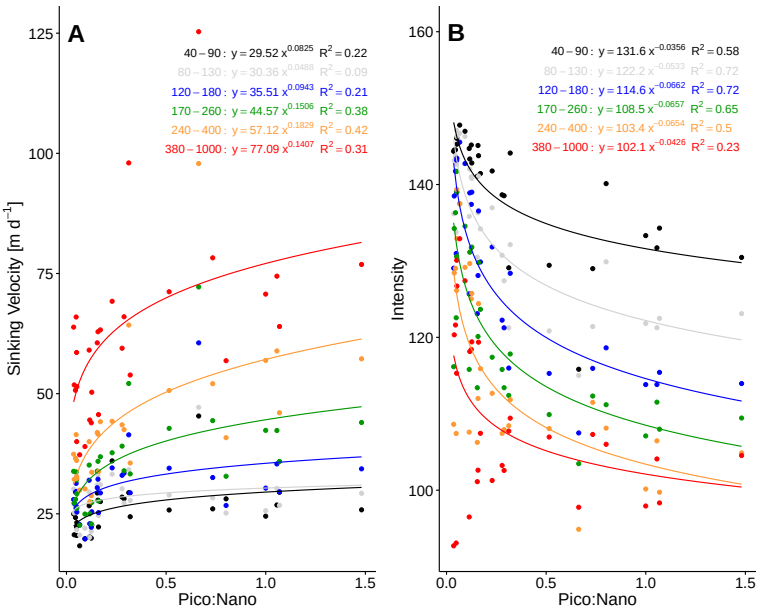

Figure 4.6: Relation between the PICO:NANO ratio and **(A)** particle sinking velocity, as well as **(B)** particle intensity. **(C)** shows the relation between intensity and sinking velocity. Each point depicts the mean of all mesocosms from one sampling day, with the colors representing the different size fractions.

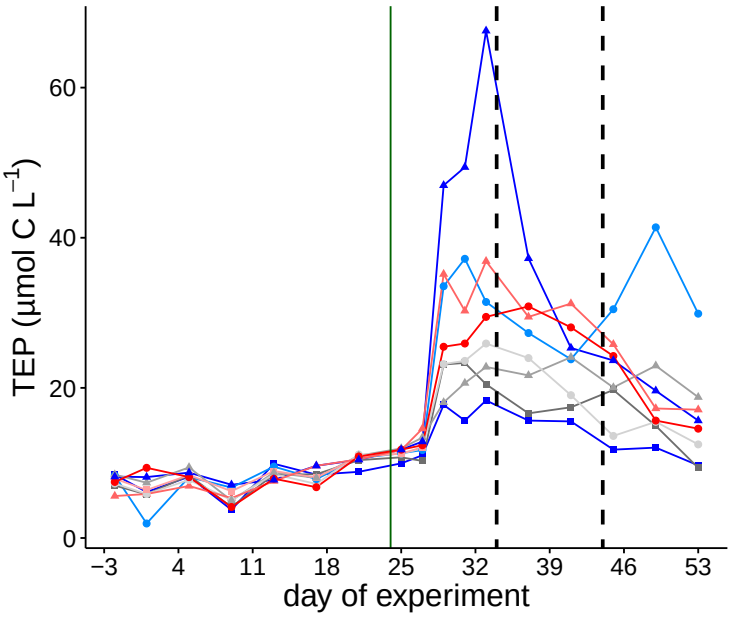

Figure 4.7: Temporal development of TEP concentrations in the water column. The green vertical line depicts the time point of deep-water addition. The dashed vertical lines indicate the experimental phases, described in Sect. 4.4.1. Colours and symbols are given in Table 4.1.

5 — Synthesis

The aim of this doctoral dissertation was to investigate how changes in plankton community structure influence export parameters and how this may affect the efficiency of the biological carbon pump (BCP). Ultimately, the goal is to identify patterns in this relation that allow for an improved parameterization of global models and accurate estimates of the BCP's strength. In the following, I will briefly summarize the key findings from chapters 2 to 4, discuss their implications for the efficiency of the BCP and outline open questions and future directions.

In chapter 2, we compared results of four *in situ* mesocosm studies with respect to the time lag between organic matter production in the surface and its sedimentation to the sediment traps. These experiments were conducted in very different biogeochemical provinces, spanning from arctic (Svalbard), over temperate (Sweden, Norway), to subtropical (Gran Canaria) regions. We found a consistent trend over all experiments, showing that the time lag decreased with an increase in the duration of chlorophyll a build-up. This correlation may partly be explained by differences in aggregation efficiencies, as well as a stronger decoupling between phytoplankton and grazer abundances during a bloom, due to the shorter generation times of autotrophs compared to their predators. Our findings indicate that *in situ* measurements of surface production and export flux have to integrate on adequate time scales in order to accurately predict the export efficiency. In chapters 3 and 4, results of an *in situ* mesocosm experiment conducted in the subtropical northeast Atlantic Ocean are presented.

For chapter 3, we investigated changes in elemental standing stocks and stoichiometry in particulate organic matter (POM) suspended in the water column and collected in the sediment traps, as well as their relative change over time. We observed clear difference in elemental stoichiometry over the course of the experiment. While C:N ratios were comparably low during a small pico-dominated bloom in phase 1, as well as during a large diatom-dominated bloom during phase 2, they rapidly increased once the blooms collapsed. These findings suggest that POM produced during the bloom was fresher and more labile compared to POM produced during times of low productivity. We further observed that sinking POM was less degraded in mesocosms with highest pCO_2, which correlated well with substantially lower abundances of zooplankton grazers.

Within the scope of chapter 4, we evaluated how changes in plankton community structure influence sinking speeds and remineralization rate of sinking POM. Based on these parameters, we also calculated changes in the remineralization length scale over time. Mean sinking velocities decreased about 20% during periods of highest mass flux, which was most likely caused by an increase in particle porosity. Carbon-specific respiration was higher in POC produced during both a small pico-dominated and a diatom-dominated bloom, compared to periods of low productivity. The temporal development of the remineralization length scale suggests that flux attenuation was highest during periods of higher productivity, which is most likely caused by an easier degradability of fresh and labile POM. Overall, these findings support the concept of a more efficient BCP in recycling systems that are commonly found in oligotrophic low latitude regions.

5.1 Towards a mechanistic understanding of the BCP

5.1.1 Assessing changes in transfer efficiency

Quantifying the efficiency of the biological carbon pump requires the assessment of the transfer efficiency (T_{eff}). I therefore used a simple one-dimensional carbon flux model, described in detail in Bach et al. (2016) with the following equation:

$$POC_z = POC_{z-1} * (\frac{R}{U} * (z - 1)) \tag{5.1}$$

In this model, POC decreases per depth interval by a rate determined through its remineralization rate R (d^{-1}) and sinking velocity U (m d^{-1}). This model further assumes that R decreases with depth as a function of temperature according to Schmittner et al. (2008):

$$R = 0.048 * 1.066^{T_z} \tag{5.2}$$

where T is the temperature in °C at a depth z in m. The temperature profile used for this model depicts the annual mean profile at N 27.5° W 15.5°, downloaded from the World Ocean Atlas data repository 2013 (https://www.nodc.noaa.gov/OC5/WOD13/). This location is in reasonable proximity (approx. 25 nm) to the mooring site of the mesocosm experiment described in chapter 2 and 3. Particle sinking velocity is parameterized to increase with depth, which is explained by the loss in organic carbon with depth (Berelson, 2002):

$$U = 0.04z + 41 \tag{5.3}$$

The parameterization of particle sinking velocity was also adapted from the University of Victoria model by (Schmittner et al., 2008), but surface sinking velocity was changed from 7 m d^{-1} to 41 m d^{-1} in order to receive a T_{eff} value of ≈24% in the control run, which corresponds to a Martin's b of ≈0.85 (Martin et al., 1987). Both particle remineralization and sinking velocity were then factorized, in order to incorporate the measured changes in each parameter over the course of the experiment. For that, I calculated the relative change of each parameter over time by dividing the daily measurement with the mean of all measurements of the respective mesocosm over the entire experiment, which was incorporated in Eq. 5.2 and 5.3:

$$R_{model} = R_{fact.} * 0.048 * 1.066^{T_z} \tag{5.4}$$

$$U_{model} = U_{fact.} * 0.04z + 41 \tag{5.5}$$

where $R_{fact.}$ and $U_{fact.}$ are the factorized changes in carbon-specific respiration rate and sinking velocity compared to the mean of the respective mesocosm over the duration of the experiment. With these assumption, I calculated the decrease in POC using Eq. 5.1 starting with the fluxes measured every second day in the mesocosms at 15 m depth. T_{eff} was then calculated as the fraction of POC at the euphotic zone depth (z=100 m) reaching the sequestration depth (z=1000 m):

$$T_{eff} = \frac{POC_{1000m}}{POC_{100m}} \tag{5.6}$$

Results of the one-dimensional model (Fig. 5.1) show a substantial change in T_{eff} over time, with an increase of ≈50% towards t33 and a steep decline afterwards. The lowest values for T_{eff} were observed on t11 (0.12, blue) and t41 (0.15, green). The resulting values for T_{eff} in this model are well within the range of T_{eff} published in other studies, where calculated T_{eff} based on POC fluxes at 2000 m depth ranged from 0.05 to 0.4 (Henson et al., 2012). In the following section, I will outline and discuss potential reasons for these differences based on the combined results of chapter 2 and 3.

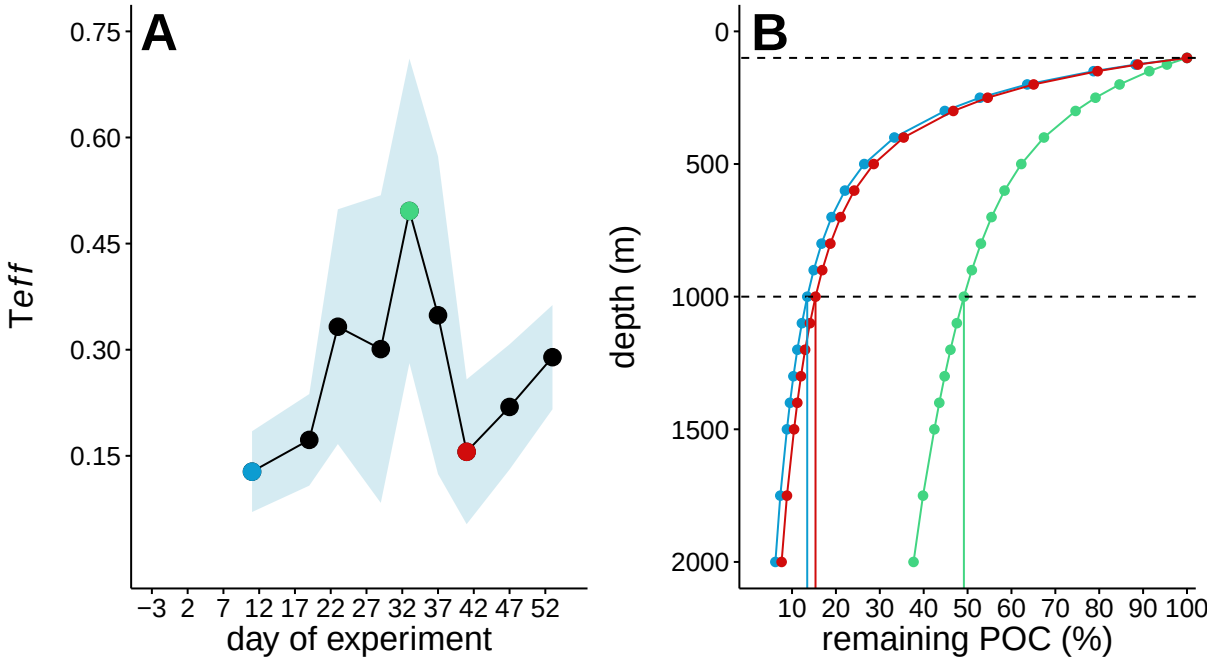

Figure 5.1: Visualisation of the results of the model described in Sect. 5.1.1. **(A)** depicts the calculated mean transfer efficiency (T_{eff}) with the standard deviation between mesocosms indicated by the lightblue ribbon. **(B)** shows the calculated mean POC decrease in %, based on the fluxes measured in the sediment traps at 15 m on days 11 (blue), 33 (green) and 41 (red). T_{eff} was calculated based on the fluxes at 1000 m and 100 m, as shown in Eq. 5.6.

5.1.2 Controls of T_{eff} and the influence of elemental stoichiometry

The fraction of POC transferred to the deep ocean primarily depends on the sinking velocity and remineralization of POM, as outlined in Eq. 5.1. The sinking velocity of particles is in turn mainly controlled by the community structure through changes in particle properties, such as the load of ballasting minerals and particle porosity. In the data presented in this doctoral dissertation, particles sank substantially faster than in previous mesocosm studies, which was most likely due to an increased aerial deposition of lithogenic material. Biogenic ballast minerals, however, only had a pronounced influence

on sinking speeds at the beginning of the experiment, when their contribution to POM was considerably high. The changes in sinking velocity over the course of the experiment were thus primarily driven by changes in particle porosity during the transition from a "regenerative" food web to a diatom bloom fueled by inorganic nutrients. These findings align well with results of a previous mesocosm experiment, where sinking velocities also decreased substantially during a diatom bloom due to increasing particle porosity (Bach et al., 2016).

Carbon-specific respiration rates were highest during times of phytoplankton blooms, both during a small bloom of *Synechococcus* and during a pronounced diatom bloom. The freshly produced organic matter during these periods was most likely rather labile and easy to degrade. Contrastingly, lowest values of carbon-specific respiration rates were observed in the period between both blooms, when productivity was very low and the produced POM was rather refractory and arguably more reworked within the food web. This illustrates that the degradability of POM has a major influence on its remineralization with depth and in combination with the sinking speeds, results in clear differences in modeled T_{eff} with highest values in periods of increased productivity and vice versa. These findings align well with current concepts in BCP research, hypothesizing that productive regions produce more labile, fluffy material, which is rapidly remineralized in the mesopelagic resulting in high export fluxes, but low transfer efficiencies (Francois et al., 2002; Henson et al., 2012; Lam et al., 2011; Wilson et al., 2012). In contrast, regions with low seasonality and "regenerative" food webs produce more refractory and densely packed organic matter, resulting in higher T_{eff} despite the comparably lower export fluxes. Results of this work further imply that the degradability of the produced POM is not necessarily dependant on phytoplankton size in controlling T_{eff}, and regions dominated by small phytoplankton species are not inevitably characterized by efficient export throughout the seasonal cycle. This conclusion is in line with a recent study by Mouw et al. (2016) who found that periods dominated by small phytoplankton can show very low T_{eff}, despite the overarching trend of higher T_{eff} in the oligotrophic ocean.

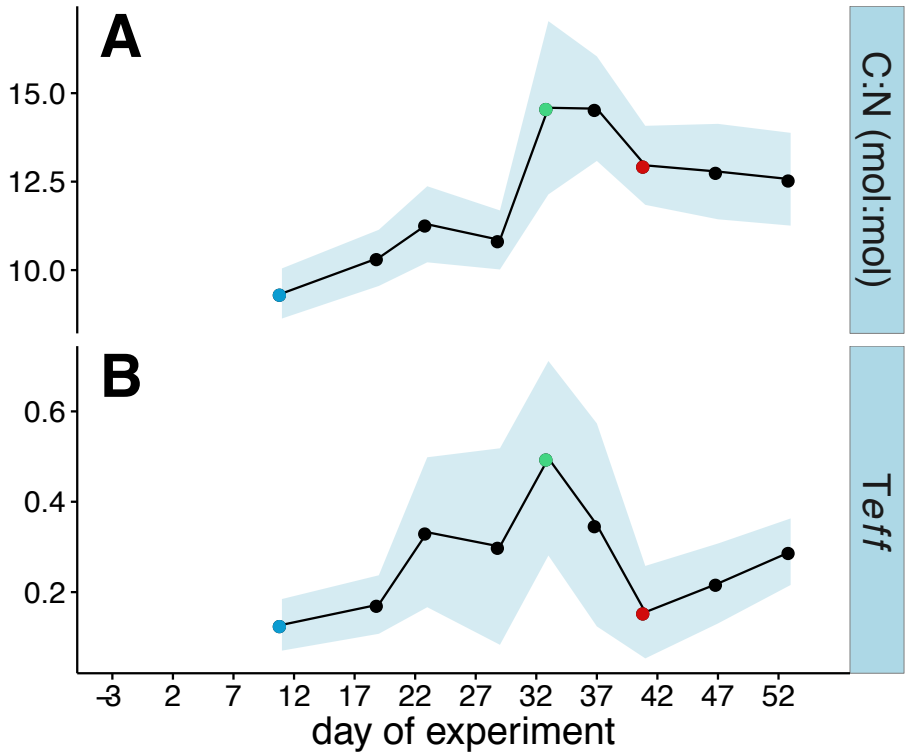

Figure 5.2: The temporal development of **(A)** the mean C:N ratio in POM collected in the sediment trap of the mesocosms and **(B)** the model results of T_{eff} described in Sect. 5.1.1. Lightblue ribbons indicate the standard deviation between mesocosms.

Furthermore, the combined results of chapter 2 and 3 reveal a second layer of complexity, namely the influence of differences in elemental stoichiometry of POM on the efficiency of carbon sequestration. With the decline in *Synechococcus* abundances, C:N ratios increased substantially from ≈9 on t11 to ≈14.5 on t33 (Fig. 5.2A). Despite the production of fresh and labile organic matter during the subsequent diatom bloom, C:N ratios in sedimented POM decreased only slightly to ≈13. This discrepancy was most likely caused by an increased production of TEP (Fig. 5.2B), which has been shown to be a typical channel for excess carbon accumulated through carbon overconsumption (Mari et al., 2001). Taking the differences in C:N stoichiometry of surface POM into account, the almost identical values of modeled T_{eff} during the *Synechococcus* and diatom bloom may not sufficiently reflect the complexity of the matter. Essentially, despite the low T_{eff}, the transport of more carbon per nitrogen to depth depicts diatoms as more efficient in our case compared to *Synechococcus* in transferring carbon to depth. The conceptual figure below summarizes this finding with the three different states of plankton community structure:

1. A phytoplankton bloom dominated by species who produce fresh material with low C:N stoichiometry (e.g. *Synechococcus*). This results in low T_{eff}, due to the high remineralization of POM. In addition, low C:N ratios of surface POM result in the removal of comparably few C per N.

2. Low production in the surface and enhanced reworking of material, resulting in

higher C:N ratios of sinking POM. This leads to high T_{eff}, due to lower remineralization, faster sinking and comparably high transfer of C per N.

3. A bloom of diatoms that results in the production of labile, yet carbon-rich compounds such as TEP. Remineralization is high, while sinking speeds are low. While this leads to T_{eff} as low as in scenario 1, C:N ratios are high resulting in proportionally more transfer of C over N.

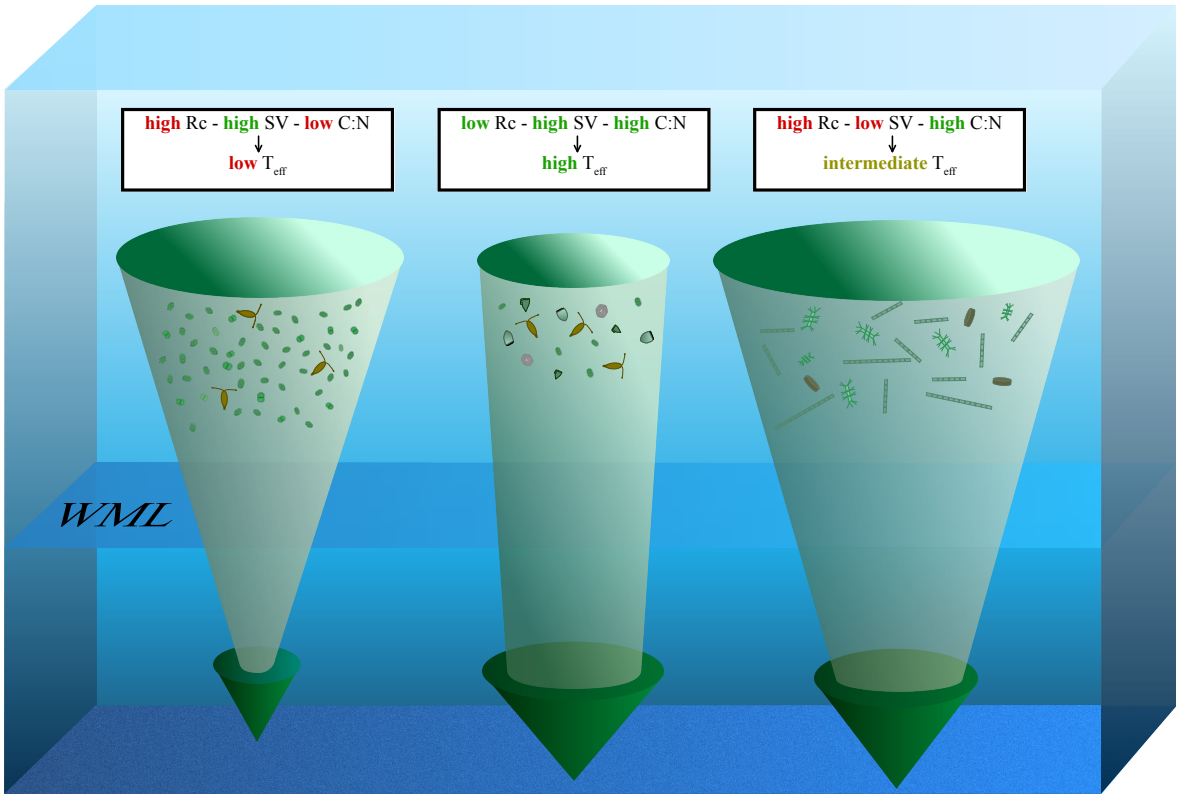

Figure 5.3: Conceptual illustration of the three different community structure scenarios, leading to differences in export relevant parameters and ultimately T_{eff}, as described in Sect. 5.1.2. The first column depicts a small bloom of picophytoplankton (*Synechococcus*) with low T_{eff}, while the second and third column show a more typical "regenerative" food web and a bloom of large diatoms with high and intermediate T_{eff}, respectively. Export relevant parameters, as presented in chapter 3 and 4 are given with colors indicating a positive (green) or negative (red) effect on T_{eff}.

5.2 Future directions

Since the first observations of marine snow by William Beebe out of a small diving bell in the early 20th century, BCP research has come a long way. Over the last decades, a growing record of *in situ* data has been acquired in the framework of several large-scale international collaborations, which created the foundation for speculation on processes

controlling the magnitude and efficiency of the BCP. Lately, the focus of the community has increasingly shifted towards processes in the epi- and mesopelagic, with particular emphasis on the link between plankton community structure and export relevant parameters. However, investigating this link in the field is difficult and requires new methodological approaches. Within the scope of this doctoral dissertation, we therefore took advantage of large-scale *in situ* mesocosms which have already proven to be a valuable tool in connecting food-web dynamics to export related parameters (Bach et al., 2016). While our results revealed a tight connection between the efficiency of the BCP and food web related differences in particle properties, key questions remain unanswered and new ones arose from this work. In this section I will thus outline what I consider necessary steps in order to further approach a mechanistic understanding of the processes that control the BCP.

5.2.1 Key question in carbon export research

This thesis emphasized gravitational settling of particles, which is considered the main pathway of carbon to depth within the BCP (Hopkinson and Vallino, 2005; Passow and Carlson, 2012). However, other means of transport have recently received increasing attention and are still largely understudied. These pathways comprise diel vertical migration (DVM) by zooplankton and the vertical transport of carbon through dissolved organic matter.

Diel vertical migration

DVMs can regionally be very important in carbon export, with an estimated contributing of 27% to total export flux in the North Atlantic (Hansen and Visser, 2016) and up to 38% at 100 m at the Bermuda Atlantic Time-series Station (BATS)(Steinberg et al., 2000). Despite its potential importance, this vertical pathway of carbon to depth is not incorporated in the majority of carbon flux models. Unfortunately, investigating this process within the scope of the experiment presented in Chapter 3 and 4 was impossible, since the depth interval of migration largely exceeds the length of mesocosms. Traditional estimations of DVM rely on zooplankton counts over a certain depth horizon and are thus very time consuming and labor intensive. As a result, our knowledge on the influence of DVM on the BCP is predominantly based on a few data sets from time-series stations such as BATS, where net samples are taken on a regular basis. Optical measurements using *in situ* camera systems (e.g. the Underwater Vision Profiler) are a promising alternative for measuring the *in situ* abundance of mesozoopankton and have become increasingly recognised within the BCP community. In combination with incubation experiments to estimate respiration and DOC excretion, ship-based assessments of the influence of DVM on carbon export could be undertaken in different biogeochemical provinces.

Grazer induced particle transformation

In addition to the quantitative influence of zooplankton on the vertical carbon flux, as described in the previous section, it is of similar importance to also investigate the qualitative change of sinking POM due to grazing. The importance of this mechanism for the BCP has been emphasized in the scope of chapter 3, where the absence of mesozooplankton grazers had a pronounced influence on the degradation of sinking particles. An elegant

way to investigate this mechanism would be to expose natural plankton assemblages to different abundances and species of zooplankton grazers, while simultaneously measuring their ingestion and excretion rates and the elemental stoichiometry of POM.

Vertical transport of DOC

The vertical transport of carbon in the form of DOC via subduction, isopycnal exchange and seasonal convective mixing is estimated with a contribution of approximately 20% to total global carbon export (Hansell, 2002). However, the high spatial and seasonal variability in this contribution is to a large extent driven by differences in DOC production and remineralization in the surface and subsurface ocean. It is therefore of great interest to investigate how these processes are affected by changes in the plankton community structure. In the light of the results presented in this work, it would be very interesting to investigate changes in the elemental composition of DOM and how the proportion of labile to refractory DOM changes over a seasonal cycle and in relation to the surface community structure.

Addressing time lag and lateral advection

As outlined in chapter 2, investigating the efficiency of the biological pump is facing two critical problems: the time lag between surface production and export measurements at depth, which conventional methods often do not account for, and lateral advection of sinking organic matter. One approach to overcome these problems is to increase and most importantly match the integration time scale of primary production and export estimates, as done recently with the introduction of the ThE_i ratio. However, the temporal resolution of this approach may be too short to unravel the short-term fluctuations in food-web structures and their influence on export relevant parameters. In contrast, experimentation in a Langrangian frame is logistically more challenging, but a very promising alternative for future investigations. The latter will be a key objective in the framework of the EXport Processes in the Ocean from Remote Sensing - project (EXPORTS, Siegel et al. (2016)).

5.2.2 The BCP in a future ocean

As a consequence of the anthropogenic perturbation of the earth's climate system, the oceanic realm already faces a variety of changes, which are predicted to intensify within the next decades. Such changes include ocean warming, acidification, deoxygenation and increased stratification. Since the mechanisms controlling the BCP are still not completely unraveled, projections about carbon export in the future are still largely uncertain.
For instance, a shoaling of the lysocline due to increasing ocean acidification could result in an overall decrease of carbon export under the premise that ballast minerals such as $CaCO_3$ exert the dominant control (Tyrrell, 2008). This in turn would result in a positive feedback to the increasing atmospheric CO_2 concentrations. However, if the concept of a community-structure controlled BCP, as outlined in this work, holds true, future scenarios may look very different. The warming-driven increase in stratification is predicted to decrease the nutrient supply to the surface ocean, resulting in the spreading of subtropical gyres and thus recycling-dominated food webs (Bopp et al., 2005; Sarmiento et al., 2004). In the past, this has been interpreted to result in a less efficient BCP, due to a decrease in

blooms of large phytoplankton such as diatoms in temperate regions (Bopp et al., 2005). However, results of this thesis in concert with a growing body of literature, portrait a different scenario, where carbon may be sequestered more efficiently in the future ocean leading to an overall decrease in atmospheric CO_2 concentrations. At the same time, the increasing temperatures are likely to directly influence the efficiency of the BCP by increasing bacterial activity, which may result in a more effective microbial loop and thus lower T_{eff} (Marsay et al., 2015). How these direct and indirect effects of ocean warming will collude is yet to be determined.
Large uncertainty also exists with regards to the influence of expanding oxygen minimum zones on the efficiency of the BCP. Possible consequences for vertical carbon transfer could be both negative due to the avoidance of migration into oxygen depleted waters by mesozooplankton (Hauss et al., 2016), and positive due to a decrease in particle remineralization compared to oxygenated waters (Keil et al., 2016; Van Mooy et al., 2002). In order to accurately predict BCP changes in a future ocean, we need to further expand our understanding of the processes controlling this mechanism on a regional and temporal scale.

5.2.3 Towards a global model of the BCP: Assembling the puzzle

As outlined in the previous sections, predictions on how the BCP may change in a future ocean require a more thorough understanding of the controlling mechanisms on a regional and seasonal scale. As suggested by Passow and Carlson (2012), a first step would be to aim for mechanistically realistic models that incorporate the regional food-web structure. As a starting point, Longhurst's concept of biogeochemical provinces (Longhurst et al., 1995) may serve as a reference for a suitable subdivision of the oceans.
Within this framework, it is recommendable that regions where anthropogenically induced stressors may be most pronounced may be given investigative priority over others. In this mindset, Eastern Boundary Upwelling Systems (EBUS), such as the Humboldt, Benguela, California or Canary system may be particularly interesting, since they are predicted to experience the simultaneous influence of ocean warming, ocean acidification and ocean deoxygenation. As outlined in Sect. 5.2.2, current knowledge on how the concurrence of these stressors will affect the plankton community structure and thus the efficiency of the BCP is very limited and understanding these systems may provide valuable insights in how the sequestration of carbon by the oceans may change in the future. While the urgency of investigating these systems with regards to the increasing anthropogenic influence is apparent, the ultimate goal of a mechanistic understanding of the BCP requires substantial effort in other regions, such as the oligotrophic gyres, the Southern ocean, the western equatorial pacific or the Indian Ocean. In consideration of the projected spreading of oligotrophic regions in a future ocean and their global contribution to primary production, they, too, should be given investigative priority to further unravel the relation of plankton community structure and carbon export in oligotrophic regions. This is further supported by the substantial variability in T_{eff} within a comparably short period of time reported in this dissertation.
Fortunately, several promising international programs have recently been initiated, such as the EXPORTS (Siegel et al., 2016) and the Controls over Ocean Mesopelagic Interior Carbon Storage (COMICS, Sanders et al. (2016)) program. These projects will take

advantage of a variety of different methodological approaches, including e.g. satellite imaging, sediment trap and glider deployments and ship-based experimentation. In addition, the vision of an increasing number of bottom-moored observational platforms like the GBF-O (Honjo et al., 2014) may extent our very limited knowledge acquired from the few time-series stations available. Unfortunately, none of the international programs involve the use of *in situ* mesocosms. This doctoral dissertation exemplifies that the latter are particularly suited for investigating the close connection between changes in plankton community structure and export relevant parameters. As such, much-needed insight can be gained by further taking advantage of this tool in BCP research.

References

Bach, L. T., Boxhammer, T., Larsen, A., Hildebrandt, N., Schulz, K. G., Riebesell, U., 2016. Influence of plankton community structure on the sinking velocity of marine aggregates. *Global Biogeochemical Cycles* , 1–21.

Berelson, W. M., 2002. Particle settling rates increase with depth in the ocean. *Deep Sea Research Part II: Topical Studies in Oceanography* 49 (1-3), 237–251.

Bopp, L., Aumont, O., Cadule, P., Alvain, S., Gehlen, M., 2005. Response of diatoms distribution to global warming and potential implications: A global model study. Geophys. Res. Lett. 32 (19), L19606.

Francois, R., Honjo, S., Krishfield, R., Manganini, S., 2002. Factors controlling the flux of organic carbon to the bathypelagic zone of the ocean. *Global Biogeochemical Cycles* 16 (4), 34–1–34–20.

Hansell, D. A., 2002. DOC in the Global Ocean Carbon Cycle. Biogeochemistry of Marine Dissolved Organic Matter , 685–715.

Hansen, A. N., Visser, A. W., 2016. Carbon export by vertically migrating zooplankton: An optimal behavior model. *Limnology and Oceanography* 61 (2), 701–710.

Hauss, H., Christiansen, S., Schuette, F., Kiko, R., Lima, M. E., Rodrigues, E., Karstensen, J., Loescher, C. R., Koertzinger, A., Fiedler, B., 2016. Dead zone or oasis in the open ocean - Zooplankton distribution and migration in low-oxygen modewater eddies. *Biogeosciences* 13 (6), 1977–1989.

Henson, S. A., Sanders, R., Madsen, E., 2012. Global patterns in efficiency of particulate organic carbon export and transfer to the deep ocean. *Global Biogeochemical Cycles* 26 (1).

Honjo, S., Eglinton, T. I., Taylor, C. D., Ulmer, K. M., Sievert, S. M., Bracher, A., German, C. R., Edgcomb, V., Francois, R., Iglesias-Rodriguez, M. D., van Mooy, B., Repeta, D. J., 2014. Understanding the role of the biological pump in the global carbon cycle: An imperative for ocean science. Oceanography 27 (3), 10–16.

Hopkinson, C. S., Vallino, J. J., 2005. Efficient export of carbon to the deep ocean through dissolved organic matter. *Nature* 433 (7022), 142–145.

Keil, R. G., Neibauer, J. A., Biladeau, C., Van Der Elst, K., Devol, A. H., 2016. A multiproxy approach to understanding the "enhanced" flux of organic matter through the oxygen-deficient waters of the Arabian Sea. *Biogeosciences* 13 (7), 2077–2092.

Lam, P. J., Doney, S. C., Bishop, J. K. B., 2011. The dynamic ocean biological pump: Insights from a global compilation of particulate organic carbon, $CaCO_3$, and opal concentration profiles from the mesopelagic. *Global Biogeochemical Cycles* 25 (3).

Longhurst, A., Sathyendranath, S., Platt, T., Caverhill, C., 1995. An estimate of global primary production in the ocean from satellite radiometer data. *Journal of Plankton Research* 17 (6), 1245–1271.

Mari, X., Beauvais, S., Lemée, R., Pedrotti, M. L., 2001. Non-Redfield C:N ratio of transparent exopolymeric particles in the northwestern Mediterranean Sea. *Limnology and Oceanography* 46 (7), 1831–1836.

Marsay, C. M., Sanders, R. J., Henson, S. a., Pabortsava, K., Achterberg, E. P., Lampitt, R. S., 2015. Attenuation of sinking particulate organic carbon flux through the mesopelagic ocean. *Proceedings of the National Academy of Sciences* 112 (4), 1089–1094.

Martin, J. H., Knauer, G. A., Karl, D. M., Broenkow, W. W., 1987. VERTEX: carbon cycling in the northeast Pacific. *Deep Sea Research Part A. Oceanographic Research Papers* 34 (2), 267–285.

Mouw, C. B., Barnett, A., McKinley, G. A., Gloege, L., Pilcher, D., 2016. Phytoplankton size impact on export flux in the global ocean. *Global Biogeochemical Cycles* 30 (10), 1542–1562.

Passow, U., Carlson, C., 2012. The biological pump in a high CO2 world. Marine Ecology Progress Series 470 (2), 249–271.

Sanders, R. J., Henson, S. A., Martin, A. P., Anderson, T. R., Bernardello, R., Enderlein, P., Fielding, S., Giering, S. L. C., Hartmann, M., Iversen, M., Khatiwala, S., Lam, P., Lampitt, R., Mayor, D. J., Moore, M. C., Murphy, E., Painter, S. C., Poulton, A. J., Saw, K., Stowasser, G., Tarling, G. A., Torres-Valdes, S., Trimmer, M., Wolff, G. A., Yool, A., Zubkov, M., 2016. Controls over Ocean Mesopelagic Interior Carbon Storage (COMICS): Fieldwork, Synthesis, and Modeling Efforts. *Frontiers in Marine Science* 3 (August), 136.

Sarmiento, J. L., Slater, R., Barber, R., Bopp, L., Doney, S. C., Hirst, A. C., Kleypas, J., Matear, R., Mikolajewicz, U., Monfray, P., Soldatov, V., Spall, S. A., Stouffer, R., 2004. Response of ocean ecosystems to climate warming. *Global Biogeochemical Cycles* 18 (3).

Schmittner, A., Oschlies, A., Matthews, H. D., Galbraith, E. D., 2008. Future changes in climate, ocean circulation, ecosystems, and biogeochemical cycling simulated for a business-as-usual CO2 emission scenario until year 4000 AD. *Global Biogeochemical Cycles* 22, 1–21.

Siegel, D. a., Buesseler, K. O., Behrenfeld, M. J., R, B.-N. C., Boss, E., Brzezinski, M. A., Burd, A., Carlson, C. A., DÂ´Asaro, E. A., Doney, S. C., Perry, M. J., Stanley, R. H., Steinberg, D. K., 2016. Prediction of the Export and Fate of Global Ocean Net Primary Production: The EXPORTS Science Plan. *Frontiers in Marine Science* 3 (22), 1–10.

Steinberg, D. K., Carlson, C. A., Bates, N. R., Goldthwait, S. A., Madin, L. P., Michaels, A. F., 2000. Zooplankton vertical migration and the active transport of dissolved organic and inorganic carbon in the Sargasso Sea. *Deep-Sea Research Part I: Oceanographic Research Papers* 47 (1), 137–158.

Tyrrell, T., 2008. Calcium carbonate cycling in future oceans and its influence on future climates. *Journal of Plankton Research* 30 (2), 141–156.

Van Mooy, B. A. S., Keil, R. G., Devol, A. H., 2002. Impact of suboxia on sinking particulate organic carbon: Enhanced carbon flux and preferential degradation of amino acids via denitrification. Geochimica et Cosmochimica Acta 66 (3), 457–465.

Wilson, J. D., Barker, S., Ridgwell, A., 2012. Assessment of the spatial variability in particulate organic matter and mineral sinking fluxes in the ocean interior: Implications for the ballast hypothesis. *Global Biogeochemical Cycles* 26 (4).

6 — Danksagung

Zuallererst möchte ich mich bei Ulf Riebesell bedanken, der mir diese Doktorarbeit ermöglicht hat, stets mit Rat zur Seite stand und Vertrauen in mich hatte. Zwar war der Start in die Arbeit mit der ersten Gran Canaria Studie nicht der Beste, jedoch passiert im Leben – wie du ja weißt – für alles Schlechte ja auch was Gutes. Dies hat sich mit den weiteren Studien mehr als bewahrheitet. Die KOSMOS Studien sind etwas besonderes, und deine Begeisterung für die Meereswissenschaften ansteckend. Ich bin daher sehr froh, dass ich ein Teil des Teams geworden bin.
Ein besonderer Dank gilt auch Lennart Bach. Diese Arbeit wäre nicht dieselbe ohne unsere Diskussionen, deinen Rat und die stets konstruktive Kritik. Danke dafür, dass deine Tür immer offen stand.
Natürlich gilt mein Dank auch der gesamten Arbeitsgruppe der "Biologischen Ozeanographie". Es war eine tolle Zeit sowohl auf den Projekten, als auch in Kiel. Danke Jan für die gemeinsame Zeit im Büro und unsere Gespräche über Gott und die Welt, Kerstin für die stetige Versorgung mit Keksen in Zeiten der Not und Allanah für die Nachhilfe in Kiwi-Accent. Fred, auch deine Tür stand stets offen und deine Kreativität hat oft zu neuen Denkanstößen geführt, als auch zu einem der Kapitel dieser Arbeit. Dafür, und natürlich für die moralische Begleitung bei meiner ersten großen Konferenz danke ich dir. Die Zeit in New Orleans mit dir war toll und lustig.
Vielen Dank auch an die ISOS, die mir mit dem großen Angebot an hochinteressanten und hilfreichen Kursen viele Dinge während der Doktorarbeit vereinfacht hat.
Mein Dank geht auch an meine Freunde in Kiel und Berlin. Vor allem an Markus und Alex, auf dass wir unser Refugium auf Fehmarn noch oft nutzen können und ihr dann auch mal Klamotten dabei habt! Olfi, Fabi, Guggi und Bolle, vielen Dank für die tollen Jahre der Freundschaft, unsere Jam-Sessions und Daddel-Abende.
Mein ganz besonderer Dank geht an Alice, die mir immer zur Seite steht und in den stressigen Phasen während Projekten und zum Ende der Doktorarbeit mein Ruhepol war und mich stets liebevoll unterstützt hat.
Zuletzt möchte ich meiner Familie Danken, die mich immerwährend unterstützt hat und stets Rückhalt gab. Danke Mama und Papa, ohne euch wäre ich nicht da, wo ich heute bin.

7 — Curriculum Vitae

Paul Stange
Biological Oceanography
Helmholtz Centre for Ocean Research Kiel GEOMAR
Eckernfoerder Strasse 82, 24116 Kiel, Germany
+49-151-75005570
pstange@geomar.de

Personal Information: *11-16-1987, Erfurt, Germany; German Nationality

Academic background

2013 – now	**Graduate student** at the Helmholtz Centre for Ocean Research Kiel GEOMAR in group of Ulf Riebesell **Topic:** The influence of plankton food-web structure on the efficiency of the biological carbon pump
2013	**Master-thesis** under the supervision of Dr. Silke Lischka and Prof. Dr. Ulf Riebesell on "The influence of ocean warming and acidification on two overwintering arctic copepod species", including a 6-week expedition to Spitsbergen
9/2011 – 9/2013	**Master of Science** in Biological Oceanography at the Helmholtz Centre for Ocean Research Kiel GEOMAR and the Christian-Albrecht-University Kiel
2011	**Co-author** of the peer-reviewed paper "Food Supply and Seawater pCO_2 Impact Calcification and Internal Shell Dissolution in the Blue Mussel *Mytilus edulis*" (PLoS ONE 6(9): e24223. doi:10.1371/journal.pone.0024223)
9/2010 - 7/2011	**One-year study-exchange** with the Ocean University of China in Qingdao, China (青岛市，山东), attending several courses in the field of Biological Oceanography and gaining basic language skills in Mandarin
9/2007 – 9/2010	**Bachelor of Science** in Biology at the Christian-Albrecht-University in cooperation with the Helmholtz Centre for Ocean Research Kiel (GEOMAR) **Thesis** under the supervision of Prof. Dr. Frank Melzner on the "Effects of food concentration and CO_2-partialpressure on calcification rates of the blue mussel *Mytilus edulis*"

Academic and field experience

5/2013 - 6/2013	**Research assistant**; Cruise (M97); Cap Verde - Brazil; Measuring Nitrogen fixation rates of key nitrogen-fixing species in the Atlantic Ocean
4/2013	**Student assistant**; Cruise (AL413); Germany/Poland/Sweden; Collecting data (length, weight, stomachs, otoliths, finclip) of key fish species (Cod, Herring, Sprat) and plankton abundances in the Baltic sea for a long term monitoring project
1/2013 - 2/2013	**Research assistant;** Ny Ålesund; Spitsbergen; Norway; 6-week experiment in the arctic winter together with Dr. Silke Lischka (GEOMAR) to estimate the vulnerability of arctic Pteropods and Copepods to Ocean warming and acidification, including work in the laboratory and collecting samples by boat in the Kongsfjord from January to February
2012	**Student assistant;** Geomar; Germany; Helping in the construction and preparation of the Mesocosms for the long-term experiment in Kristineberg, Sweden (Prof. Dr. Ulf Riebesell)
2011 - 2012	**Student assistant;** Geomar; Germany; Measuring Total Alkalinity for an ocean acidification incubation-experiment on coralline red algae under Dr. Jan Büdenbender and Prof. Dr. Ulf Riebesell
2009 - 2010	**Student assistant;** Geomar; Germany; Assistant of Prof. Dr. Syee Weldeab (University of California / Santa Barbara) on the topic of the thermal, salinity, and productivity history of the oceans. Working on cores of the gulf of Bengal.
2009	**Volunteer;** La Tortuga feliz; Costa Rica; Voluntary work for the WWF-, and NCDO-supported project “La Tortuga feliz”. Experience in the field of environmental protection and preservation of sea-turtles.

Publications (peer-reviewed)

Stange, P., Bach, L. T., Taucher, J., Achterberg, E. P. and Riebesell, U. (2017): The influence of plankton community structure on particle sinking velocity and respiration rates, Manuscript in preparation

Stange, P., Taucher, J., Bach, L. T., Algueró-Muñiz, M., Horn, H. G., Krebs, L., Boxhammer, T., Nauendorf, A. and Riebesell, U. (2017): Ocean acidification-induced restructuring of the plankton food-web can influence the degradation of sinking particles, submitted to *Frontiers in Marine Science*

Stange, P., Bach, L.T., Le Moigne, F.A.C., Taucher, J., Boxhammer, T., and Riebesell, U. (2017): Quantifying the time lag between organicmatter production and export in the surface ocean: Implications for estimates of export efficiency, *Geophysical Research Letters* 44 (1), 268-276

Melzner, F., Stange, P., Trübenbach, K., Thomsen, J., Casties, I., Panknin, U., Gorb, S.N., Gutowska, M.A., (2011): Food supply and seawater pCO_2 impact calcification and internal shell dissolution in the blue mussel Mytilus edulis, *PloS one* 6 (9)

8 — Eidesstattliche Erklärung

Hiermit bestätige ich, dass die vorliegende Arbeit mit dem Titel:

The influence of plankton food-web structure on the efficiency of the biological carbon pump

von mir selbstständig verfasst worden ist und keine weiteren Quellen und Hilfsmittel als die angegebenen verwendet wurden. Die vorliegende Arbeit ist unter Einhaltung der Regeln guter wissenschaftlicher Praxis der Deutschen Forschungsgemeinschaft entstanden und wurde weder im Rahmen eines Prüfungsverfahrens an anderer Stelle vorgelegt noch veröffentlicht. Ich erkläre mich einverstanden, dass diese Arbeit an die Bibliothek des GEOMAR und die Universitätsbibliothek der CAU weitergeleitet wird.

Kiel, den 06. April 2017 Paul Stange